Technical Report 1247

The PHD: A Planar, Harmonic Drive Robot for Joint Torque Control

Bruce R. Thompson

MIT Artificial Intelligence Laboratory

AI-TR 1247 The PHD: A Planar, Harmonic Drive Robot for Joint Torque Control Bruce R. Thompson

The PHD: a Planar, Harmonic Drive Robot for Joint Torque Control

by

Bruce Robert Thompson

B.S.M.E. Carnegie Mellon University
(May 1988)

Submitted to the Department of Mechanical Engineering
In Partial Fulfillment of the Requirements
For the Degree of
Master of Science in
Mechanical Engineering
at the
Massachusetts Institute Of Technology
May 1990

The PHD: a Planar, Harmonic Drive Robot for Joint Torque Control

by

Bruce Robert Thompson

Submitted to the Department of Mechanical Engineering on July 5, 1990 in partial fulfillment of the requirements for the degree of Master of Science in Mechanical Engineering.

Abstract

Many efforts are underway to extend the abilities of robots into the domain of space, where they can be used to perform simple tasks in environments where it is difficult or dangerous for humans to work. One such effort, the Flight Telerobotic Servicer (FTS) is being undertaken for NASA by Martin Marietta.

The FTS is a two arm manipulator system mounted on a mobile platform. A third arm is used to anchor the platform while working. The two manipulators on the FTS are seven degree of freedom arms which will be used to perform a variety of tasks. MIT was contracted, in conjunction with the University of Iowa, to build an accurate simulation of a seven degree of freedom manipulator similar to that proposed for the FTS. This thesis documents the development of that model.

In order to perform some tasks, the FTS will need some sort of force control ability. To assist in the development of that ability a robot, the PHD, was designed and built with the capability to be used for two purposes. First, it can be used to perform research on joint torque control schemes, and second it can be used to determine the important dynamic characteristics of the Harmonic Drive gear reducer.

The PHD, is a planar, three degree of freedom arm with torque sensors integral to each joint allowing joint torque feedback to be implemented. Preliminary testing using the PHD has shown that a simple linear spring model of the Harmonic Drive's flexibility is suitable in many situations. Future work with the system could include a more detailed Harmonic Drive model, as well as development of joint torque feedback schemes for force control.

Thesis Supervisor: Warren Seering
Professor of Mechanical Engineering

Acknowledgements

There are numerous people who I wish to thank for making this work possible, but first and foremost I must give thanks to the Lord and God of my life, Jesus Christ. It is only through His power and constant grace that I am able to meet and overcome the day to day challenges in my life.

Next, I sincerely thank my advisor, Warren Seering, whose careful, and sometimes hidden, plan exposed me to a very well rounded experience, which I'm not sure I would have gotten elsewhere. Next, I thank the other students in our group—both past and present—Brian Avery, Michael Caine, Andy Christian, Jim Hyde, Neil Singer, Lukas Rueker, Kamala Sundaram, Erik Vaaler and Al Ward for their help and also for putting up with my antics.

A very special thanks goes to Kamala, both for being an excellent research partner and friend, providing a pressure relief when things got hectic. Thanks also to Marc Filerman, who has been a friend and accomplice in many enjoyable times. Special thanks go to Andy, whose help on the design and especially control of the robot saved me immeasurable time and whose patience with me has been tested (you passed) in the last few weeks of generating this document. Also, I must thank Erik, whose immense size is rivaled only by his immense knowledge of design (and control and dynamics and...). Some credit also goes to the support staff of the Artificial Intelligence Lab, who take on the formidable task of keeping this place running on a daily basis.

Thanks to my two roommates Dave and Dave (Kowalick and Otis) who have provided much support, both physical and spiritual and to my many friends at The Church of the Open Bible, especially Lynne Steele, who have taught me what is really important in life. I will never be able to thank Liz and Pete Coxon enough for showing me the way to my eternal salvation.

Finally, I greatly thank my parents, Ann and Don, and my brother and sister, Pete and Sherri, for always being there with support and encouragement when I need it. I love you all.

This report describes work done at the MIT Artificial Intelligence Laboratory. This material is based on work supported in part by the Office of Naval Research University Research Initiative Program under Office of Naval Research contract no. N00014-86-K-0685. Funding was also provided by NASA Goddard Space Flight Center through the University of Iowa, contract no. V80380.

Table of Contents

Chapter 1: Introduction

This thesis describes research in two different areas. The first is the creation and verification of a model for the simulation of a commercially produced robot arm purchased by NASA's Goddard Space Flight Center. The second is the construction and testing of the PHD robot, a planar robot built using the Harmonic Drive used as a gear reduction. The PHD will be used for the testing of joint torque control strategies as well as determining a suitable simulation model of the Harmonic Drive. The following chapter introduces the research and discusses its relevance.

1.1 Control Background

In order for robots to perform useful tasks we must be able to control them. This control can either be done using a human being teleoperating the robot, or by a computer generating high level commands. In either case these commands must be converted into lower level commands to be executed by the robot. In many applications, robotic systems are being discovered to require more and more precise control in order to accomplish their chosen task. This is seen in areas such as parts assembly, where robots are required to accurately position parts to thousandths or even ten-thousandths of an inch. Other tasks such as surface grinding require force control—the ability of a robot to exert a commanded force—in order to be successful. The remainder of this section gives a brief overview of control, beginning with position control, then moving to force control and finally examining one particular force control scheme called joint torque control.

1.1.1 Position Control

Position control allows robots to move from one place to another. The most common scheme for doing this is a simple P.I.D. control loop based on a position and velocity feedback signals. Many more intricate and complex schemes have been devised which allow higher precision control, usually at the expense of requiring more computing power. Some examples of these include estimator design and full state feedback. Position control has significant limitations when it comes to doing many robotic tasks as it has little ability to deal with uncertainties in its environment or errors in its task. For example, when a position control scheme is being used to assemble parts, the tolerances on the parts must be very accurate in order to achieve a reasonable success rate. If parts are out of tolerance and they collide during assembly then there is no means for the system to recover. Alternatively, if a robot is picking up an object, monitoring its force output is a good way of telling whether or not it has been successful, position control lacks this ability.

A good way to solve some of these problems involves sensing the force being exerted by the robot and incorporating that signal into the feedback control system. This allows the system to react to its environment. One such method proposed by Paul [15] involves integrating position and force control into a hybrid scheme, allowing position control in some directions and force control in others.

1.1.2 Force Control

In some tasks, it is desired is to generate a commanded force in a certain direction with position being of secondary concern (e.g. grinding). Various approaches have been taken to allow accurate force control and many of these are documented by Whitney [20]. Research has been done by Maples [10] to classify the different schemes based on their method and some arguments have been made that certain approaches are inherently better than others. Good [6] and Eppinger [4] have worked to explain the reasons for limitations of force control by building more complex models and using them to show why problems occur in certain strategies. Both of these researchers stress the importance of analyzing the drive system elements when looking at a robotic system.

In force controlled systems, issues that are unimportant in position control suddenly become critical. When modelling such systems, parameters which have little effect on the position control model become more important. Therefore, to be able to generate a successful force control scheme it is important to build a relatively accurate system model. Such a model should include any structural modes, the characteristics of the drive train (motor, gearing, etc.) and any significant non-linearities in the system (Coulomb friction, amplifier current limits). Analyses of these types of models have offered much insight into the problems that occur in force controlled systems.

More recently, other issues have emerged as important with regard to force control. These issues relate to whether the actuator and sensor are located together (collocated) or there is some flexibility between them (noncolocated). The rigid body bandwidth as well as dynamically collocated and noncolocated modes often serve to dictate the maximum achievable bandwidth of the force controller. Specifically, Eppinger [5] states that it is important to boost the lowest frequency noncolocated modes in order to improve performance of the system. According to Maples [10] another way to enhance performance is by controlling the robot in Cartesian space as opposed to joint space. This allows more flexibility in the control scheme which more than offsets the added computational burden.

1.1.3 Joint Torque Control

Another recent advancement is the use of joint torque feedback. This method proposes to feed back the torque across each joint to improve control. This was proposed by Hashimoto [7] and Tilley [18] as an effective method for improving position control strategies as it significantly improves disturbance rejection. This method is used predominantly in systems where an actuator is driving a joint through a large gear ratio although Asada [1] showed it is also useful in minimizing the effects of non-linearities in direct drive joints. As documented by Pfeffer [16] and Luh [9] the torque sensor located on the output of the gear reduction allows the system to compensate for friction and nonlinearities present in the drive and gearing. As shown by Tilley [19] it also improves backdrivability. Now researchers such as Sundaram [17] are interested in probing the advantages of using joint torque sensing in force control strategies. This approach provides a middle ground between directly measuring endpoint force and simply using motor current to control endpoint force. This type of scheme, if successful, will provide a means for robots

to perform tasks in unstructured environments where the need for force control is more important.

1.2 NASA Background

One area where robots can be of great use assisting humans is in space. The planning required to send a robot into space to repair a satellite or assemble a structure is significantly less than that required to send a human. Therefore, teleoperating robots in space either from the Space Shuttle or even earth, is a useful goal. Since the tasks being done by the robot would often be in uncertain or unstructured environments this is an area where force control is indispensable.

1.2.1 FTS Program

The Flight Telerobotic Servicer (FTS) is one such robot system being built by NASA to operate remotely in space. Its main purpose is to assist astronauts with the construction and maintenance of the U.S. Space Station proposed for the mid 1990's. It will be teleoperated from within the Space Station, allowing astronauts to perform assembly, inspection, and servicing without having to leave their protected environment. The FTS will also be able to operate from the Space Shuttle to perform initial assembly of the Space Station or perform maintenance on satellites in earth orbit.

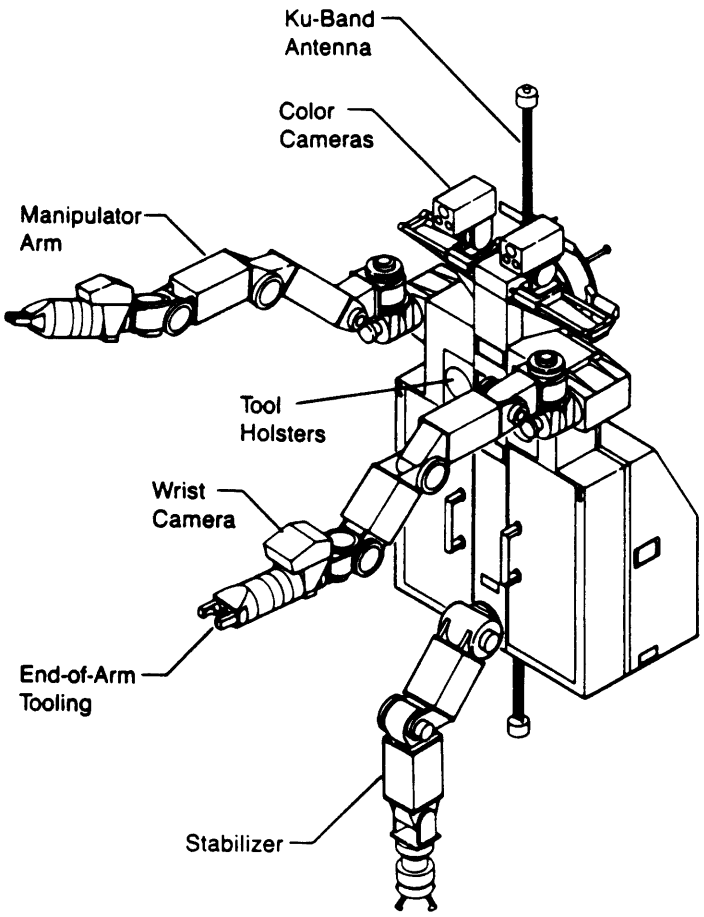

Figure 1.1 Layout of the Flight Telerobotic Servicer
(courtesy of Martin Marietta)

The FTS will consist of a base platform mounted to a modified MMU (Manned Maneuvering Unit) allowing the FTS to move from place to place as shown in Figure 1.1. Three manipulators will be mounted on the platform, one five degree of freedom stabilizer arm used to hold the platform stationary, and then two seven degree of freedom manipulator arms for performing whatever tasks are necessary. A full complement of end effector tooling will allow the robot to perform a wide variety of tasks. Operator feedback will be accomplished via two adjustable color cameras mounted on the platform as well as smaller

wrist cameras mounted on each of the manipulator arms. This will allow the robot to perform tasks out of the operator's direct view.

1.2.2 Martin Marietta's Work

The primary contractor selected to design and build the FTS system is Martin Marietta's Space Systems Division. The planned schedule is to launch a partial prototype system with the Space Shuttle on a test flight in 1991, followed by a full prototype test in 1993. The final system should be operational in the mid 1990's as Space Station construction commences. Currently, Martin Marietta is involved in designing the seven degree of freedom manipulator to be used, additionally they are developing the platform and stabilizing arm.

To allow the FTS to perform tasks such as replacing electronic components or manipulating delicate instruments research is needed in developing robust force control strategies. Also, Martin Marietta is interested in being able to accurately predict the robot's performance, so they need to develop detailed computer models and simulations of all parts of the FTS. They want to be capable of building models of differing complexities so that simulations can be run faster or slower depending on the desired accuracy of the results. In order to do this it is necessary to develop detailed models of the components of the arm. One particular area where work is needed is in exploring the performance characteristics of the Harmonic Drive.

1.2.3 Harmonic Drive

The Harmonic Drive (H.D.) is a commercially produced gear reducer based on a principle of using a non-rigid, continuous deflection wave to achieve large gear ratios in a small package. Its main advantages are:

- large ratios can be obtained (up to 200:1) in a small module
- input and output rotations are coaxial
- units can be produced with zero backlash
- high output torques can be achieved

The drive consists of three parts, a "circular spline', a "flexspline" and a "wave generator". The common configuration is to have the wave generator serve as the input driven by a motor at high speed. The circular spline is then attached to "ground" and the flexspline rotates at the motor speed divided by the gear ratio and has an output torque of roughly the gear ratio times the input torque. Typical efficiencies for the drives are between 60% and 85% and maximum torque outputs range from 30 in lb to 7500 ft lb. A picture of the Harmonic Drive is shown in Figure 1.2.

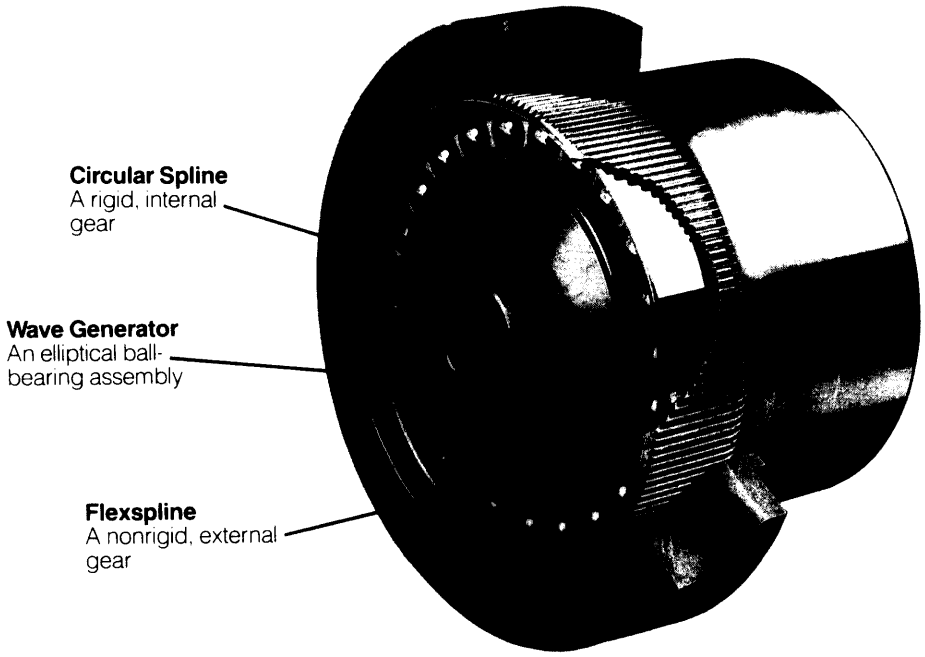

Figure 1.2 Harmonic Drive

The operational principle of the drive is to place the elliptical wave generator inside of the flexspline causing it to deflect into an ovular shape. The flexspline has small gear teeth on its outside which mate in two places (along the major axis of the ellipse) with similar teeth on the inside of the circular spline. Then, as the wave generator is rotated consecutive teeth mesh between the flexspline and circular spline. Since the circular spline has two more teeth than the flexspline one revolution of the wave generator causes the flexspline, to move backward two teeth with respect to the circular spline, thus giving the desired gear ratio (see Figure 1.3). The best way to understand the operation is to examine one up close. The

Harmonic Drive was "invented" by Walt Musser in 1955 and modified little since, although currently some research has been done by Kondo [8] on modified tooth profiles in order to optimize performance.

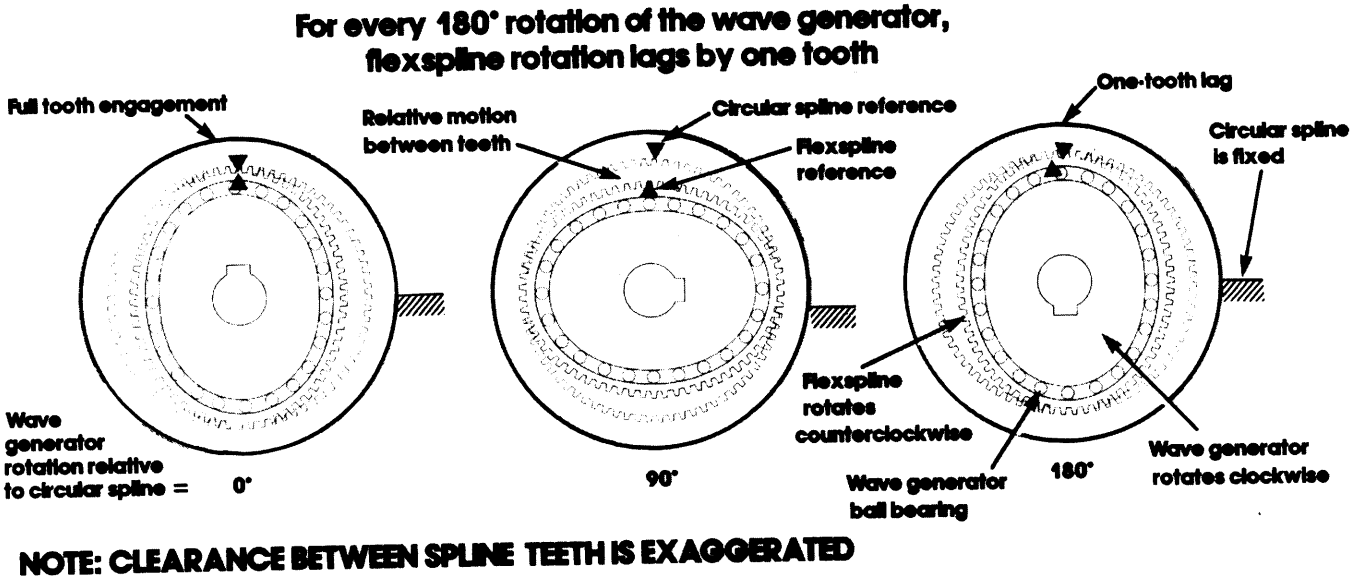

Figure 1.3 Description of Harmonic Drive Operation

1.3 Design of a Test System

The PHD is a Planar, Harmonic Drive robot built as a research tool to study two separate issues, joint torque control and Harmonic Drive performance characteristics. It has three joints: shoulder, elbow, and wrist which all rotate in the same plane. The PHD was designed to be modular and easy to assemble and disassemble. Each of the joints consists of two parts, the joint housing and the drivetrain. There are three main components that make up the drivetrain: the motor, the Harmonic Drive and the torque sensor. The torque sensor is designed to measure the torque across the joint, allowing various joint torque control schemes to be tested using the robot.

The PHD has been designed primarily as a robot to study joint torque control strategies. Another goal of the design is to allow the robot to be used to study the dynamic performance of the Harmonic Drive gear reducer. Each joint has a torque sensor allowing the measurement of the torque across the joint which can then be fed back to the controller.

Additionally, the shoulder and elbow joints have tachometers integral to the motors to permit velocity feedback and all three motors are equipped with encoders to allow position feedback. All three joints rotate in the same plane, the shoulder having 180° rotation, the elbow having 270° rotation, and the wrist being able to rotate continuously. The shoulder joint is equipped with an extra encoder allowing the joint position to be measured directly. This data can be combined with the motor encoder data allowing the position of both the input and output of the Harmonic Drive to be monitored. This, in conjunction with the torque sensor, allows more accurate dynamic characterization of the Harmonic Drive.

The remainder of this thesis is divided into the following chapters:

Chapter 2: Presents the details of our efforts to build an accurate simulation of the performance of the RRC arm purchased by NASA. The chapter shows the model development and revision based on experimental results obtained from the arm. Finally, a brief discussion is presented of what is required to extend the model to predict force control behavior.

Chapter 3: Discusses the important issues considered while designing the PHD robot. The motivation for many of the numerous design decisions is provided. Also, details as to the configuration and mechanical layout of the robot are presented.

Chapter 4: Shows experimental results detailing the PHD's behavior. The first section outlines the tested capabilities of the robot. The second section presents the results of tests conducted on the Harmonic Drive, and presents a suitable model of the drive.

Chapter 5: Conclusions of this research are given along with suggestions of areas for future research using the PHD.

Chapter 2: NASA Modelling Research

As stated earlier, NASA's work on the Flight Telerobotic Servicer (FTS) included the need to produce an accurate simulation of the performance of the hardware. To build this simulation, research was needed to determine an accurate model of the seven degree of freedom manipulator arms to be used. In order to initiate research in this area, NASA's Goddard Space Flight Center purchased two commercially produced robot arms from Robotics Research Company (RRC) of Cincinnati, Ohio. These arms are seven degree of freedom arms similar to the design proposed for use in the FTS system. This chapter discusses our efforts to build a good simulation of these manipulators

MIT was contracted in conjunction with researchers at the University of Iowa and Cambridge Research (a local company in Cambridge) to produce a dynamic simulation of these arms. The initial commitment from MIT was to research and determine a reasonable model of the controller of the robots. That is, to determine a set of equations that would predict the motor current given the input command and feedback signals. It was the responsibility of the group at the University of Iowa to develop the required kinematic model of the seven degree of freedom arm. Then Cambridge Research was to coordinate the integration of the full model into a suitable simulation package.

2.1 RRC Arm

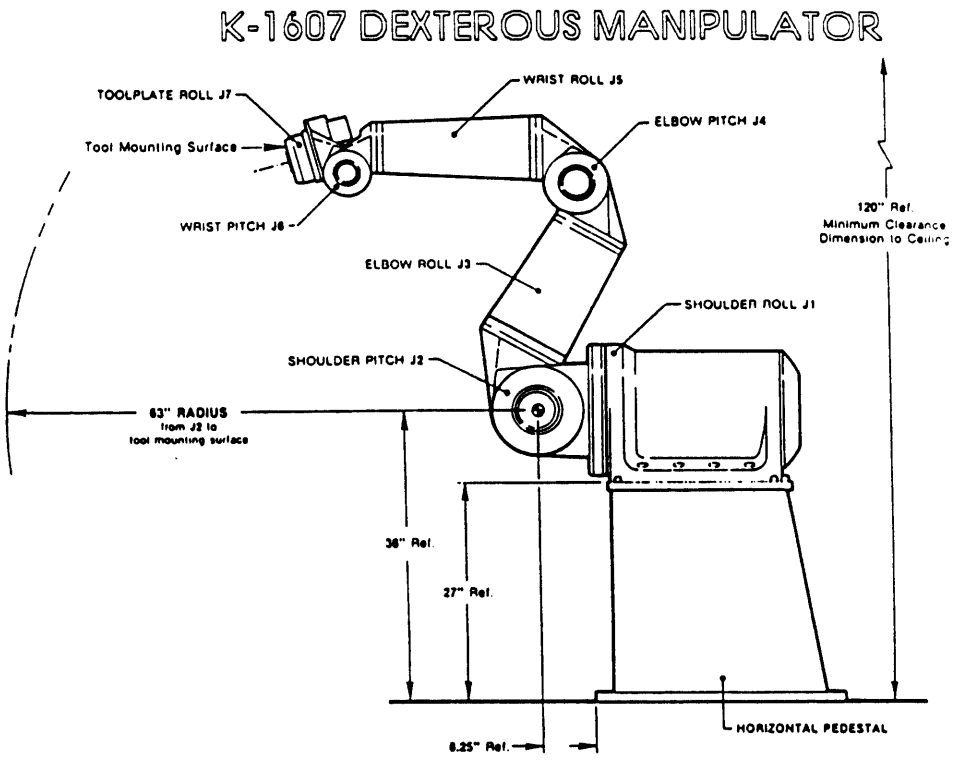

Figure 2.1 Robotics Research Co. K-1607 Manipulator (courtesy of RRC)

The specific arm chosen by NASA is the RRC K1607 manipulator. It is the anthropomorphic seven degree of freedom arm shown in Figure 2.1. Some of its more important specifications are listed in Table 2.1.

Model Specification:	MPS K-1607-0986-1B
Configuration:	Jointed Arm
Servoed D.O.F:	7
Max. Reach:	63 in.
Working Envelope:	~600 cu. ft.
Positioning Repeatability:	0.005 in.
Weight:	500 lb.
Max. Payload:	25 lb.
Construction:	Cast Aluminum & Steel

Table 2.1 Specifications for RRC K-1607 Manipulator (courtesy of RRC)

The RRC arm has seven independent degrees of freedom: shoulder roll and pitch, elbow roll and pitch, wrist roll and pitch and toolplate roll. The drivetrain is similar to that proposed for the FTS system and consists of a DC servomotor turning a Harmonic Drive which drives each joint. Each joint has a torque sensor measuring the torque output of the Harmonic Drive (or the torque across the joint). Two of these arms are mounted side by side at NASA's Goddard Space Flight Center. They are being used to study what tasks can be performed and how two manipulators can be used together to perform more complex tasks than one single arm. Also, these arms were used to gather data to verify our simulation model.

2.2 Position Control Model

In order to build and test an accurate simulation of the controller of the RRC arm it was necessary for us to incorporate some physical dynamics into the model. Since it was not our responsibility to develop the kinematics for the seven degree of freedom arm, we chose to treat each joint separately so that no dynamic coupling was present. To implement this we started with a relatively simple model of the controller moving a simple load inertia. This model, when proven to be accurate, could be incorporated into the more advanced kinematic

model. This method of decomposition—MIT working on the one degree of freedom controller model and Iowa working on the seven degree of freedom kinematic model—made it simpler for research to happen in parallel as well as verify our own results at each successive step.

2.2.1 Controller Modelling

Since each joint of the robot is equipped with torque sensing capability this data is used in the controller. As mentioned earlier, this form of torque feedback serves to remove the nonlinear effects present in the Harmonic Drive and motor as well as frictional effects present in their bearings. Figure 2.2 shows a block diagram which outlines the basic model used for position control.

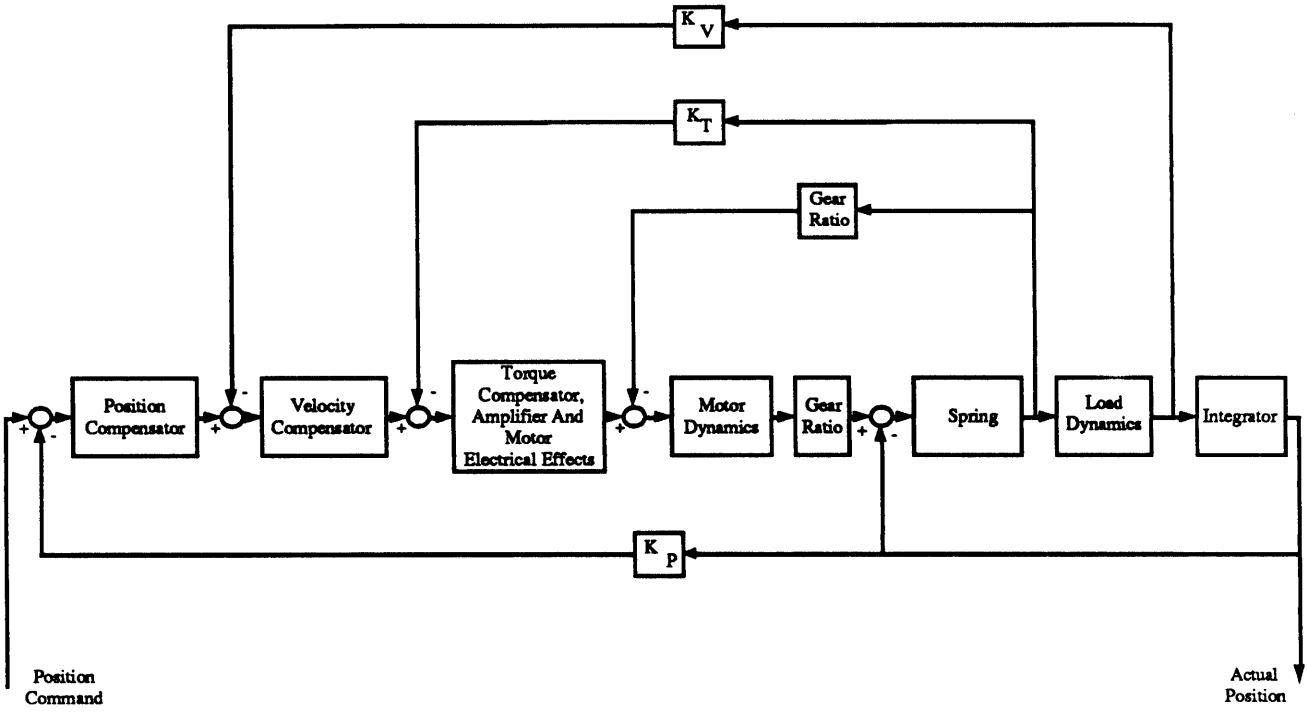

Figure 2.2 Block Diagram of Position Control Model

In this scheme the joint position is fed back and compared to the desired position and fed into the position compensator. This produces a velocity command which is compared to the actual velocity and fed to the velocity compensator. Finally, this generates a torque

command which is compared to the measured torque and fed to the torque compensator. Thus, there are three feedback loops in the model, corresponding to the position, velocity and joint torque. The innermost loop on the block diagram is not an electrical feedback signal but a block diagram representation of what is physically happening in the system. It accounts for the reaction torque from the transmission which acts on the motor rotor. This representation presumes that the transmission can be modelled as an inertia (lumped in with the motor rotor inertia), a 100% efficient gear ratio, and a spring representing the flexibility of the Harmonic Drive.

The controller model ends internal to the torque compensator block, when it sends a signal to the amplifier. Therefore, we were primarily interested in the first three blocks and feedback loops in the diagram. The torque compensator block also takes into account the amplifier and motor electrical dynamics. Its output is the motor torque, which then has the reaction torque subtracted from it. The result is the total torque acting on the motor rotor, which accelerates the motor rotor and acts to "wind up" the spring which drives the joint. This representation is kind of subtle but it is consistent with the physical system. It is the inherent "springiness" of the Harmonic Drive that allows this representation to work. Essentially, the motor and joint are on opposite ends of a spring. The available feedback signals are the torque through that spring and the position of the joint. On the RRC arm there is no direct position feedback available from the motor, instead the joint position is measured.

For the simple model shown in Figure 2.2, the amplifier/motor pair is represented by a perfect torque source, taking the motor current and turning it directly into a torque acting on the motor rotor. This assumption is justified because the amplifier coupled with the motor electrical effects responds very quickly, driving the motor inertia with the commanded torque almost immediately. As we will show later, this assumption breaks down when we begin to develop a force control model. The dynamic model includes the motor inertia and viscous damping, the gear ratio of the transmission, a spring rate associated with the transmission flexibility, and a load inertia and damping. The values for the inertia and viscous damping in the motor were obtained from the motor manufacturer, the transmission stiffness was quoted in the Harmonic Drive literature, and the joint inertia and damping were obtained from RRC.

Since we were building a dynamic model of a single degree of freedom, we needed to decide which physical properties were important to include. In a system with a transmission such as this, it is important to consider the motor mechanical dynamics (rotor inertia and

damping) in any model because for large gear ratios, motor dynamics can become more significant than joint and load dynamics. It must be recalled that when accelerating the system, the motor must drive an inertia equivalent to the motor inertia plus the joint inertia divided by the gear ratio squared; for example on the RRC arm a typical gear ratio is 200, so that the equivalent inertia the motor is accelerating is the joint inertia divided by 40,000 plus the motor inertia. In many cases the equivalent joint inertia is small compared to the rotor inertia, allowing the controller to drive a load which is roughly constant regardless of the robot configuration. However, due to the RRC arm's rigid, heavy design (and therefore large joint inertias), the joint inertias are significant for the inner joints (shoulder, elbow). Pasch [14] gives a detailed discussion of these considerations.

It is important to emphasize at this point that our goal in this exercise was to model the existing RRC arm and not to optimize its performance. The models of the compensators were provided by RRC. The first model we arrived at is shown in Figure 2.3.

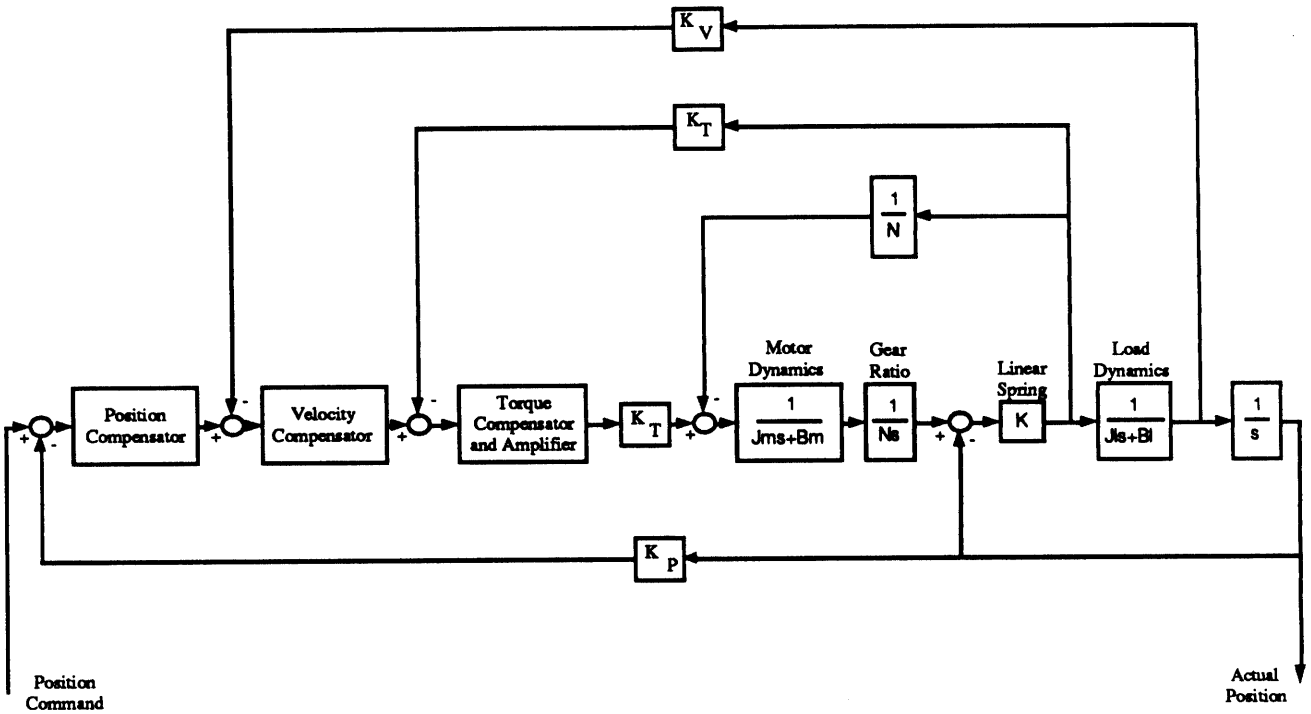

Figure 2.3 Linear Model of Typical Joint

This linear model seemed to provide reasonable response for the larger joints but when simulations were run on the smaller joints (wrist pitch and toolplate roll) they were

found to exhibit some instabilities (see Figure 2.4). Since the real robot is stable, this implies that either our model was inadequate or its parameters were incorrect. Since we were relatively confident about the parameters, we decided to pursue a more detailed system model.

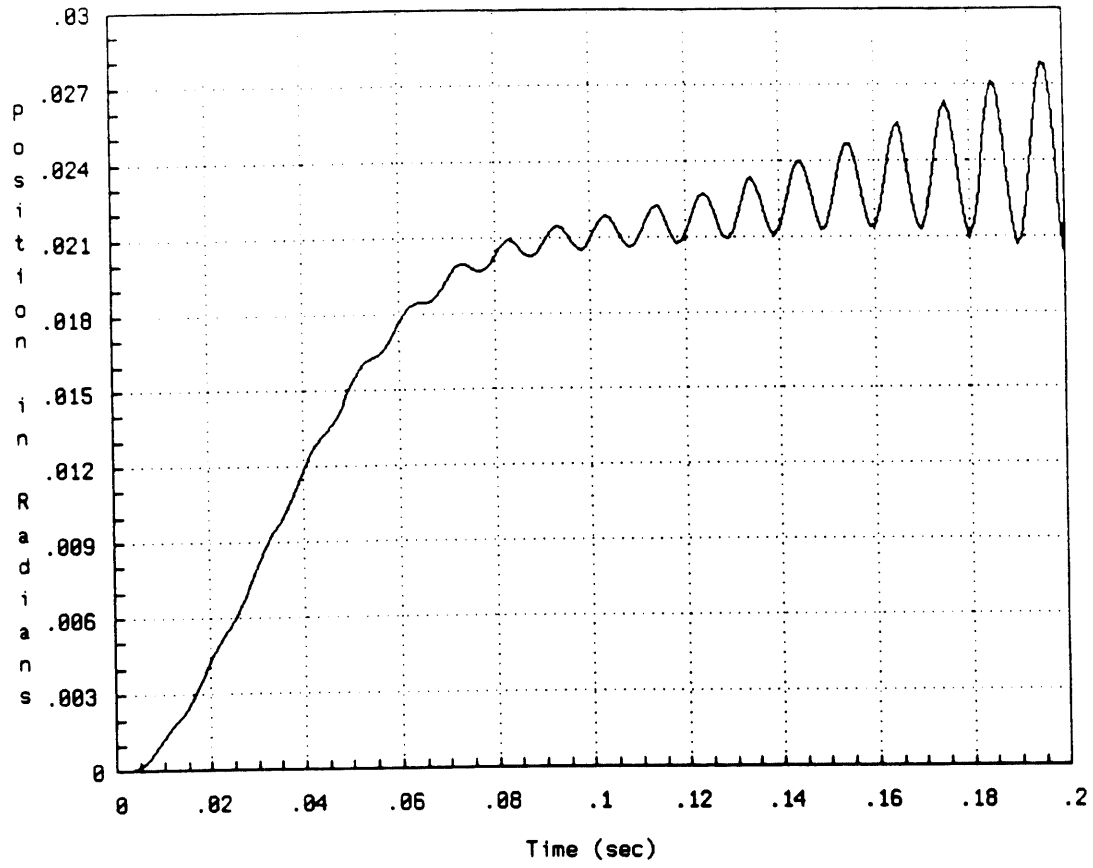

Figure 2.4 Simulated Step Response for Wrist Pitch – Linear Model

2.2.2 Non-linear Model

The most apparent elements missing in the linear model were the quoted non-linear spring characteristics of the Harmonic Drive and the unmodelled Coulomb friction in both the motor and joint. We added these effects to the model and again looked at simulation results and found that all seven joints were stable and well behaved using this model. Now that we had a stable model we needed to verify its accuracy. The non-linear model is shown in Figure 2.5.

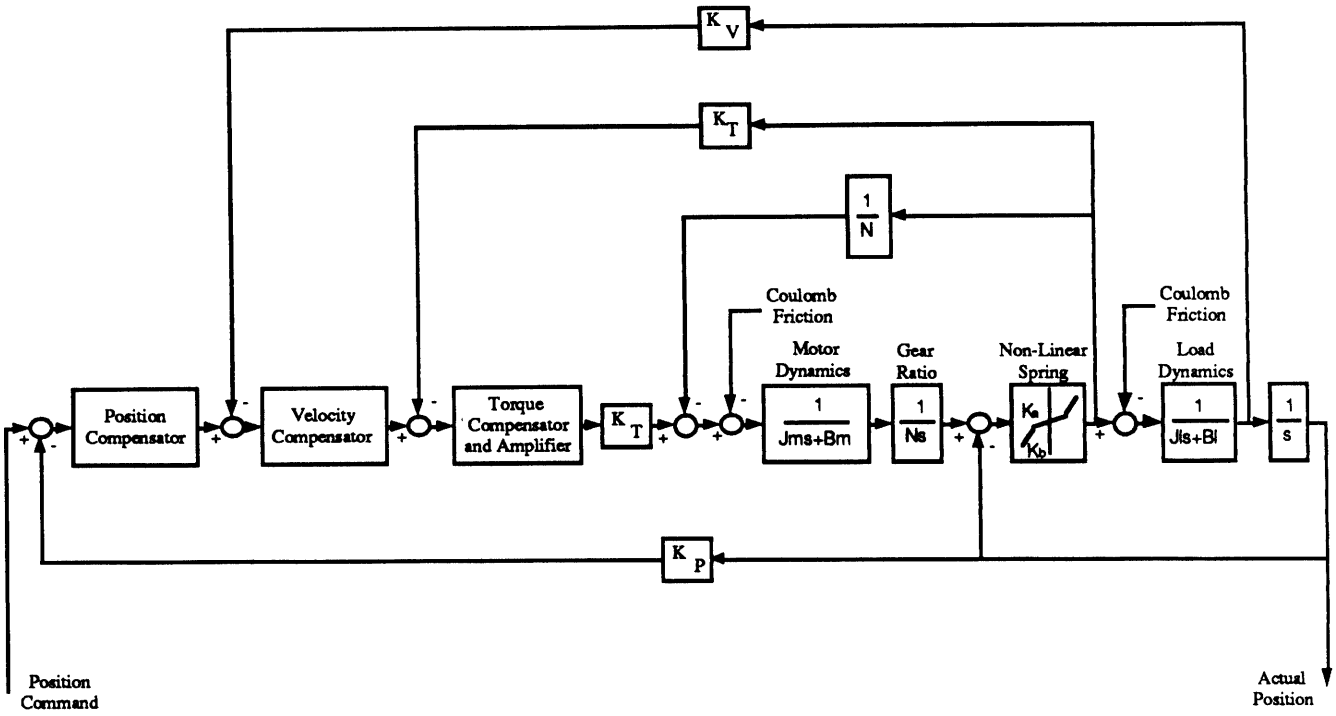

Figure 2.5 Non-linear Model of Typical Joint

2.2.3 Testing

The next step was to obtain actual experimental data from the RRC arm which we could compare to our model's predictions. To do this, we first designed a test plan which would yield results we could correlate to our model. Since our model represents only one single degree of freedom, all of the tests were run on only one joint with the others commanded to zero. The robot was always placed in a configuration such that the tested joint's motion would be in the horizontal plane, in order to keep the load inertia from changing during motion. The joint inertia for the model was calculated based on the testing configuration and it consisted of the equivalent inertia of all of the joints on the distal (outboard) side of the joint being tested. Also, the test configurations were chosen in order to minimize any dynamic interactions between the joints. This was accomplished, as much as possible, by keeping the tested joint's rotation perpendicular to all other joints' axes of rotation.

The experimental data compares favorably with the simulation results, although there are some differences. The comparisons for the elbow roll and wrist pitch joints are shown in Figures 2.6 and 2.7. The simulation results have the same rough shape as the experimental data but there are still discrepancies. Performing parameter studies of our position control model enabled us to evaluate the simulation's sensitivity to the various modelling quantities. This was done by choosing a confidence interval for each parameter, within which we believed the true value to lie. The simulation results were examined to see if their outcome was strongly affected by changing the parameter within this interval.

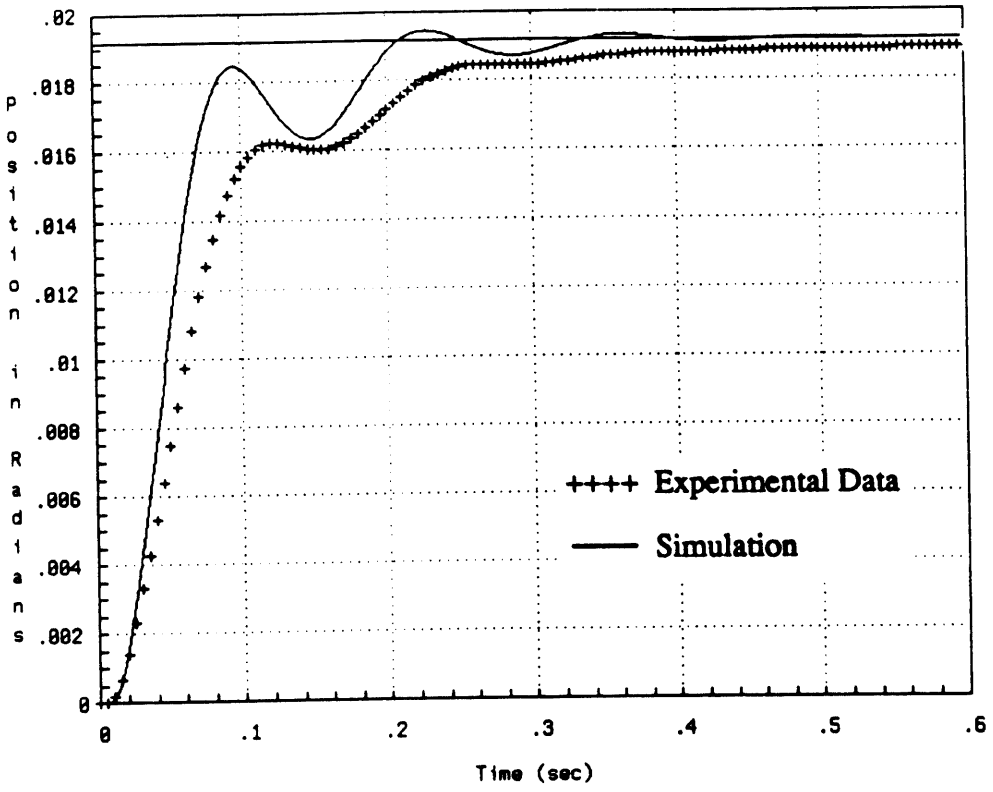

Figure 2.6 Step Response for Elbow Roll – Non-linear Model

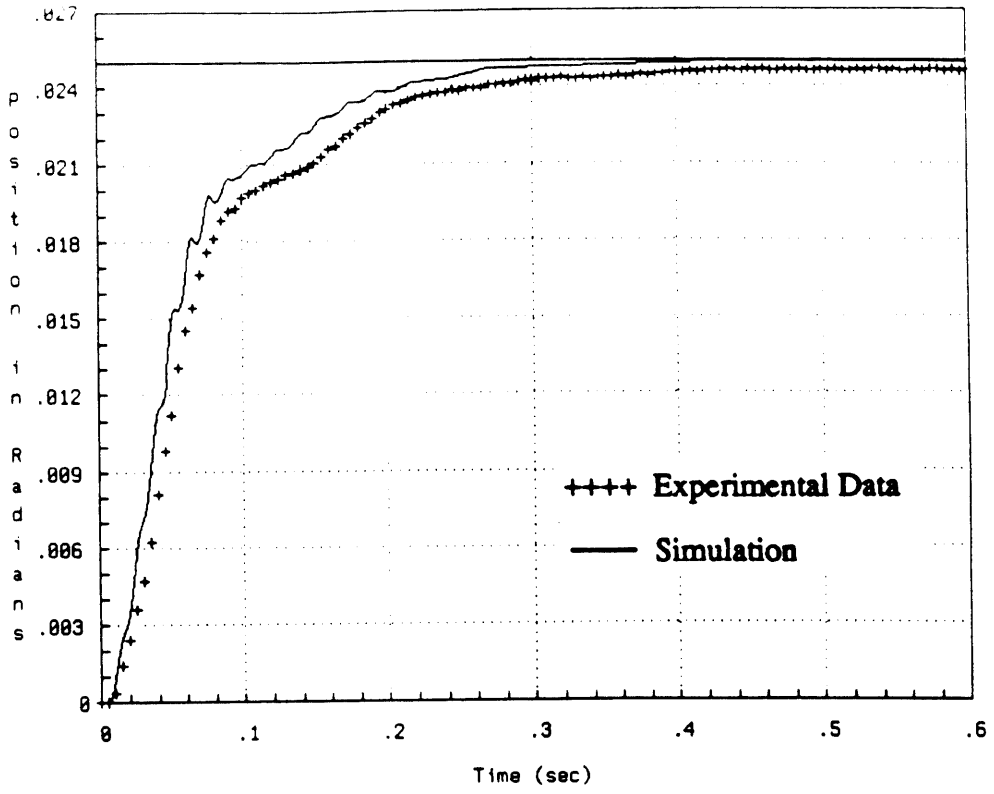

Figure 2.7 Step Response for Wrist Pitch – Non-linear Model

The results showed, as expected, that our position control simulation was most sensitive to the parameters in the outer loop, that is the position feedback and compensator gains. For the joints closer in to the base (shoulder roll and pitch, elbow roll and pitch) the effective joint inertias are significant with respect to the motor inertias so their values are also important. For the outer joints (wrist roll and pitch, tool plate roll) the motor inertia dominates so the joint inertia becomes less significant. The value of the motor rotor inertia also affects the results considerably for all the joints. The position control simulation is not particularly sensitive to values of either the motor or joint viscous damping and, although it was important to include the Coulomb friction in the model, changing its value up to an order of magnitude does not affect the results significantly.

2.2.4 Model Improvements

With regard to the reported compensator gains, the simulation output is affected considerably for values within the confidence range. Based on this knowledge we obtained

more accurate estimates of their values and subsequently improved our results substantially. Figure 2.8 shows simulation and experimental results for the tool plate roll with old and new values for the position compensator gain. Possible inaccuracies in the reported joint inertias also affect the simulation for the inner (shoulder and elbow) joints and we have not yet been able to refine their values.

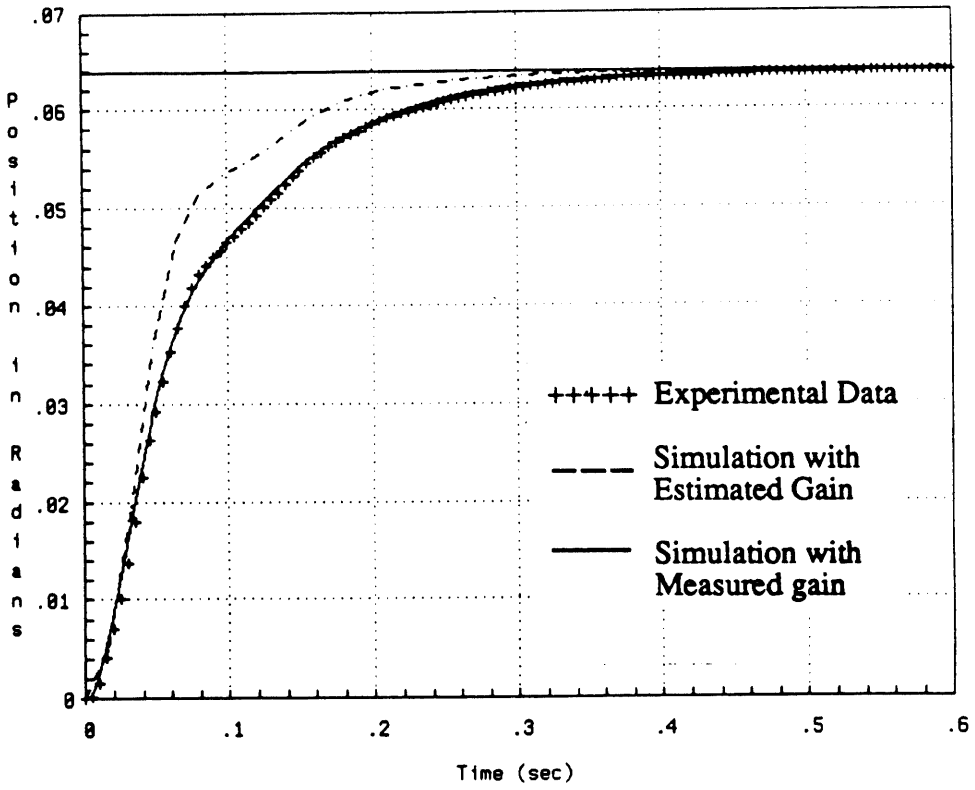

Figure 2.8 Comparison of Step Responses for Toolplate Roll – Non-linear Model

2.3 Force Control Model

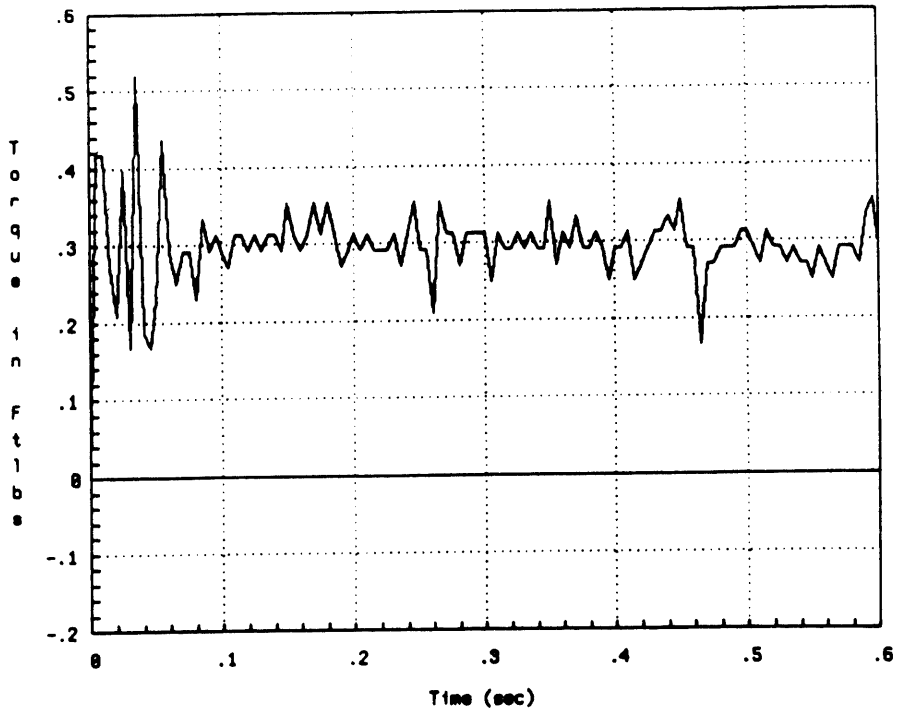

Figure 2.9 Transmission Torque Data for Toolplate Roll – Experimental Results

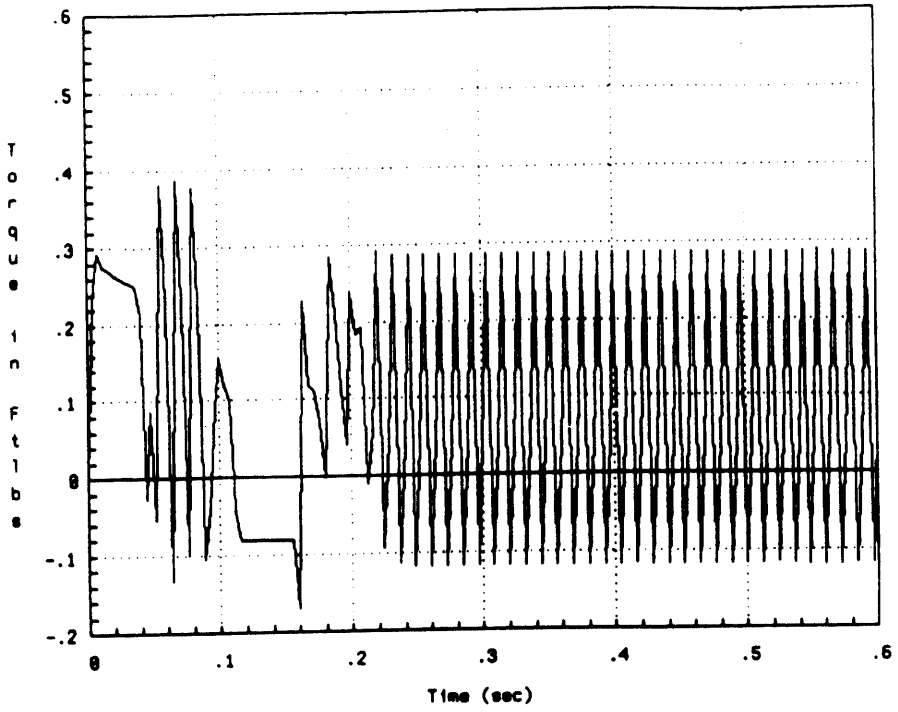

Figure 2.10 Transmission Torque Data for Toolplate Roll – Simulation Results

The next step was to try to extend the position control model into the force/torque control domain. Initially, this simply involved comparing the simulated motor current and torque output of the joint to the experimental data under position control. To build a suitable model for force control, it is important to verify that the simulated and experimental torque output of the drive correspond closely. Similarly, the motor current has a strong influence on the motor torque, which is also significant in predicting force control performance. Figure 2.9 and 2.10 show simulation and experimental torque outputs for toolplate roll and as it can be seen there are significant differences. Further research into the cause of these discrepancies has been performed and important elements were found to be missing in the model. Two of these effects are current and voltage limits in the amplifier which dictate the maximum capabilities of the amplifier. The simple and revised models for the amplifier and motor are shown in Figures 2.11 and 2.12. The results obtained using the new model are shown in Figure 2.13. As you can see, the revised model provides simulation results that better correlate to the experimental data. The noise in the experimental data is due to the fact that we were making very small moves, and thus the torques produced were small (i.e. near the resolution of the torque sensor). Sundaram [17] presents more research into improving the model for torque control as well as modelling and developing torque control strategies in general.

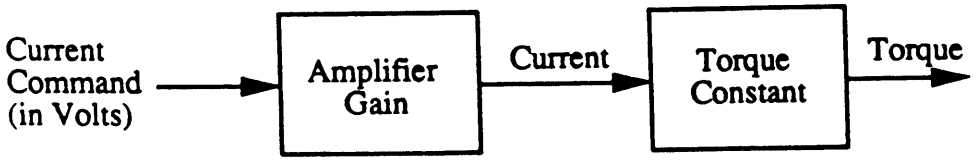

Figure 2.11 Simple Model of Amplifier and Motor

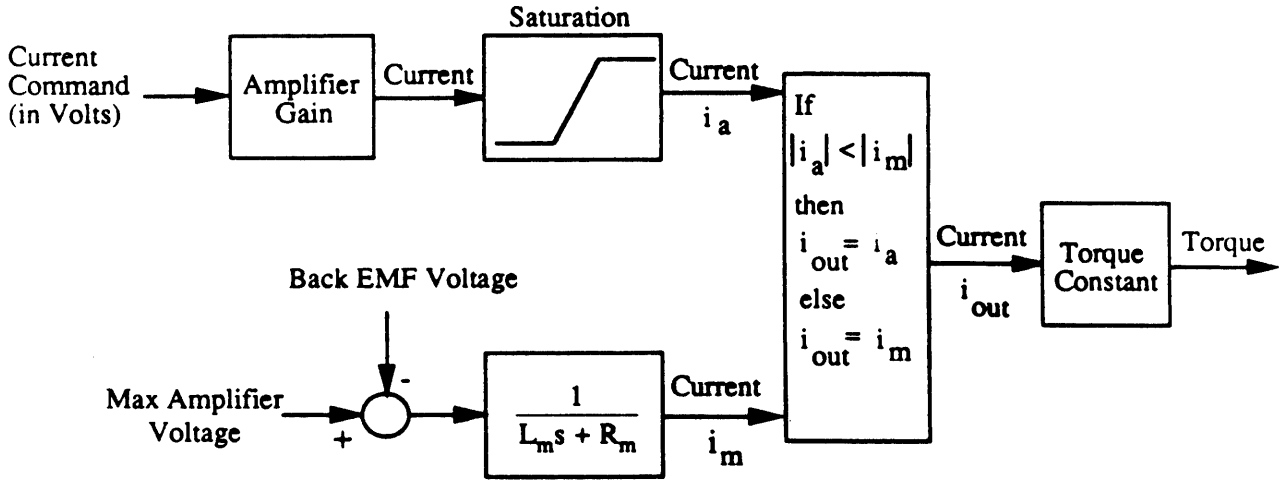

Figure 2.12 Revised Model of Amplifier and Motor

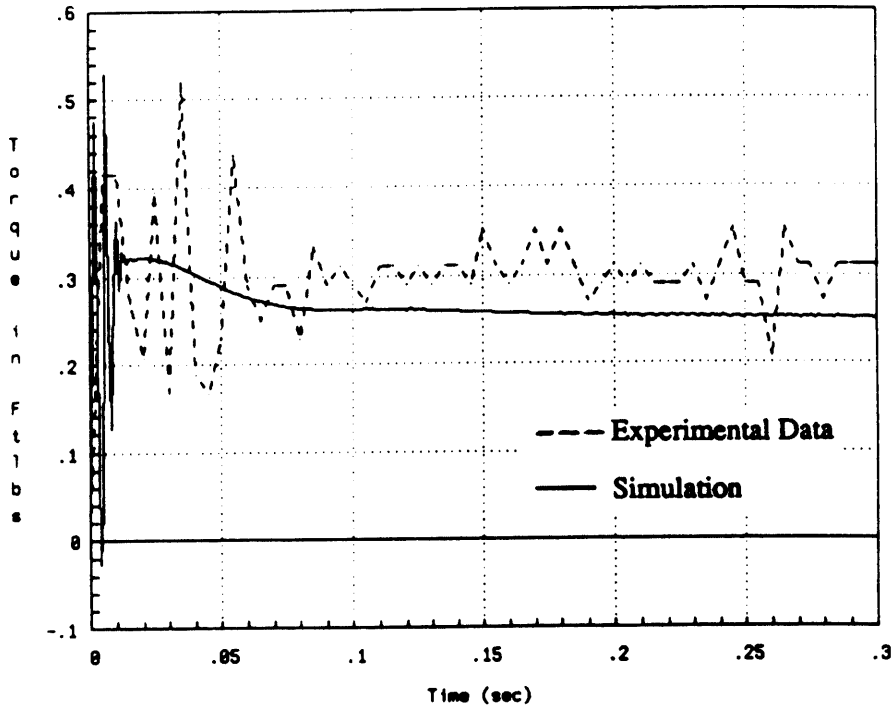

Figure 2.13 Transmission Torque Data for Toolplate Roll – Revised Motor/Amp Model

Chapter 3: Robot Design

This chapter details the design and construction of the PHD. It begins with a discussion of the motivation for the robot and the selection of the various attributes of the design. Then the mechanical configuration of the robot is shown in detail. Finally, the wiring and computer control issues associated with the robot are discussed.

3.1 Motivation/Goal

The primary goal of the PHD was to produce a research tool which could be used to research joint torque control strategies. In order to achieve joint torque control each axis is equipped with a sensor measuring the torque across that joint. This allows us to explore different methods of using torque feedback to control the endpoint force. A secondary goal of the PHD was to be able to research the performance characteristics of the Harmonic Drive. The overall design was aimed at satisfying both of these goals.

3.2 Attributes

In the design of any robot, there are many decisions which must be made and usually these decisions are made to satisfy the constraints posed on the problem. There were several constraints initially imposed on the design of the PHD. Some of these were dictated by us and others were inherent in the design goals. The first important choice we made was that the robot would be planar. Since many force control schemes have been demonstrated with moderate success on single degrees of freedom systems, we felt a one axis system was overly simple. Alternatively, very few schemes have been successful in achieving useful

force control on systems with multiple degrees of freedom. Therefore we chose to go with a multiple degree of freedom robot. We did not feel it was necessary to build a six (or more) degree of freedom arm, but that a three degree of freedom arm would be complex enough to develop strategies applicable to more complex systems, while not being as computationally intensive as larger systems. The choice to build a planar robot was made in order to allow the robot to accomplish simple tasks, such as planar assembly tasks (board insertion, 2-D peg in hole). Next, issues such as size, strength, and configuration had to be addressed.

3.2.1 Size

The size of a robot often is dictated by the tasks it will do. In the case of the PHD a nominal task we chose was computer board insertion. This implied that we needed a work envelope of at least a few square feet. We chose to use the 2' by 4' platform of another robot we had in the Artificial Intelligence Lab (the Cartesian robot) as a base since it was of reasonable size to perform the nominal tasks we had in mind and also since it was very rigid (well, as rigid as the 9th floor of a building built on a marsh can be). This constrained the work envelope and thus gave a rough idea of the size of the robot. Another constraint on the size came from the desire to build a stiff system, this requirement will be discussed below (section 3.2.5).

3.2.2 Joint Configuration

The joint configuration of a robot dictates what kind of motions it will be able to make and what the shape of its useful work envelope will be. The configuration for the joints (and links) of the PHD allow the robot to reach most parts of the base it is mounted on. Since the goals of the PHD were to test joint torque control and look at Harmonic Drive performance, we decided that three planar, rotary joints would be more useful than any sort of linear motion. After considering a few different configurations it became apparent that having the robot capable of folding back on itself (i.e. the tip could touch the base) was important in increasing the usable workspace. This also dictated that the links between the base and first joint and first joint and tip be about the same length. Of the several different configurations considered, the one we selected is depicted in Figure 3.1.

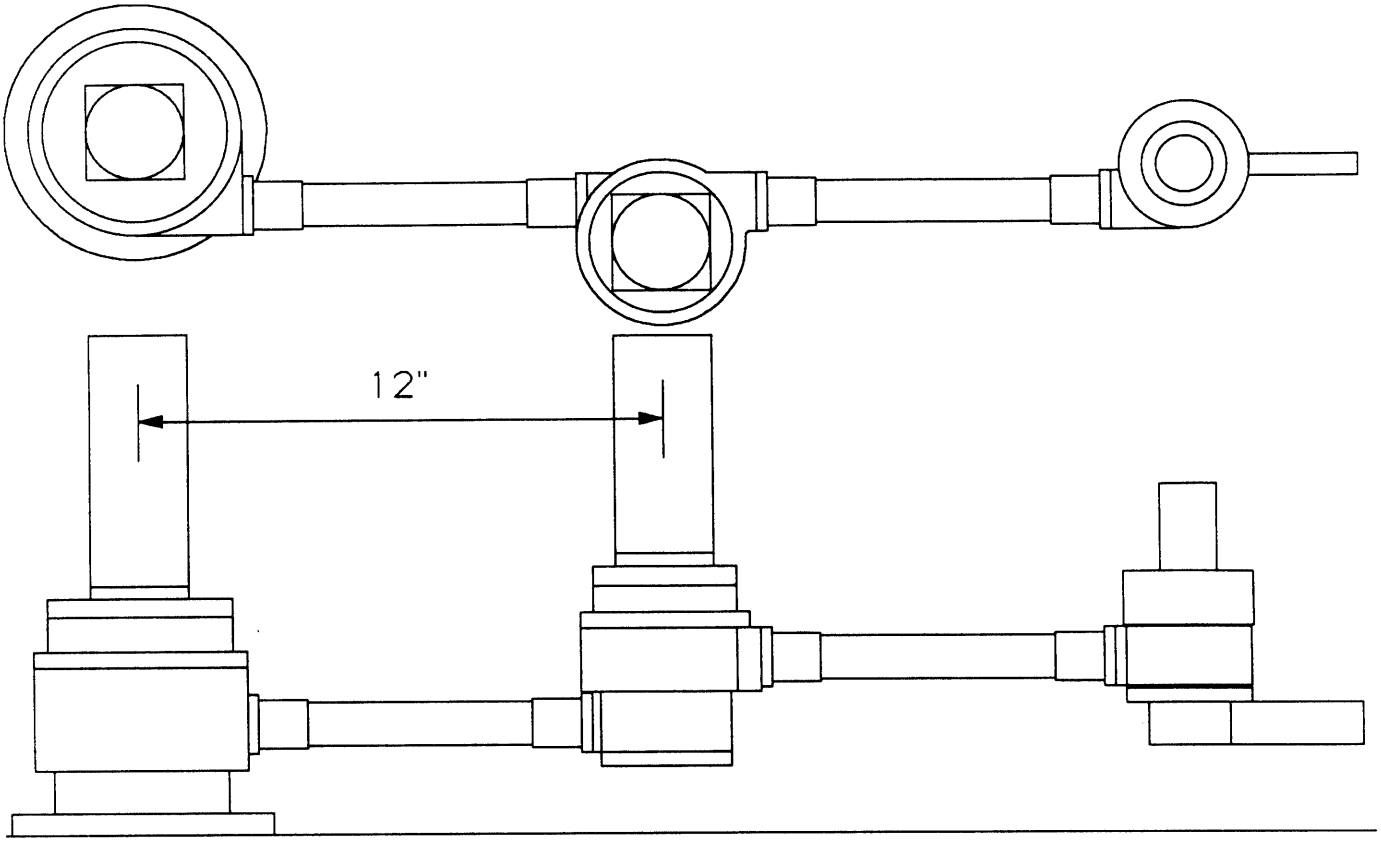

Figure 3.1 Top and Side View of the PHD Robot

The chosen configuration is an anthropomorphic design with three joints. The first joint, or shoulder, is fixed to the base and rotates 180° (it could rotate continuously, except the cables would fail). The second joint, or elbow, is just over 12" (center to center) from the shoulder. The incoming and outgoing links are connected to the elbow joint in such a manner as to allow it to rotate all the way back on itself on one side. Due to the cable routing, it can only turn halfway back on the other side, giving it a total of 270° of rotation. The final joint, or wrist, is mounted 12" from the elbow. This joint's output is a continuous rotation of its bottom plate. Currently, a 4" link is mounted as the output, but in general this plate serves as the mounting point for any end effector. An outline illustrating the PHD's work envelope is shown in Figure 3.2.

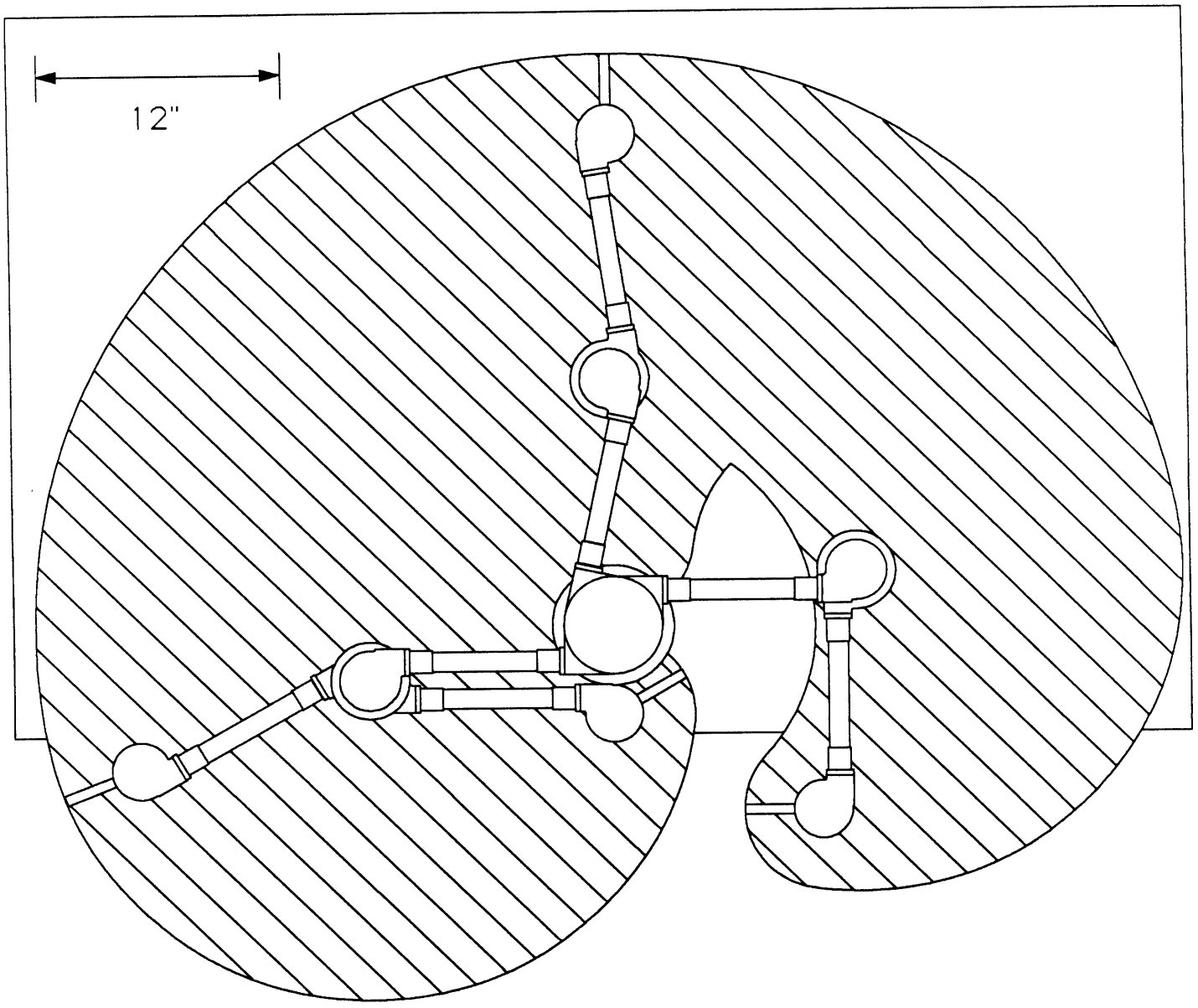

Figure 3.2 Work Envelope of the PHD Robot

3.2.3 Modularity

One feature that we tried to include in the design was modularity. Each joint is a separate unit and it is relatively easy to disconnect a joint and run it alone. There are three links, the first between the shoulder and elbow, the second between the elbow and wrist and

the third serving as the end effector. The ends of first two links are identical so the joints can be swapped into different configurations. For example, the elbow joint could be eliminated, producing a simpler two degree of freedom system. Alternatively, the design for the elbow could be reproduced with the same size Harmonic Drive but a different gear ratio and motor giving a four joint arm to experiment with. Also, the joints can be turned 90° so the robot no longer has simple planar motion. One final feature is that the links can be changed with relative ease, so the robot could be used to explore the advantages and disadvantages of different ratios of inner link length to outer link length. The only limiting factor here is the length of the cables, which was chosen to suit the current configuration.

3.2.4 Power/Strength

The PHD's strength was chosen so as to be appropriate for a typical task. As mentioned earlier, a typical force control task we would be interested in would be inserting a computer card into a cage. Roughly speaking the nominal force needed to complete such a task is about 5 lbs., so we decided a continuous force of 10 lbs. as the spec for minimum linear force output at the endpoint. The actual capabilities of the PHD are somewhat higher, in order to provide some adaptability if the configuration is changed. Each joint is powered by a brushed D.C. motor driving a Harmonic Drive gear reducer. The H.D.'s were all purchased as backlash free units in order to give the robot improved performance and added stiffness.

3.2.5 Natural Frequency

The final important characteristic of the robot is its natural frequency of vibration. As stated earlier, the first mode of vibration of the system is dominant in determining the achievable bandwidth of the system. In order to obtain an estimate of the lowest natural frequency of the robot we can use a convenient formula relating endpoint deflection to natural frequency. This formula is based on a simple model of a mass at the end of a cantilever beam suspended in a gravity field as shown in Figure 3.3.

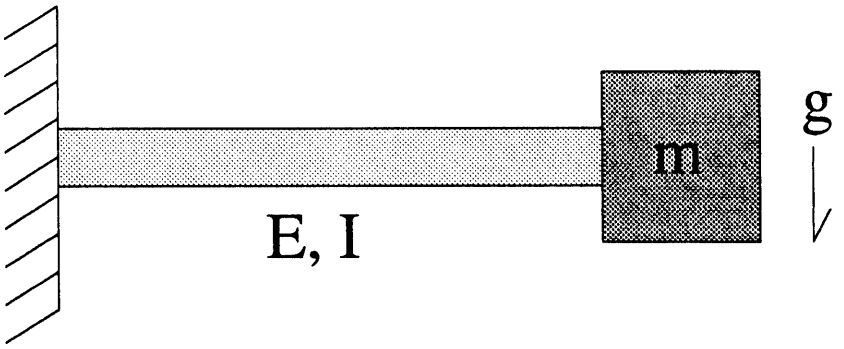

Figure 3.3 Cantilever with Suspended Load

To derive this relationship for the natural frequency of this system we start first with the formula for the deflection, ∂, of a simple cantilevered beam with a load at its tip (see Blevins [2]).

$$\partial = \frac{PL^3}{3EI} \tag{3.1}$$

where

$$P = mg \tag{3.2}$$

This formula assumes that the mass of the beam is negligible in comparison to the end load. Now that the tip deflection is known, the equivalent spring constant for the beam, K, can be expressed as

$$K = \frac{P}{\partial} = \frac{mg}{\partial} \tag{3.3}$$

A reasonable (first order) approximation of the natural frequency (in Hz.) of this beam is given by

$$f = \frac{1}{2\pi}\sqrt{\frac{K}{m}} \tag{3.4}$$

and by substituting equation 3.3 for K in this expression we find

$$f = \frac{1}{2\pi}\sqrt{\frac{g}{\partial}} \tag{3.5}$$

This gives a convenient relationship between endpoint deflection and natural frequency. It can be shown that this formula is also a good approximation for two link systems, as long as the joints are of the same relative stiffness. Some work showing this was done by Christian [3]. For a system such as the PHD we must analyze each joint as if the robot was hanging sideways, so that gravity would cause the joints to sag. By knowing the stiffness of the joints, the total amount of endpoint sag can be predicted, and thus a reasonable prediction for the natural frequency can be obtained.

For our robot we wanted to push this frequency as high as possible. This meant building a system as stiff as possible (or minimizing the endpoint deflection). After evaluating the different elements of the system it became evident that the torque sensor and the Harmonic Drive were the most flexible elements in the drive system. All the other elements could be made comparatively stiff. Since we were designing the torque sensor ourselves (see section 3.3.2), we chose to make it significantly stiffer than the H.D. For the H.D., there was little we could do about the stiffness, so it became the deciding factor in determining the first mode of vibration of the robot. Using the method discussed above, the predicted natural frequency for the robot in a fully extended configuration is around 22 Hertz.

3.3 Mechanical Configuration

An isometric drawing of the PHD is shown in Figure 3.4. It decomposes into six basic parts; the shoulder joint, the first link, the elbow joint, the second link, the wrist and the output link or end effector. The design of the three joints of the PHD are very similar. The shoulder and elbow joints are almost identical except for their size, and the wrist is slightly different due to the desire for continuous rotation at the output. The joints were designed to be as light and compact as possible. All the machined parts of the joints (everything except the H.D. and motor) are made from aluminum. To provide sufficient stiffness, the links were made out of steel tubing silver soldered into two (steel) end caps which are then bolted onto the joint. The joints decompose easily into two parts, the joint housing and the drivetrain.

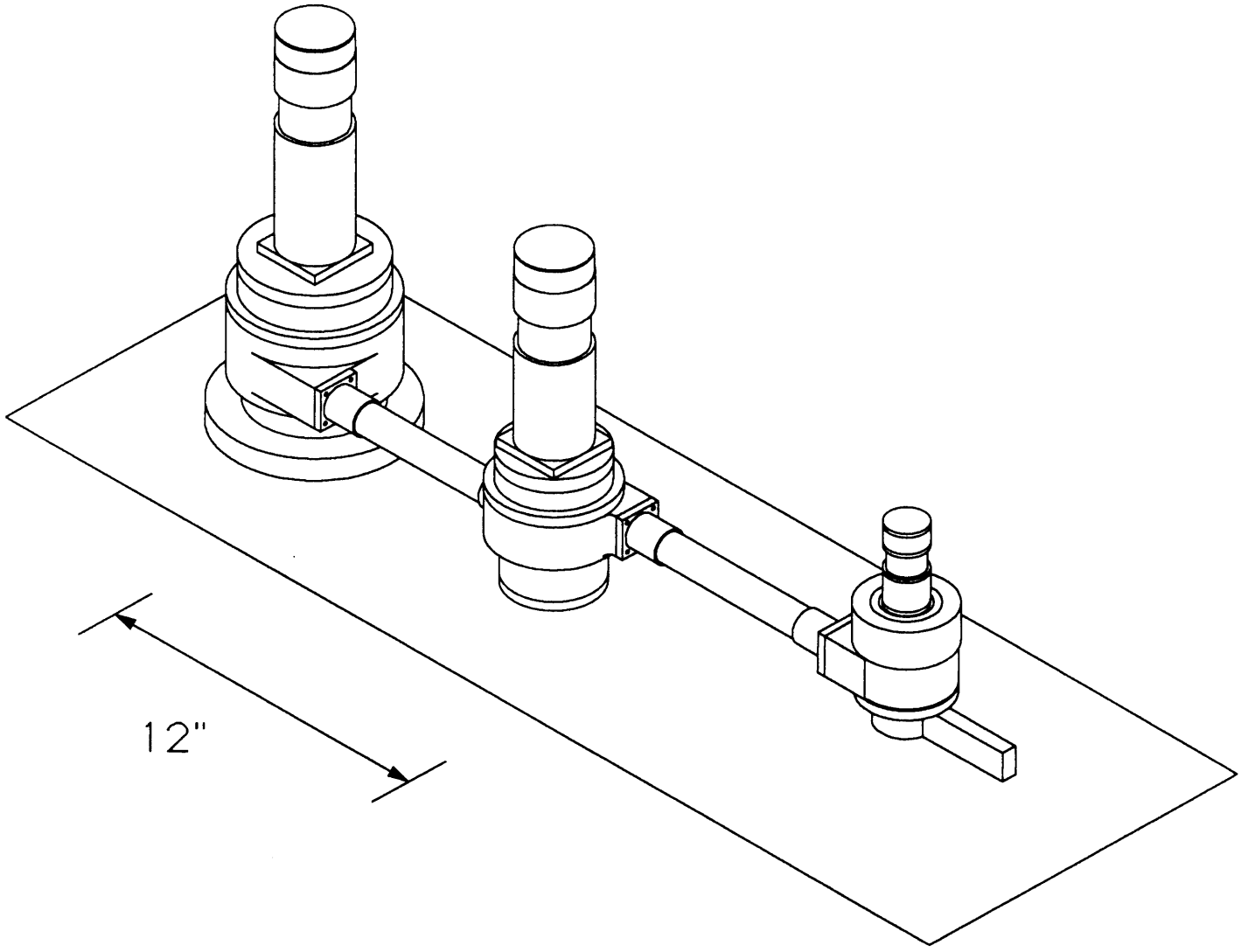

Figure 3.4 Isometric View of the PHD Robot

3.3.1 Joint Housing

The joint housing consists of an inner cylinder and an outer cylinder separated by bearings to allow them to rotate with respect to each other. A cross sectional view of the elbow joint housing is shown in Figure 3.5a and the wrist in Figure 3.5b (both joints are shown without the drivetrain). The bearings are thin section angular contact bearings mounted back to back to achieve the maximum moment load capabilities. The bearings are

pressed into the outer cylinder and then slipped over the inner cylinder. They are held in place between a lip on the bottom of the outer cylinder and its cover (the top plate), which is bolted into the cylinder on its top face. Then the cover on the top of the inner cylinder is used to preload the bearings enough to remove all backlash. There is also a bottom plate on the inner cylinder which forms the base on the shoulder, the input or base on the elbow, and the output rotation on the wrist. Finally, the links are bolted into the sides of the cylinders.

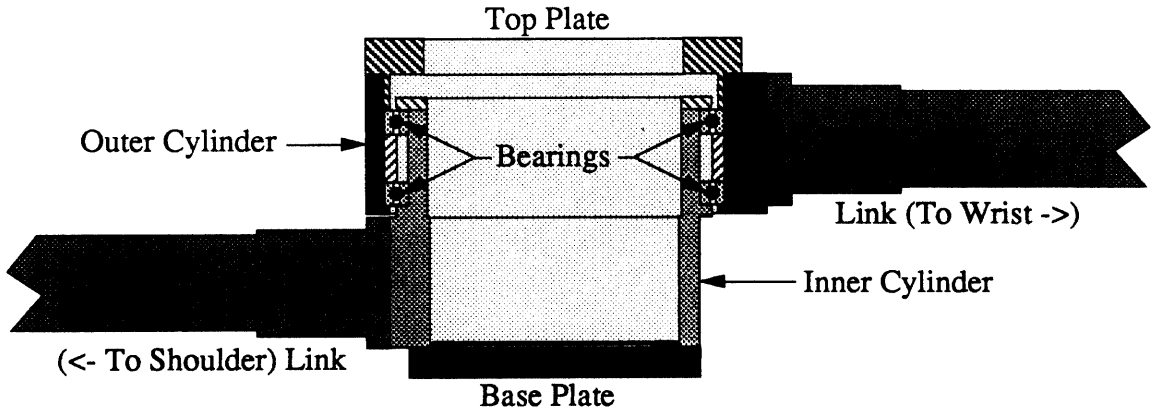

Figure 3.5a Cross Section of Elbow Joint Housing

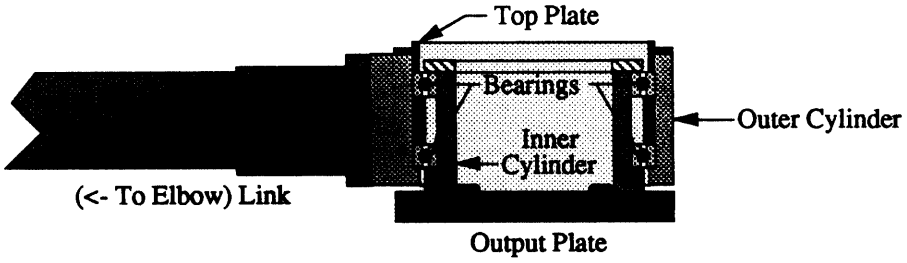

Figure 3.5b Cross Section of Wrist Joint Housing

3.3.2 Drivetrain

The drivetrain consists of three main parts: the motor, the Harmonic Drive and the torque sensor. A cross section of the drivetrain for the shoulder and elbow joints is illustrated in Figure 3.6a and the wrist is shown in Figure 3.6b. The motors for all three

joints are brushed D.C. servomotors. The first two are Aerotech permanent magnet motors with integral tachometers (see Appendix B for hardware specifications), and the third is a Clifton Precision samarium cobalt magnet motor without a tachometer. All three motors have Hewlett Packard optical encoders to allow motor position feedback. The motor case is mounted to an adapter plate which also holds the Harmonic Drive circular spline. The motor rotor then spins with the H.D. wave generator. This, in turn, causes the flexspline to turn relative to the circular spline (at the motor speed divided by the gear ratio). On the shoulder and elbow the torque sensor is bolted to the flexspline output. For the wrist, the torque sensor is mounted to the circular spline as shown in Figure 3.6b. This is done so that the torque sensor rotates with the input instead of the output, and therefore the joint can rotate continuously without worrying about the torque sensor cable winding up.

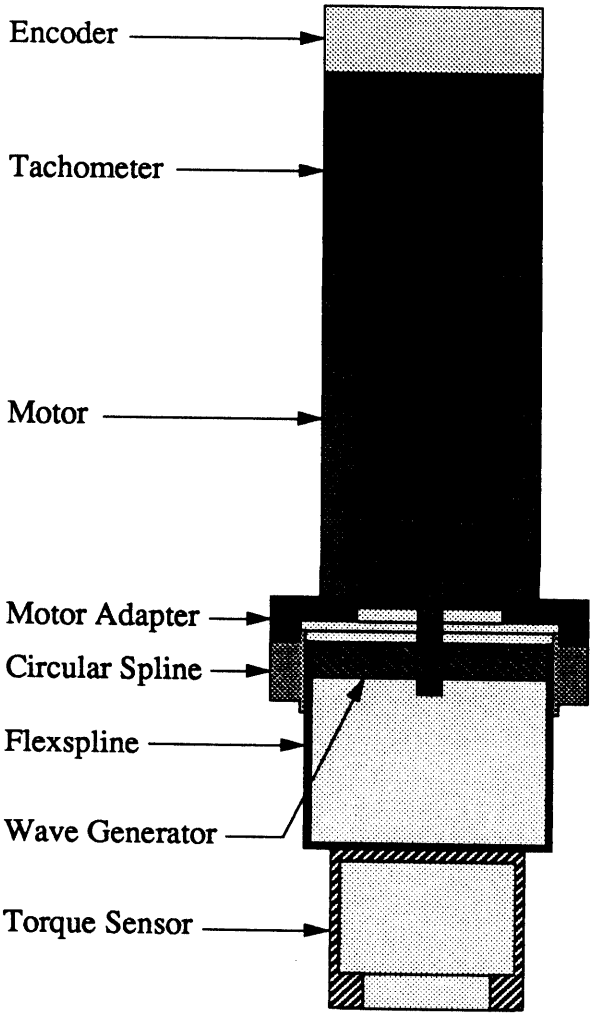

Figure 3.6a Cross Section of Elbow Drivetrain

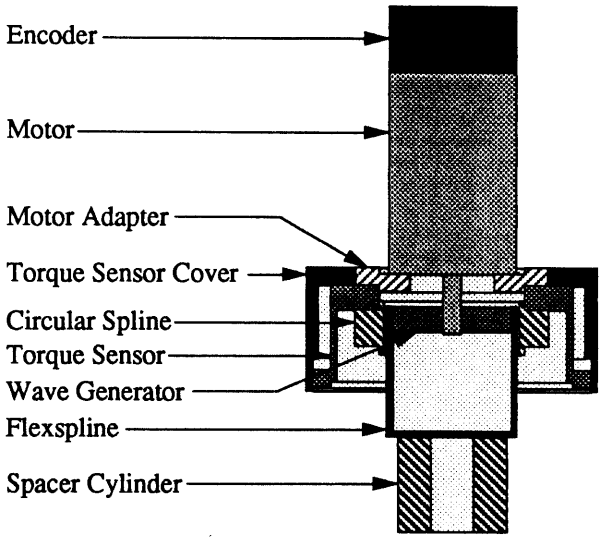

Figure 3.6b Cross Section of Wrist Drivetrain

The drivetrain and joint housing can be are assembled separately and then mounted together. The drivetrain is placed inside the joint housing and the bottom of the torque sensor is bolted to the base plate on the bottom of the inner cylinder. Next, the circular spline and motor adapter plate are bolted to the top of the outer cylinder. The relative motion of the circular spline and flexspline then causes the joint to rotate. A cross section of the assembled joints are shown in Figures 3.7a and 3.7b.

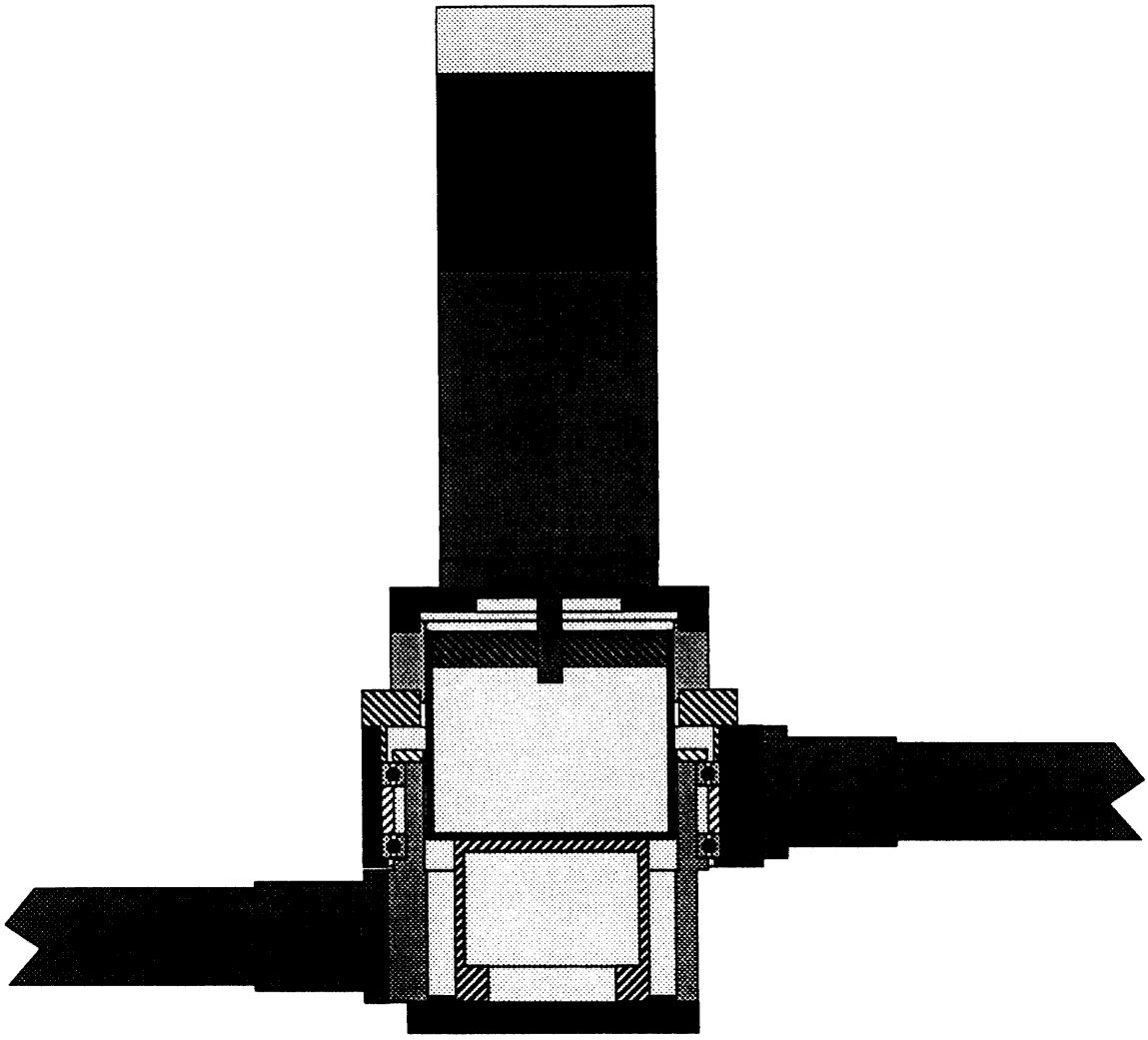

Figure 3.7a Cross Section of Assembled Elbow Joint

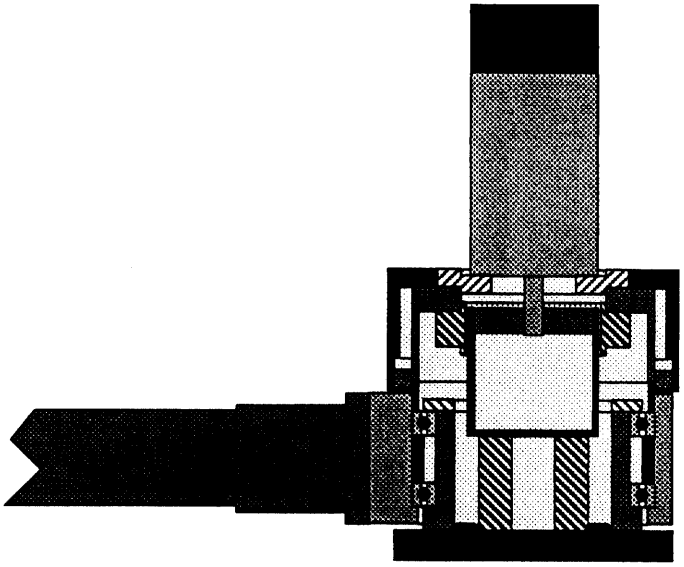

Figure 3.7b Cross Section of Assembled Wrist Joint

Harmonic Drive/Motor Selection

The choice of motor and Harmonic Drive is an important factor in determining the performance characteristics of the robot. The motor and gear ratio combine to determine the speed with which the system can react. Additionally, as discussed above, the Harmonic Drive provides the majority of the flexibility in the system, so this decision must be considered carefully. Many different motor and reducer sets were considered using a spread sheet to analyze the different combinations, as shown in Appendix D.

Selecting the Harmonic Drive was the first consideration. Harmonic Drives are available in a range of models (sizes) and then each model is available in a variety of gear reductions. The output rotational stiffness of the drive depends solely on the model and not on the reduction (the input stiffness is influenced by the ratio chosen). Since we were concerned about keeping the first mode of the system as high as possible we wanted to choose the stiffest drive possible, which meant choosing as large of a Harmonic Drive as possible. Since the largest drive is 13" in diameter we decided on a more moderate size which could be accommodated in our design.

The next decision was to choose an appropriate reduction, but this had to be done in conjunction with selecting the motor. The method we used for doing this was to first identify

an appropriate set of motors for each joint representing a range of different torque, speed and weight characteristics. These were then entered into a spread sheet and paired with different H.D. ratios to select drives for each joint. It is important to have comparably powered drives for each joint so that one of the joints is not overpowered or underpowered with respect to the others. The final motor and Harmonic Drive selections are documented in Table 3.1. These combinations provide a maximum linear output force of around 30 lbs. with the arm at full extension.

Joint	Motor	Harmonic Drive
Shoulder	Aerotech 1035DC	Model 1M-160 Reduction
Elbow	Aerotech 1017DC	Model 3C-160 Reduction
Wrist	Clifton SmCo AS-780	Model 1C-80 Reduction

Table 3.1 Motor/Drive Choices

Torque Sensor Design

As the PHD's design evolved, the design of the torque sensor became a major part of the joint design. Initially, we examined several commercially produced sensors but soon decided that they would be difficult to integrate easily into the design. Additionally, these sensors are expensive and most are not as stiff as we desired. Therefore, we concluded that we would design and build our own strain gage based torque sensor. This decision had a significant influence on the design as it allowed us to locate the sensor where we wanted and also choose its stiffness. We chose to use a strain gage bridge mounted on a cylindrical sensor to measure torque across the joint as shown in Figure 3.8. This design prevented us from increasing the sensor stiffness arbitrarily since too stiff of a sensor would not provide enough strain for the gages to measure. There is an intricate coupling between the physical dimensions of the sensor, its stiffness and the sensitivity of its readings. We decided that we desired the stiffness of the sensor to be about an order of magnitude higher than the Harmonic Drive for that joint. This would keep the sensor from significantly affecting the joint stiffness and lowering the system bandwidth.

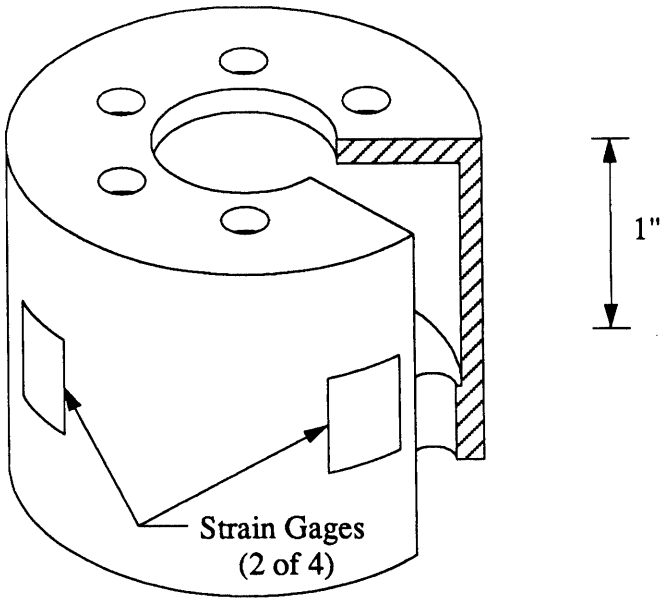

Figure 3.8 Design for the Shoulder Torque Sensor

The location for the sensor was chosen to accommodate the joint design. In the shoulder and elbow designs, the sensor is placed between the H.D. flexspline and the base plate on the joint. This allows it to measure the torque acting across the joint. In the wrist the location is slightly different in order to allow continuous joint rotation. The wrist sensor is mounted between the circular spline and the joint housing. This allows us to still measure the torque across the joint but at the other end of the drivetrain.

As mentioned, the dimensions of the sensor were chosen so that the sensor would be about an order of magnitude stiffer than the H.D. It was important to verify that we could accomplish this while still having enough strain in the sensor to allow the strain gages to measure accurately. The basic approach was as follows. First the sensor was modelled as a tube in torsion whose angular deflection, Θ, is given by

$$\Theta = \frac{TL}{GI_p} \tag{3.6}$$

where T is the torque acting on the tube, L is the length of the tube, G is the shear modulus of elasticity and I_p is the polar moment of inertia of the tube. Solving this for the rotational stiffness, K_θ, we get

$$K_\theta = \frac{T}{\Theta} = \frac{GI_p}{L} \tag{3.7}$$

Since the length was roughly fixed by the design, this gives us the required polar moment of inertia for the sensor. The outer diameter (D_o) was selected to be as large as physically possible to allow the maximum strain for a given torque and stiffness. Given the O.D. of the sensor the inner diameter (D_i) can be found using the following formula for the polar moment of inertia of the cylinder

$$I_p = \frac{\pi}{32}\left(D_o - D_i\right) \tag{3.8}$$

Next, it was necessary to verify that the stress on the sensor was within the limits for the chosen material (aluminum). This was done by calculating the stress on the outside surface while the joint was exerting its maximum torque. The formula used for the stress, τ, is

$$\tau_{max} = \frac{T_{max} D_o}{2I_p} \tag{3.9}$$

Finally, it was important to verify that the strain on the outer surface was large enough to be measured using a conventional strain gage bridge. The gages are mounted on the outer surface and measuring strain in the 45° direction, so the formula for the strain, ε, is

$$\varepsilon_{max} = \frac{\tau_{max}}{E}(1 + \nu) = \frac{T_{max} D_o}{2EI_p}(1 + \nu) \tag{3.10}$$

where E is the modulus of elasticity and ν is Poisson's ratio for the material.

Finally, it must be verified that this strain will produce a reasonable voltage difference using a Wheatstone bridge configuration. The gages we chose have two opposing 45° resistances with one common terminal as shown in Figure 3.9. Four of these gages were mounted at 90° increments on the cylinder and wired as shown in Figure 3.10. Each leg of the bridge had two 350Ω resistances in series. Mounting the gages at 90° increments on the cylinder surface (see Figure 3.8) minimizes any bending strain that may occur in the torque sensor.

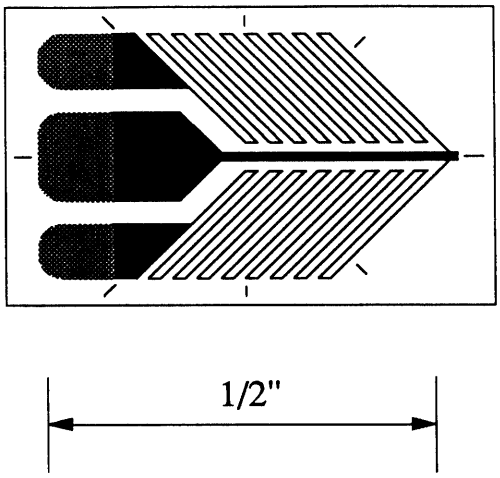

Figure 3.9 Strain Gage

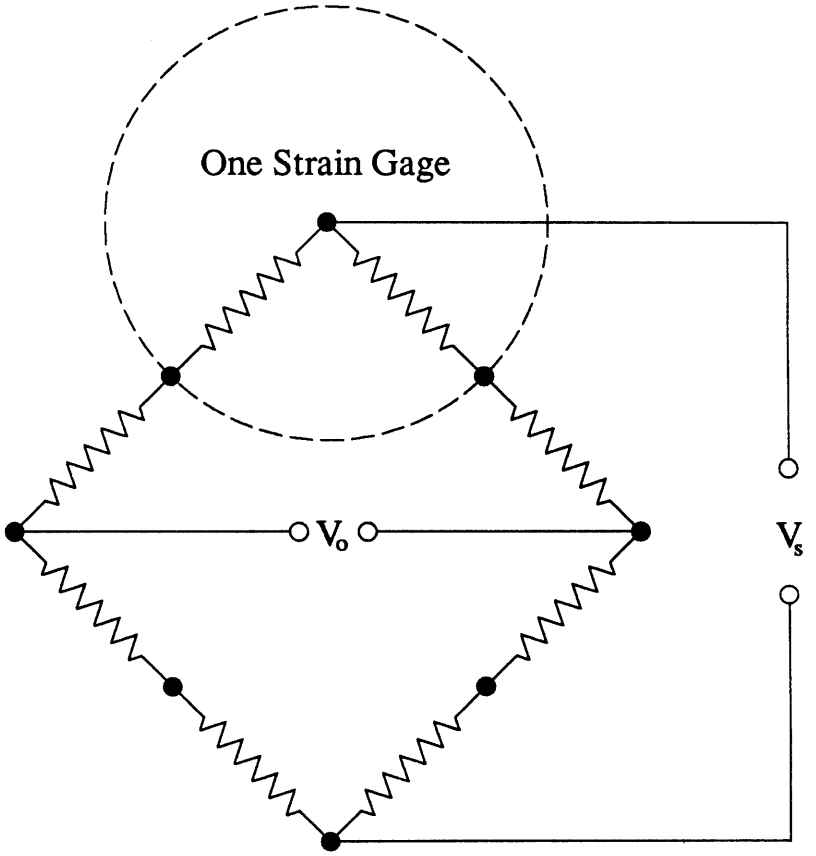

Figure 3.10 Layout for Strain Gage Wiring

The formula relating output voltage, V_o, to input voltage, V_s, is

$$V_o = \frac{V_s \Delta R}{R} \tag{3.11}$$

Where the resistance change, ΔR, is related to the strain by the gage factor, γ, as

$$\gamma = \frac{\Delta R/R}{\Delta L/L} = \frac{\Delta R/R}{\varepsilon} \tag{3.12}$$

This factor, γ, is dependent on the composition of the gage which is chosen to closely match the thermal properties of the material it is being mounted on. If the gage and sensor material have similar coefficients of thermal expansion then the effect of strain due to temperature changes will be minimal. Temperature changes will affect the gage resistance slightly, but having a four (or eight) gage Wheatstone bridge minimizes these effects. Therefore, for this configuration the formula that relates the strain to the output voltage is

$$V_o = \varepsilon \gamma V_s \tag{3.13}$$

and the maximum output voltage of the sensor is

$$V_{o,\,max} = \frac{\gamma V_s T_{max} D_o}{2EI_p}(1 + \nu) \tag{3.14}$$

This voltage must be high enough to be transmitted to the electronics box where it is amplified. This location was chosen over an earlier idea of placing the amplifier on board the joint, due to packaging and noise problems. In Appendix A, the final design for the sensors are shown along with their important characteristics, such as maximum strain and sensor voltage levels.

The formulas for the strain gages were applied iteratively until a combination was found that satisfied the stiffness requirement with acceptable strain sensitivity. This method worked for the shoulder and elbow gages but the wall thickness for the wrist sensor was too thin (1/64") to be robust. The design for the wrist sensor was modified by removing the wall completely in some spots, leaving six posts where the gages are mounted. The wrist torque sensor is shown in Figure 3.11.

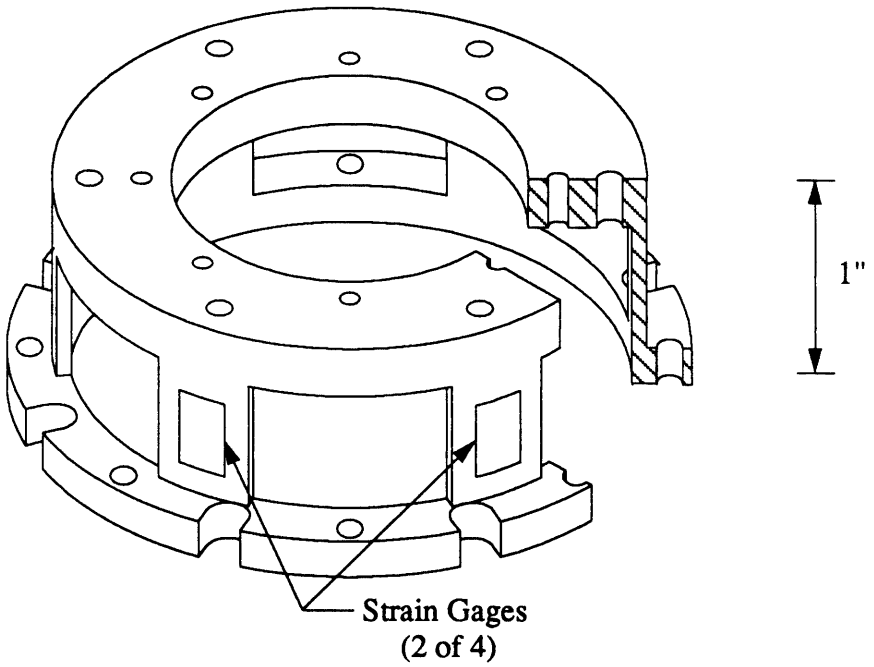

Figure 3.11 Isometric Drawing of Wrist Torque Sensor

3.3.3 Shoulder Position Sensor

One additional component was added to the design to accommodate the goal of testing the Harmonic Drive. This is an extra encoder mounted on the outside of the shoulder to allow direct measurement of the joint position. This encoder will provide us with the joint position or position of the H.D. output whereas the motor encoder measures the motor position or position of the H.D. input. Therefore, we can monitor position on both sides of the Harmonic Drive. This data, in conjunction with the torque sensor data will allow us to gather data on the H.D. and determine its important dynamic properties.

The extra encoder body is a 2500 line optical encoder mounted to the base of the shoulder. It is driven through a large diameter (6") precision gear which meshes with a smaller gear mounted on the encoder shaft. The smaller gear is an anti-backlash gear to prevent slip between the two gears. The pair of gears give a reduction of eight yielding a net resolution of 20,000 counts/joint revolution, which is about one-eighth as good as the motor encoder (1000 counts/motor revolution = 160,000 counts/joint revolution).

3.4 Computer Considerations

A significant part of any robot is the computer hardware and software used to control the system. For the PHD, this system consists of four main components: a computer rack, an amplifier rack, and two junction boxes located near the robot base. The computer rack is where all the data processing and control takes place. The amplifier rack is where the motor amplifiers are located as well as the power supply for the torque sensors. Finally, there are two junction boxes, a "motor box" and an "electronics box". The motor box provides a junction point between the cables running from the amplifier rack and those running to the motors. The electronics box provides junctions for all of the other cables as well as space for electronics to filter and amplify the strain gage signals coming from the torque sensors. The reason for two boxes was to shield the low level torque sensor signal and electronics from the motor power.

The computer system being used was originally chosen and integrated by Andrew Christian, and gratefully, it was his effort that allowed us to get the PHD up and running relatively quickly. The base of the computer control system is a VMEbus card cage housing several boards including: a system controller, three single board processors, a digital to analog converter board, two analog to digital converter boards, six optical encoder reading cards, a digital I/O board and extra memory. The backplane of the VMEbus is tied directly to the backplane of a Sun 3/180 Workstation. This is a Unix based workstation used for software development, compilation, and down loading to the processors. All real time control is executed through the VME box. More detailed descriptions of the layout and capabilities of this system are given by Christian [3].

3.4.1 Cabling/Wiring

A potpourri of cables are needed to get all the signals back and forth from the robot and the racks. There are 5 cables running from the computer rack to the junction boxes, three of them are encoder/tach cables and the other two carry the torque sensor signals. Four cables run from the amplifier rack to the junction boxes, three of them are motor power and the other carries power for the torque sensors. In total, there are 11 cables running from the junction boxes to the robot. Each joint has an encoder cable, a motor power cable, and a

torque sensor cable. Then the first two joints also have another cable carrying the limit switch and tachometer signals. Since the wrist has no tach or limit switches, its connection is used for two limit switches on the edge of the base platform, to keep the robot from hitting the user in the back of the head. Another cable carries the limit switch signals from the motor box to the electronics box. Finally, there is one other cable taking the signal from the extra encoder on the shoulder directly back to the computer rack. The details of all of these cables as well as an overall wiring layout are presented in Appendix C.

3.4.2 Junction Boxes

Two junction boxes were required to re-route the signals coming from the racks to the various sensors. Additionally, they provide electronics for amplification for the strain gage signals near to the robot, so that the low level signal is not required to travel over large distances. One other purpose for the junction boxes is to provide a good location for other "fixes" that became necessary, such as "pull-up" resistors used to improve the encoder signals and a voltage divider used to keep the tach signals within the range of the A/D converters. Wiring diagrams for these boxes are also presented in Appendix C.

3.4.3 Software

The low level software system which handles board setup and communication for us is the Condor system, a computational architecture and programming environment developed at the MIT Artificial Intelligence Laboratory. The system was developed primarily by two graduate students, Sundar Narasimhan and David Siegel [11,12,13]. Condor provides convenient subroutines for handling inter-board communications as well as communication between the Sun computer and the VMEbus. It also has standard frameworks for building timed, interrupt driven servo loops running at user specified rates. The interface between the Sun and VME systems is done by a related program called Xcondor, which allows the user to send commands directly to the processor boards and monitor their actions. The effect of the Condor system is to separate the user from having to deal with issues such as getting the various boards to communicate properly and being able to communicate with them.

The program used to run the PHD is run on two of our three processors. The code is written in C and then compiled and downloaded to the boards using the Condor system. The

main processor handles the I/O from the Sun and generates commands for the joints. The commands take the form of a series of joint angle setpoints which are then used in the servo controller. The other board is the servo board which runs the servo loop, sampling all the sensors, generating a command and saving the current system status at each step. The current control strategy is a simple PD loop on the shoulder and elbow and just proportional control on the wrist. The fastest this loop can currently run the three joints is about 500 Hz but this can be improved if all the sensor data is not needed (such as in force control). Alternatively, the third processor could be used to speed up the control loop. Future research will focus on building a better control strategy or implementing some form of joint torque control using this system.

Chapter 4: Experimental Results

This chapter discusses the results of the experiments that have been performed using the PHD robot. This includes experiments to identify the important characteristics and capabilities of the system, and then tests to determine and verify an acceptable model of the Harmonic Drive gear reducer.

4.1 Capabilities

One of the first things we wanted to do with the PHD after we got it running was to determine a few of its important performance characteristics. We ran some simple tests and Table 4.1 shows some of the measured capabilities of the robot.

Capabilities of the PHD Robot	
Servoed D.O.F:	3
Max. Reach:	28.4 in.
Weight:	500 lb
Max. Shoulder Slew Rate:	130 °/sec
Max. Elbow Slew Rate:	145 °/sec
Max. Wrist Slew Rate:	450 °/sec
Max. Tip Speed (at full extension):	90 in/sec
Max. Shoulder Acceleration:	450 °/sec^2
Max. Elbow Acceleration:	975 °/sec^2
Max. Wrist Acceleration (no end effector):	15,600 °/sec^2
Max. Tip Acceleration (at full extension):	1392 in/sec^2

Table 4.1 PHD Capabilities

The main factor limiting the slew rates of the joints is the top motor speed, which is limited by our amplifiers. The maximum speed the amplifier is capable of driving the motor is 3600 RPM for the shoulder and elbow and 6000 RPM for the wrist , although the maximum speeds quoted in the motor product literature is 6000 RPM for the shoulder and elbow and 8000 RPM for the wrist. This is predominantly limited by the amplifier current and voltage limits which allow a maximum of 40 Volts and 10 Amps. The maximum acceleration and force output are determined by the current limits of the amplifiers. The motors are actually capable of taking 25 or 30 amps in order to produce their quoted peak torque.

4.2 Surprises/Problems

As with any piece of hardware several problems were encountered in getting the robot up and running. Some of the more important of these problems are discussed in the following sections.

4.2.1 Addressed

One issue that I never appreciated was the wiring of the robot. I learned the hard way that this is an issue that is best addressed early in the design process. There are signals for 8 sensors, 2 limit switches, 2 tachometers and 3 motors running between the junction boxes and the joints. I had originally planned to run the cables for the two outer joints inside of the links, but as it turned out only the tach/limit switch cables and the torque sensor cables would fit. Had I taken the time to think about the required cables, I would have made the links out of larger diameter tubing.

Another problem that came up after the robot was assembled was backlash. After the initial assembly there was a slight backlash in the shoulder joint. The cause of this backlash was determined to be the Harmonic Drive not being assembled tightly. This means that the wave generator was not pressed far enough down into the flexspline to remove all backlash. The reason for this is that as the elliptical wave generator is pressed into the round flexspline, the flexspline's walls are deflected outward. This causes the flexspline teeth to be pushed out against the circular spline teeth, removing all backlash from the drive. The solution for removing the backlash in the shoulder was to mount the wave generator further out on the motor shaft in order to make the H.D. truly backlash free. Unfortunately, this pointed out the importance of mounting the wave generator squarely onto the motor. If the wave generator is not square to the shaft, it causes a noticeable "bump" in the output as it spins. This caused us to have to redesign and re-machine the part holding the wave generator onto the motor shaft.

4.2.2 Unaddressed

There are a couple of problems that came up which we have not yet had time to repair. The first is the bearing preloading, which is not quite even. This causes the joint's velocity to vary slightly as it rotates. The cause of this problem is that the rings which preload the bearings are hand tightened in 12 places. If you tighten them down all the way it produces too much preload in the bearings (and thus too much friction). Therefore, there is a

small gap between the ring and the inner cylinder and it is nearly impossible to get an even preload. The solution to this problem would be to place a shim under the ring of the proper thickness so that the ring could be tightened down hard against it and still remain square.

Another issue we have yet to address is the servo loop speed. As it stands now we can not run our servo any faster than 500 Hertz, and in the future we may need a faster loop. The main thing slowing the loop is reading all of the sensors. This consists of having to convert 5 Digital to Analog channels (3 for the torque sensors, and 2 for the tachometer) and 4 encoder channels (two for the shoulder and one each for the elbow and wrist). There is a relatively easy fix for this problem, which is already partly underway. We have purchased another D/A card and have another microprocessor board. Ideally, the other processor board could be used to continuously sample the sensors, then the servo loop could run significantly faster.

4.3 Harmonic Drive Testing

One of the stated goals of the PHD was to research Harmonic Drive performance characteristics. Preliminary research has begun and this section presents the results obtained from that testing. It first details the testing already completed and then goes on to propose some further areas of interest for expanding and improving the model. Our initial research took place using just the shoulder joint of the PHD. To perform all of our tests the elbow and wrist joints were removed allowing us to look at the shoulder alone. Some of the characteristics of the shoulder Harmonic Drive are given in Table 4.2.

Model:	1M
Ratio:	160
Max. Input Speed:	7000 RPM
Max. Output Torque:	2470 in lb
No-Load Starting Torque (at input):	11 oz in
Circular Spline O.D.:	4.25 in
Weight:	2.6 lb

Table 4.2 Specifications for Shoulder Harmonic Drive

4.3.1 Static Testing

The first area we wanted to examine with regard to the Harmonic Drive was whether we could confirm the properties reported in the product literature. This involved testing to determine the rotational spring rate for the drive. Our goal was to measure experimentally the spring rate from both the input and output sides of the drive. Since both sides of the drive were outfitted with optical encoders this process was relatively straight forward. First, we looked at the input stiffness. This was done by fastening the output link firmly to the base. It was very important to firmly lock the output so that there would be no backlash as it was tested. This was accomplished by machining a piece of 1" thick aluminum plate with a slot which the link would fit into snugly. This plate was then bolted to the steel base plate the robot is mounted on as shown in Figure 4.1.

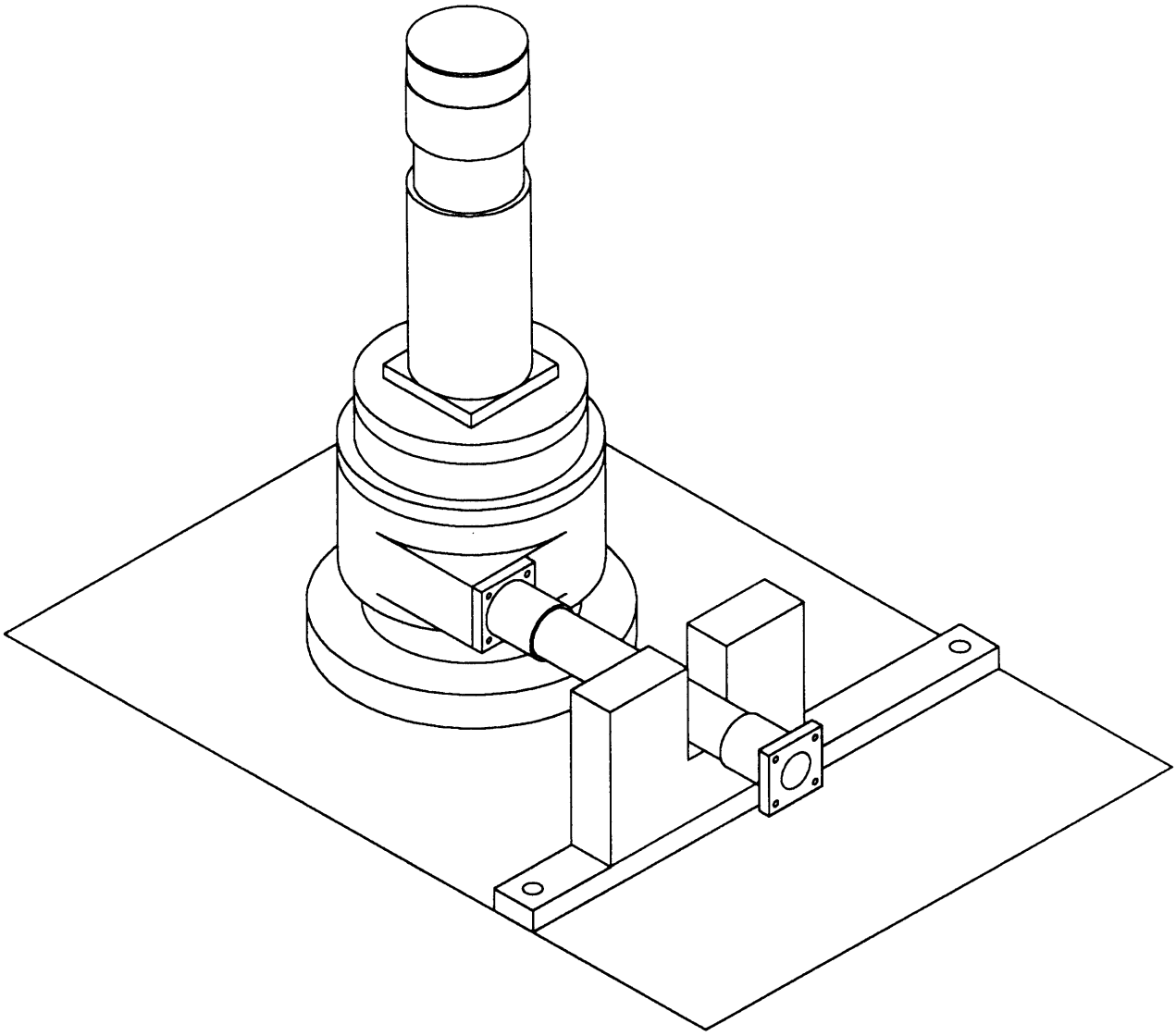

Figure 4.1 Isometric of Input Stiffness Test Setup

This setup then allowed us to load the Harmonic Drive input using the D.C. motor and measure the flex using the encoders. Additionally, the torque sensor provided data as to how much torque the drive was seeing. Given the position and torque data we could determine the stiffness. A graph showing the torque vs. position for the input is shown in Figure 4.2. The position is the equivalent output position (e.g. the motor angle divided by 160). In Figure 4.3 the same data is shown plotted next to a linear spring approximation

with a stiffness of 320,000 in lb/rad, which is our best linear approximation to this data. As you can see the Harmonic Drive does have a slight non-linearity—the stiffness increases as the torque increases. This effect presumably continues as the torque climbs but we were incapable of increasing the input torque to the motor's full capabilities due to current limits on the amplifier driving the motor (10 Amps). The motor is capable of delivering 260 in oz at peak which would give 2600 in lb at the H.D. output, but this requires an input of 30 Amps. We did run some tests with a larger amplifier but ran into difficulties with noise since the amplifier was pulse-width modulated. This caused noise in the low level torque signal which affected the results considerably.

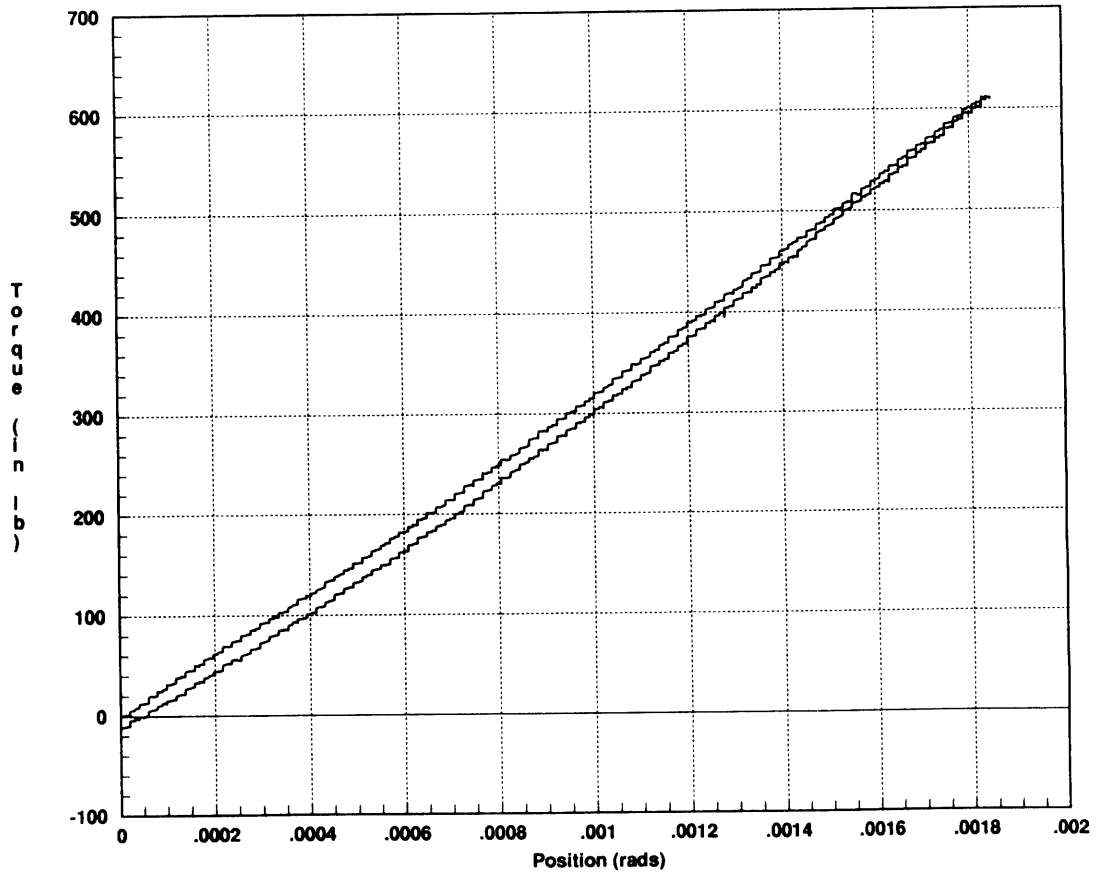

Figure 4.2 Test Results for Determining Harmonic Drive Input Stiffness

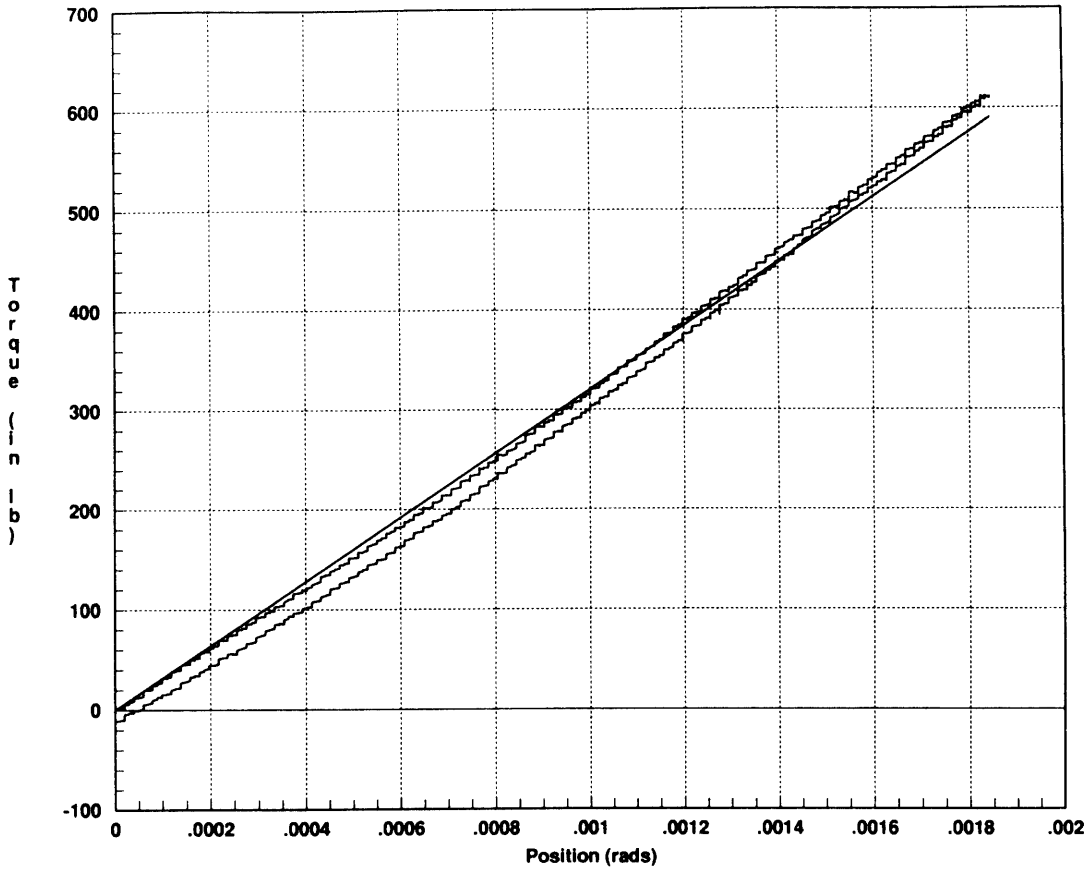

Figure 4.3 Tested H.D. Input Stiffness with Linear Approximation to Data

Shown in Figure 4.4 is the input stiffness plotted against the stiffness quoted in the H.D. literature. The quoted stiffness is 250,000 in lb/rad up to 20% of the rated torque (at 1750 RPM) and then it jumps to 515,000 in lb/rad. It can be seen that for low torques this approximation isn't too bad but for higher torque the results do diverge. There are several possible explanations for this discrepancy. The first is that the H.D. we have has a slightly different spring rate. Another is that the actual torque was higher than what we measured. This difference could possibly be due to some inefficiency in the drive, although this seems unlikely since the drive was not moving very quickly (0 to 0.002 radians and back in 20 seconds).

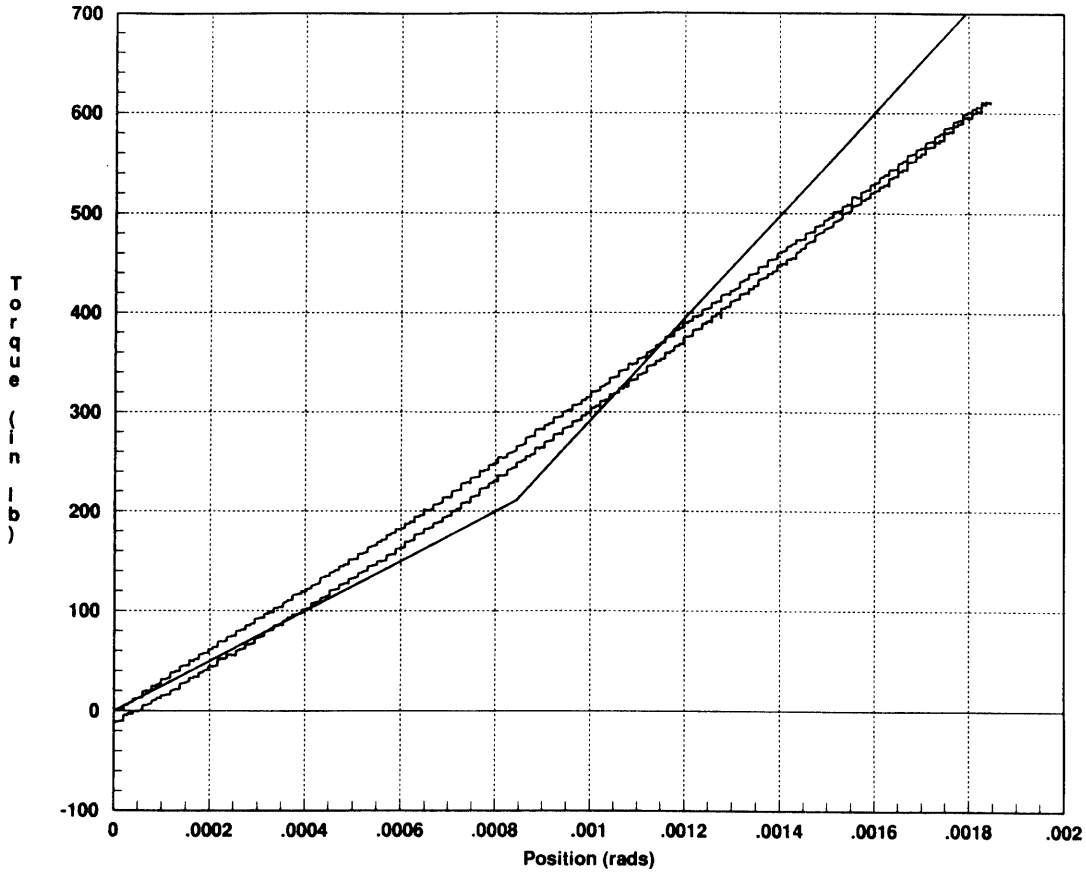

Figure 4.4 Tested H.D. Input Stiffness with Factory Quoted Stiffness

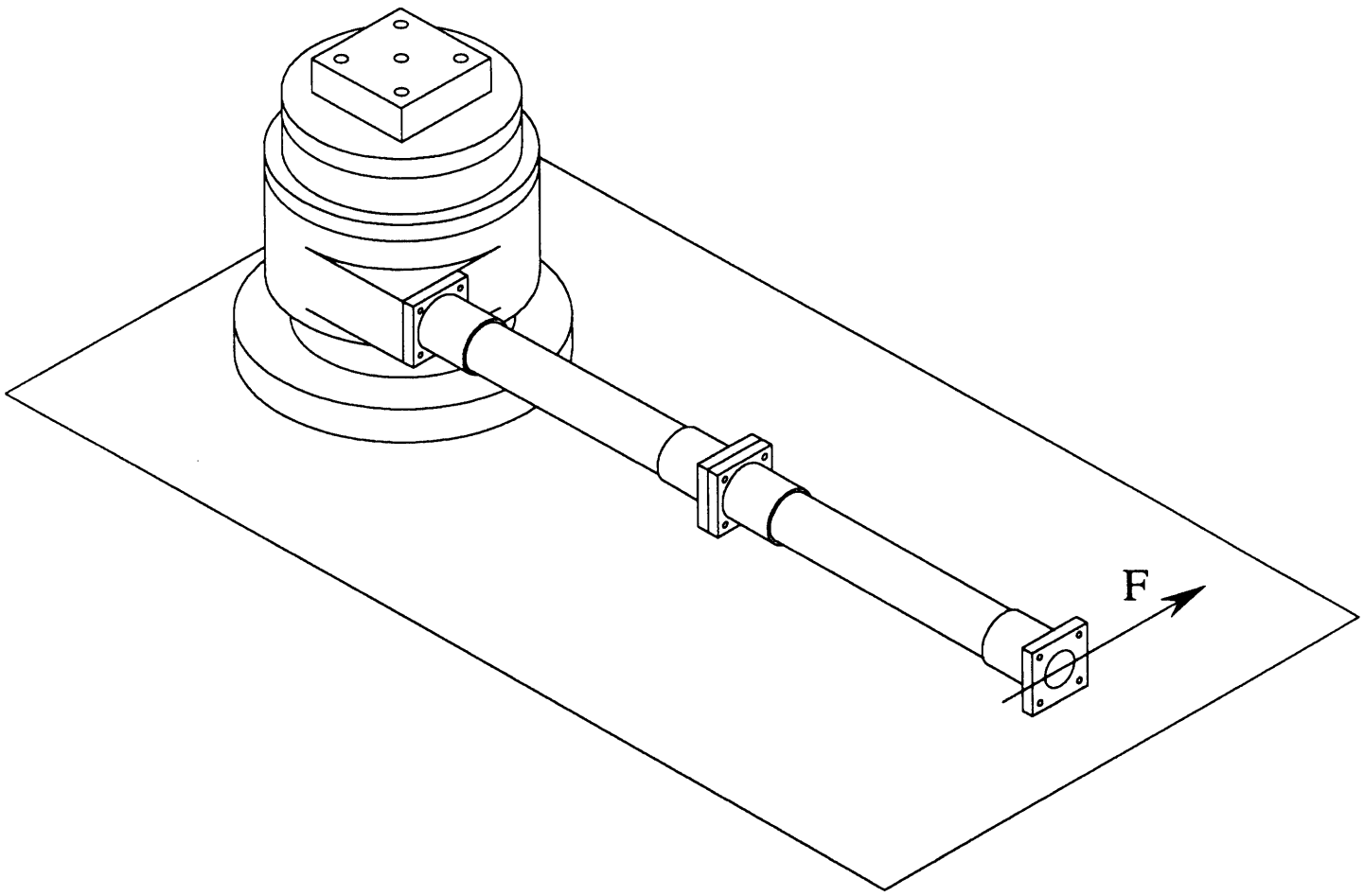

Figure 4.5 Isometric of Output Stiffness Test Setup

The second static test we ran was to determine the stiffness from the output as shown in Figure 4.5. To do this, we removed the motor and replaced it with a part which locked the H.D. wave generator to the top plate. Then a spring scale was used to pull on the end of the link and apply a torque on the joint. The data for this is test graphed along with a spring rate approximation of 265,000 in lb/rad in Figure 4.6. Again, the linear approximation is the best fit to the available data. The steps in the data are due to the output encoder, which has a resolution of 0.0000785 radians per count. As you can see, the data again shows a pronounced non-linearity, stiffening as the torque increases. Figure 4.7 shows the output stiffness compared again to that reported in the company literature. In this case the measured stiffness is somewhat less than that given by the company.

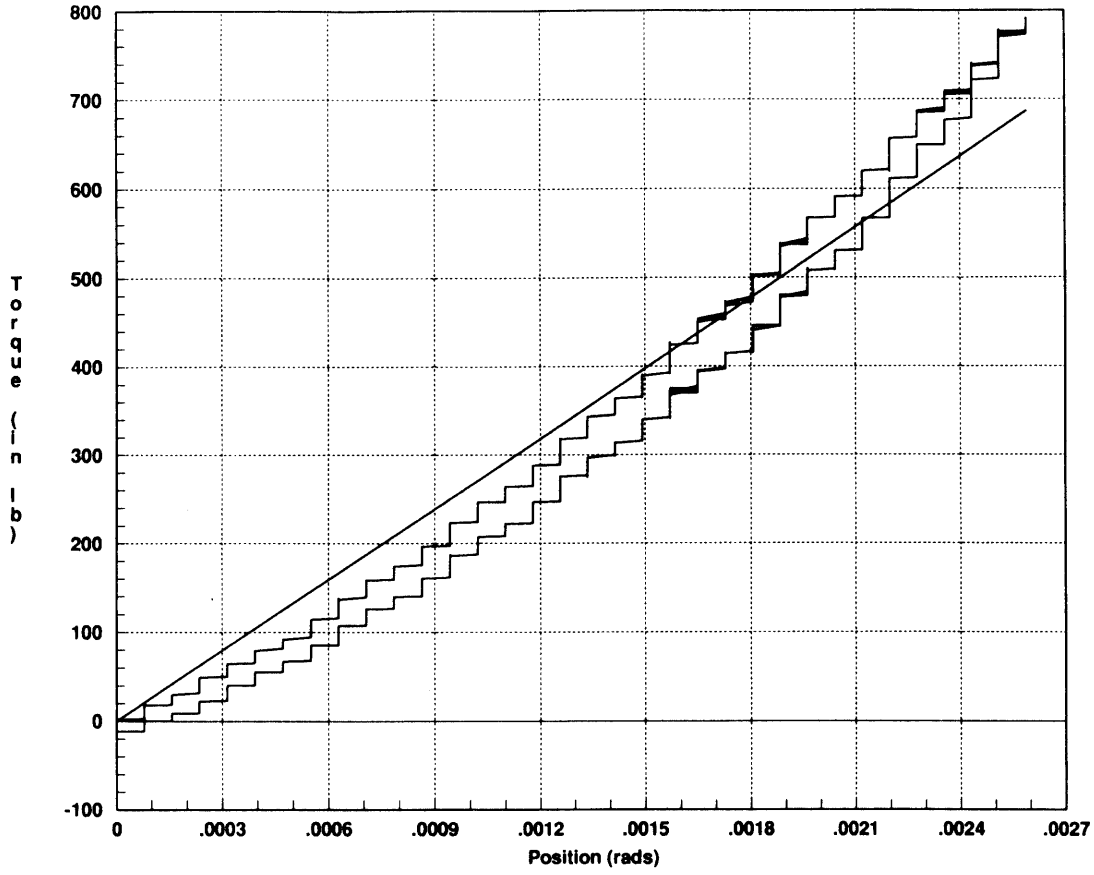

Figure 4.6 Tested H.D. Output Stiffness with Linear Approximation to Data

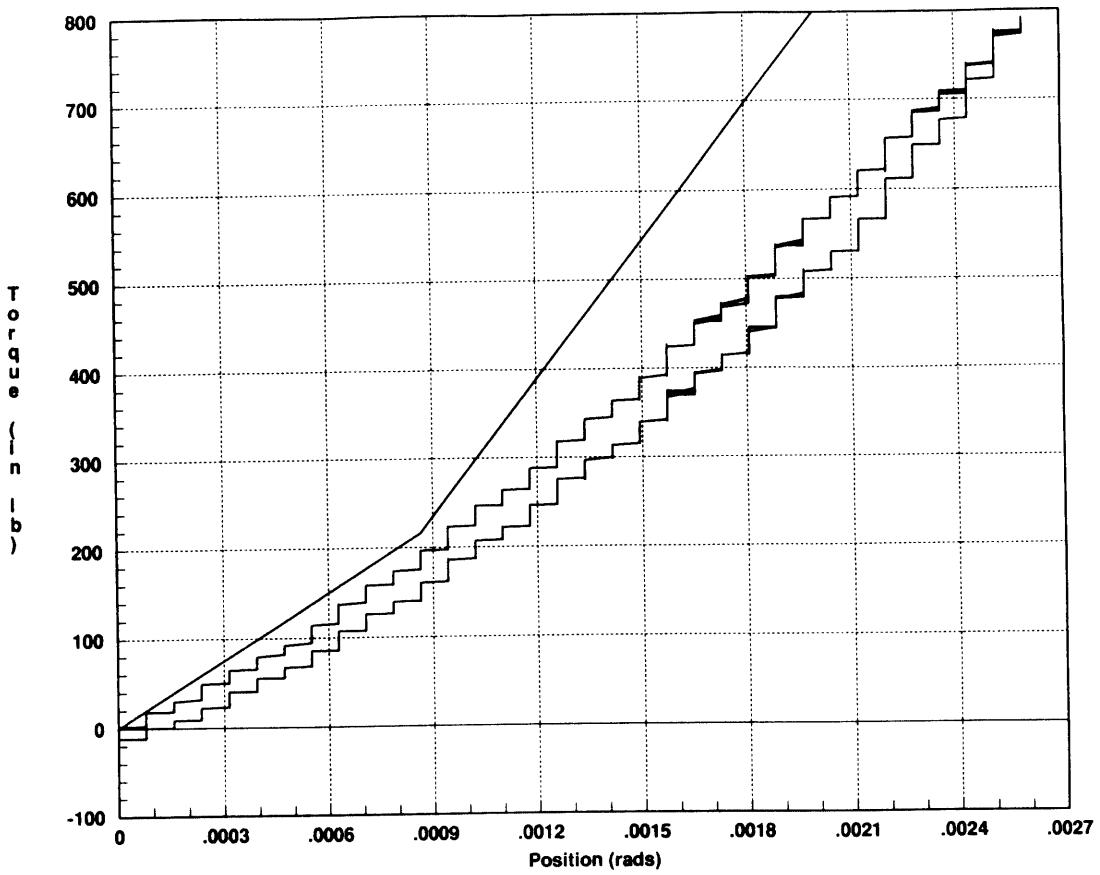

Figure 4.7 Tested H.D. Output Stiffness with Factory Quoted Stiffness

Another interesting result that we noticed was that the drive is slightly stiffer in counterclockwise direction than it is in the clockwise direction. Table 4.3 shows the average linear spring stiffnesses we measured for different tests of the Harmonic Drive. We were not surprised to find a difference between the input and output stiffnesses, as the mechanism of running the drive forward and backward are significantly different. The slight change in stiffness dependent on direction is a much more interesting effect. We have not yet been able to pin down the cause of this, but we feel it must be within the H.D. since it happens on both the input and output sides.

Directional Stiffnesses	Clockwise	Counterclockwise
Input	290000 in lb/rad	330000 in lb/rad
Output	280000 in lb/rad	300000 in lb/rad

Table 4.3 Tested Harmonic Drive Stiffnesses for Shoulder Joint

4.3.2 Theoretical Model

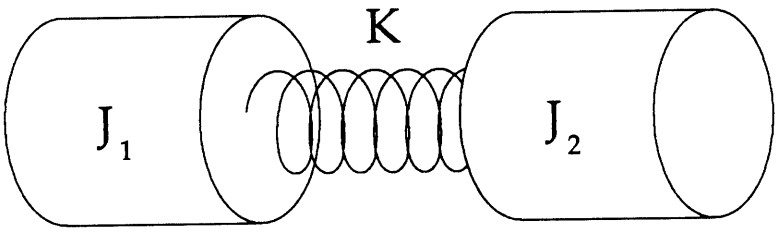

Figure 4.8 Schematic of Model

Based on the tested stiffnesses, we decided that the next thing we wanted to do was construct a simple model of the drive and test its validity. The simplest model is that of a linear, rotational spring connecting two inertias, one being the joint and load inertia and the other being the motor inertia reflected through the gear ratio. A schematic of this model is illustrated in Figure 4.8. Basically, this model represents the motor driving the shoulder, with a load mounted at the end of the first link as shown in Figure 4.9.

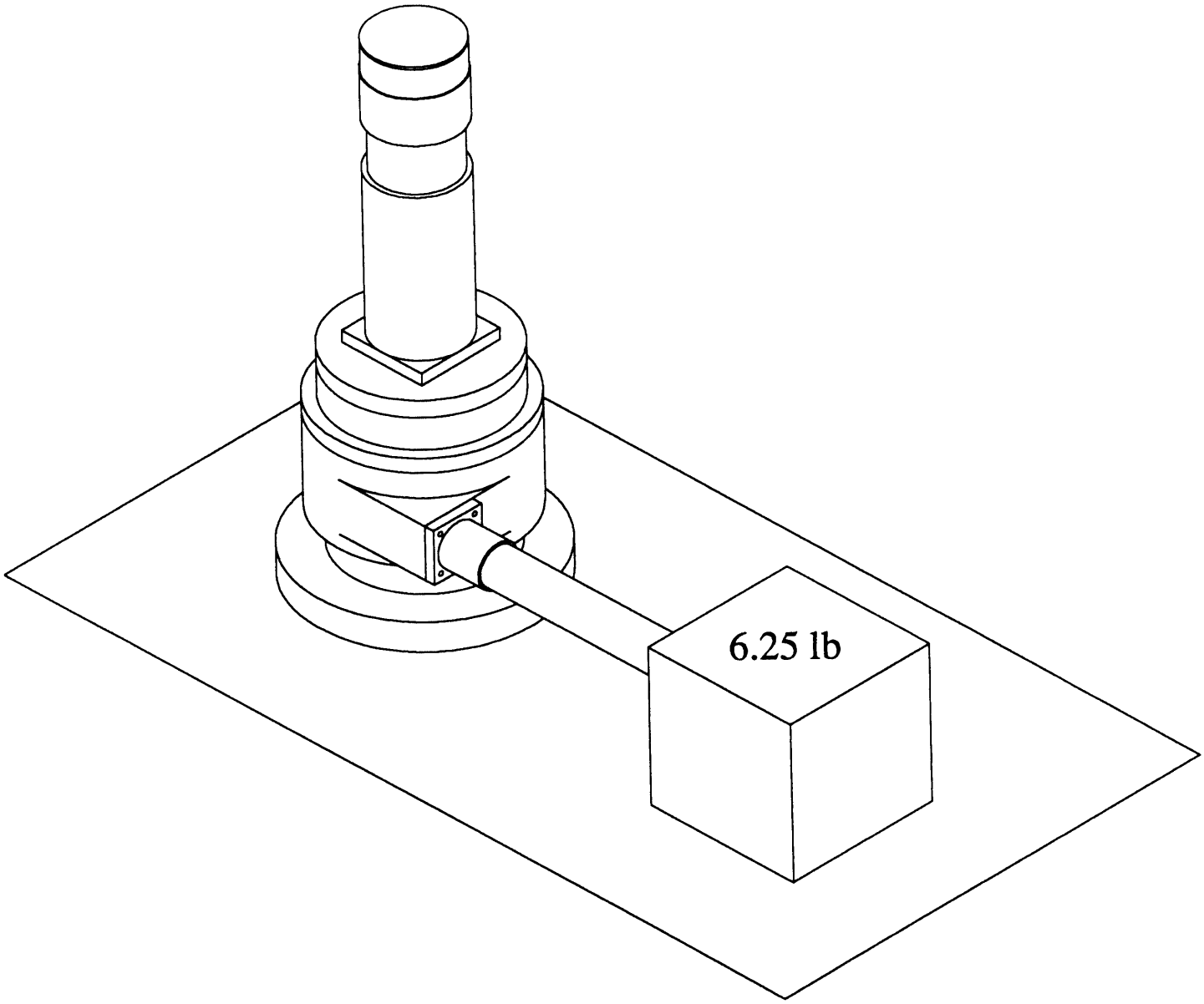

Figure 4.9 Isometric Drawing of Test Setup

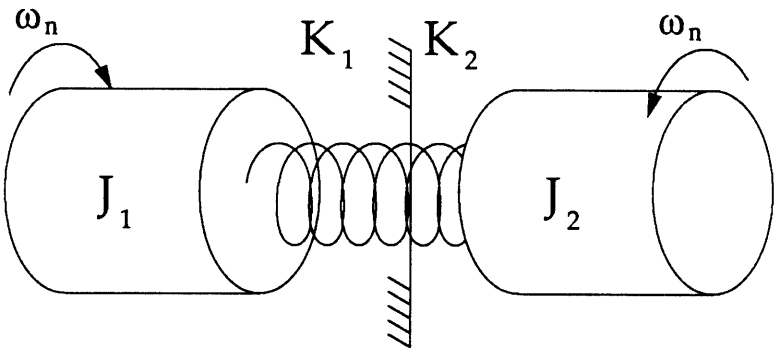

Figure 4.10 Schematic of Model

Analyzing this model, we wish to determine the natural frequency, which can be calculated in a number of ways. We chose to use the inherent symmetry, by noting that there is some point on the spring which remains still as the two inertias vibrate as illustrated in Figure 4.10. The spring can then be divided into two stiffnesses, k_1 and k_2, which must yield the overall spring constant, k, according to the following equation

$$\frac{1}{k} = \frac{1}{k_1} + \frac{1}{k_2} \tag{4.1}$$

Since both sides must vibrate at the same frequency we know

$$\omega_n = \sqrt{\frac{k_1}{J_1}} = \sqrt{\frac{k_2}{J_2}} \tag{4.2}$$

where J_1 and J_2 are the load and equivalent motor inertias, respectively. Since we also know k for the H.D. we can then solve to find

$$\omega_n = \sqrt{k\left(\frac{1}{J_1} + \frac{1}{J_2}\right)} \tag{4.3}$$

For the PHD this test was run with a 6.25 lb load mounted where the elbow would usually be, so the parameters are:

$$J_1 = 160^2(2.6 \times 10^{-5}) \text{ ft lb s}^2$$

$$J_2 = 0.2267 \text{ ft lb } s^2$$

The stiffness we measured for the shoulder joint was

$$k = 300{,}000 \text{ in lb/rad} = 25{,}000 \text{ ft lb/rad}$$

so we get a predicted natural frequency of

$$\omega_n = 384.5 \text{ rad/s} = 61 \text{ Hertz}$$

4.3.3 Experimental Results

The next step was to try to experimentally prove that the shoulder would resonate at this frequency. We began by performing a sine sweep using the control system, by inputting sine waves of varying frequencies to the motor and looking at the motor and output positions. From this information we could then derive the necessary magnitude and phase information to construct a Bode plot. Unfortunately, since the frequency we were looking for was so high it was difficult to get good data. Due to the limits of the motor and amplifier pair, we could only achieve a servo bandwidth of around 40 Hertz using this method. Above this frequency we could not take useful data.

To alleviate this problem we obtained a Hewlett Packard Spectrum Analyzer. This allowed us to analyze the frequency response of the shoulder without having to worry about amplifier limits or servo loop bandwidth. The analyzer generates a white noise signal and then, based on a feedback signal and that noise, determines the frequency response of a system. In testing the PHD, we took the white noise signal and ran it into the amplifier as the current command. Then we fed back either the tachometer or torque sensor signal depending on whether we wanted to look at the input or output side of the H.D.

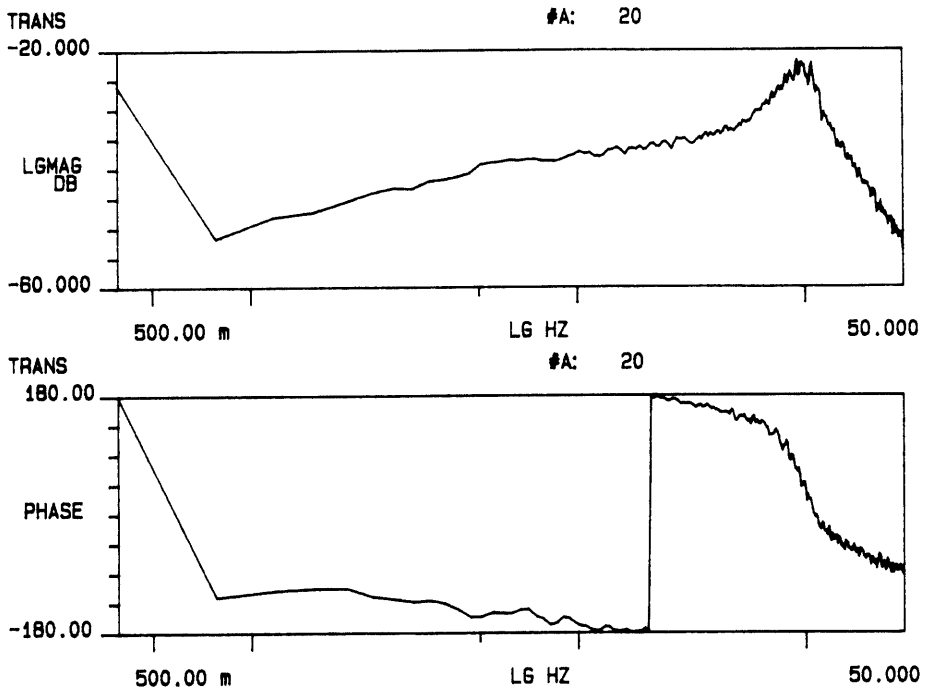

Figure 4.11 Bode Plot of System Response with Load

Figure 4.11 shows a Bode plot taken of the shoulder with the load inertia mounted. The values on vertical scale on this plot are not relevant, these plots were used only to determine where peaks occurred. The horizontal scale tick marks are located at 0.5, 1, 5, 10 and 50 Hertz, which is not clear in the plot. From the data you can see there is a peak in the magnitude plot at 50 Hz, which is slightly lower than the predicted frequency 61 Hz peak for the mode between the motor and load inertia. There are several probable reasons for this difference. First, our calculation considered only the flexibility in the H.D., and not any in the link or joint. Although we designed all the other elements to be much stiffer than the H.D. they will still have some effect on lowering the frequency of this mode. Second, the white noise did not generate very large motions in the joint, so the H.D. was operating in the range where its stiffness is lowest. Our stiffness estimate was an average for the whole range of tested torques. If we examine the plot again and just use the initial slope we get a spring rate of about 255,000 in lb/rad. This corresponds to a natural frequency of 56 Hz which is closer to the measured frequency.

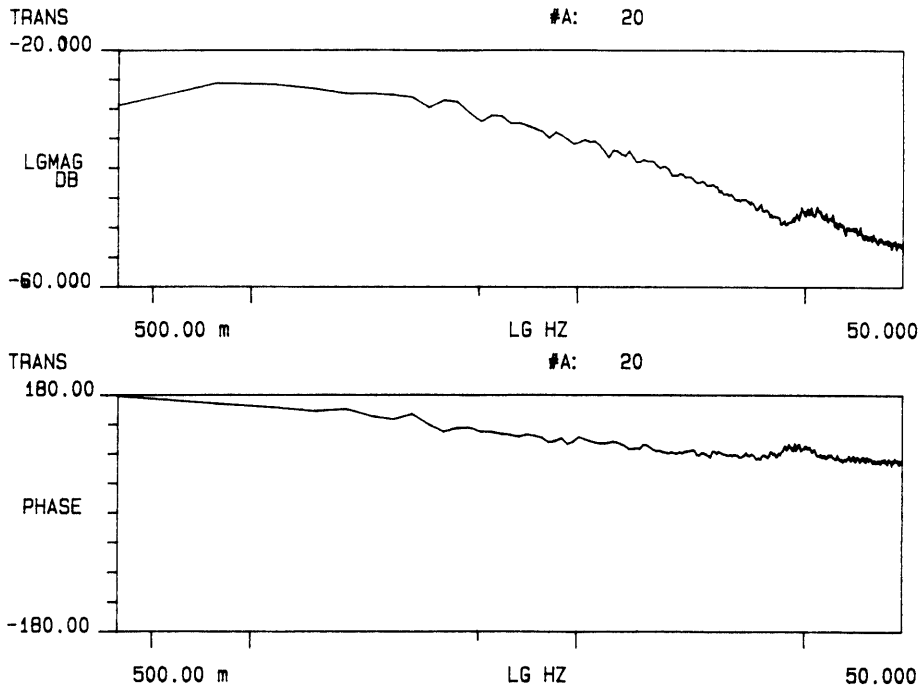

Figure 4.12 Bode Plot of Motor Response with Load

Shown in Figure 4.12 is a Bode plot of the transfer function between the motor (actually the amplifier) and the tachometer. As you can see the response just rolls off at 20 dB/decade with a small resonance at 50 Hz which is due to the resonance of the load inertia. This means that the motor/amplifier pair essentially looks like an integrator which is what we would expect from Newton's Third Law

$$T_{motor} = J\,\alpha = J\,s\,\omega \tag{4.4}$$

or

$$\frac{\omega}{T_{motor}} = \frac{1}{s} \tag{4.5}$$

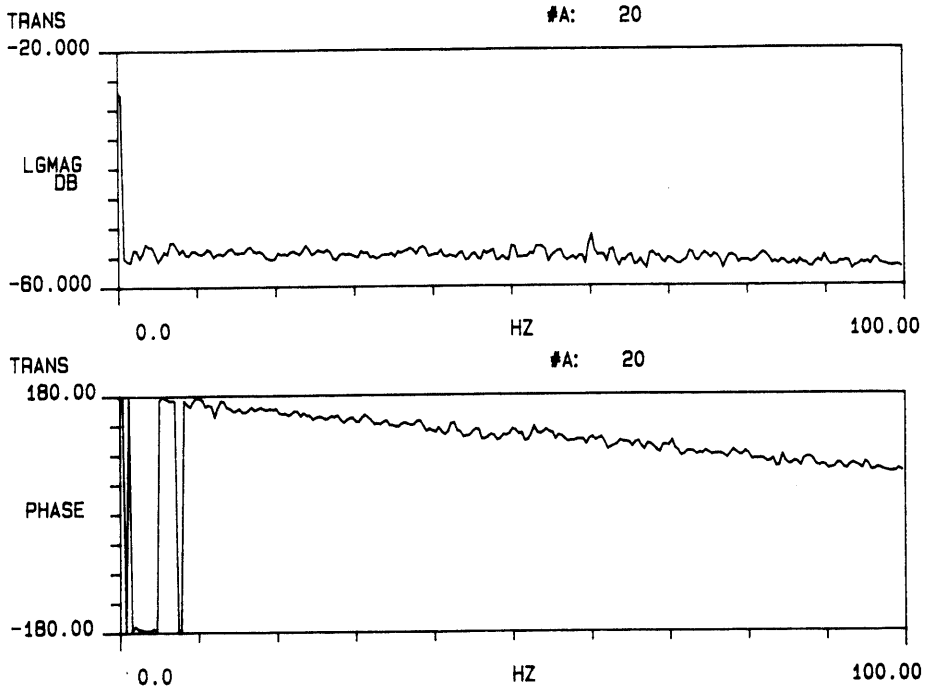

Figure 4.13 Bode Plot of System Response without Load

The next test we performed was to remove the load inertia to check if the joint had a flat response and, as shown in Figure 4.13, there are no surprises. One final set of tests we wanted to run was to look at the response with the output locked. If the simple spring model is valid we would expect a simple second order response from this test. Figure 4.14 shows the result and it does, to a large degree, look like a second order response. There are some other effects but the spring model predicts the behavior reasonable well.

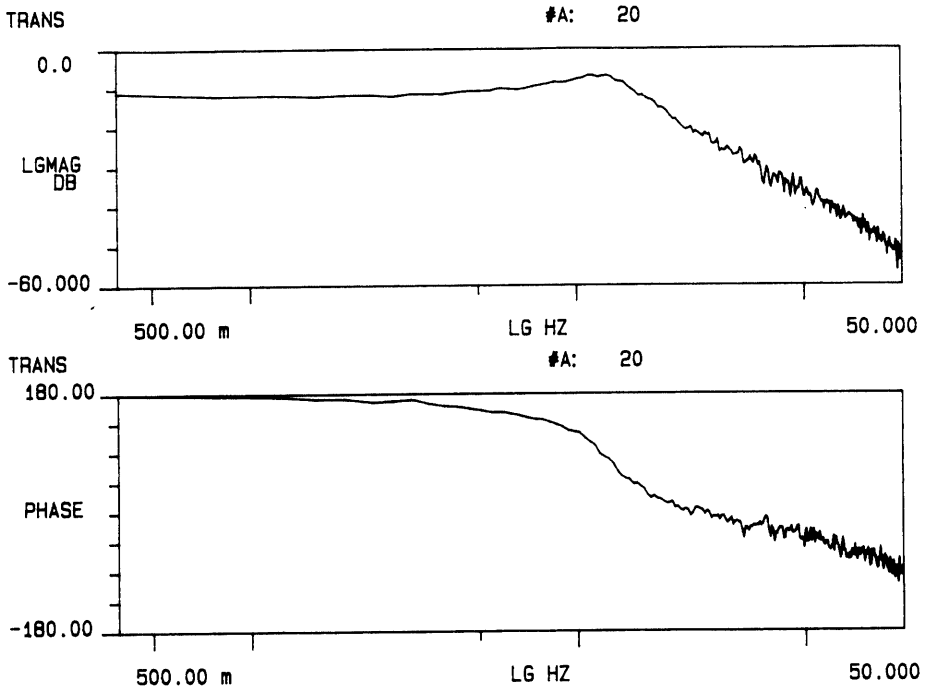

Figure 4.14 Bode Plot of System Response with Output Locked

4.3.4 Model Weaknesses/Improvements

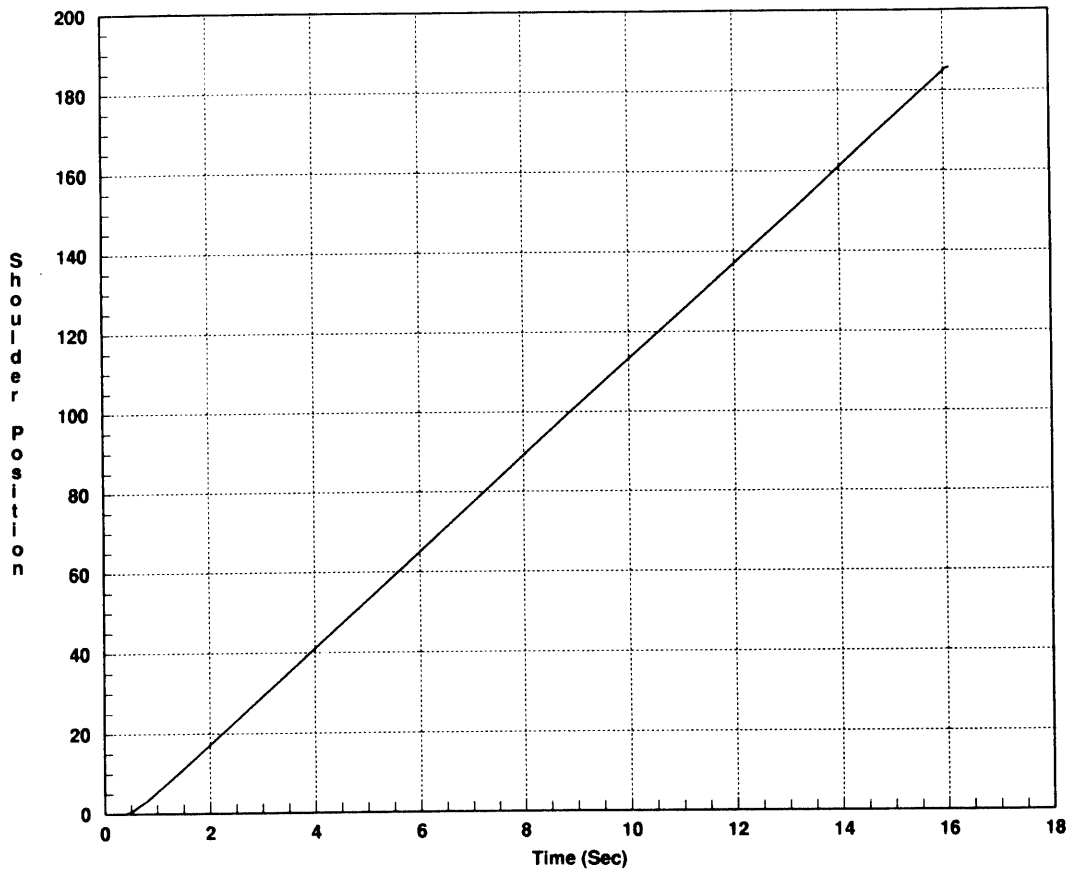

Figure 4.15 Position Data for a Low Speed Move

There are still some effects that are not predicted by the simple linear spring model of the H.D. Figure 4.15 shows a plot of the shoulder position for a slow move of the joint. Although it looks smooth on this plot if you draw a parallel line next to it and subtract the data from that line you get the plot shown in Figure 4.16. As you can see there are definitely some higher order effects going on here. The large scale variation is due to velocity changing, which is caused by unequal bearing preloading. The frequency of the small wave is the same as that of the motor and wave generator. This effect seems likely to be caused by the Harmonic Drive and it is obviously not something predicted by our simple spring model.

In order to build a model to predict effects such as this we would have to build a more detailed model of the interactions of the three parts of the drive.

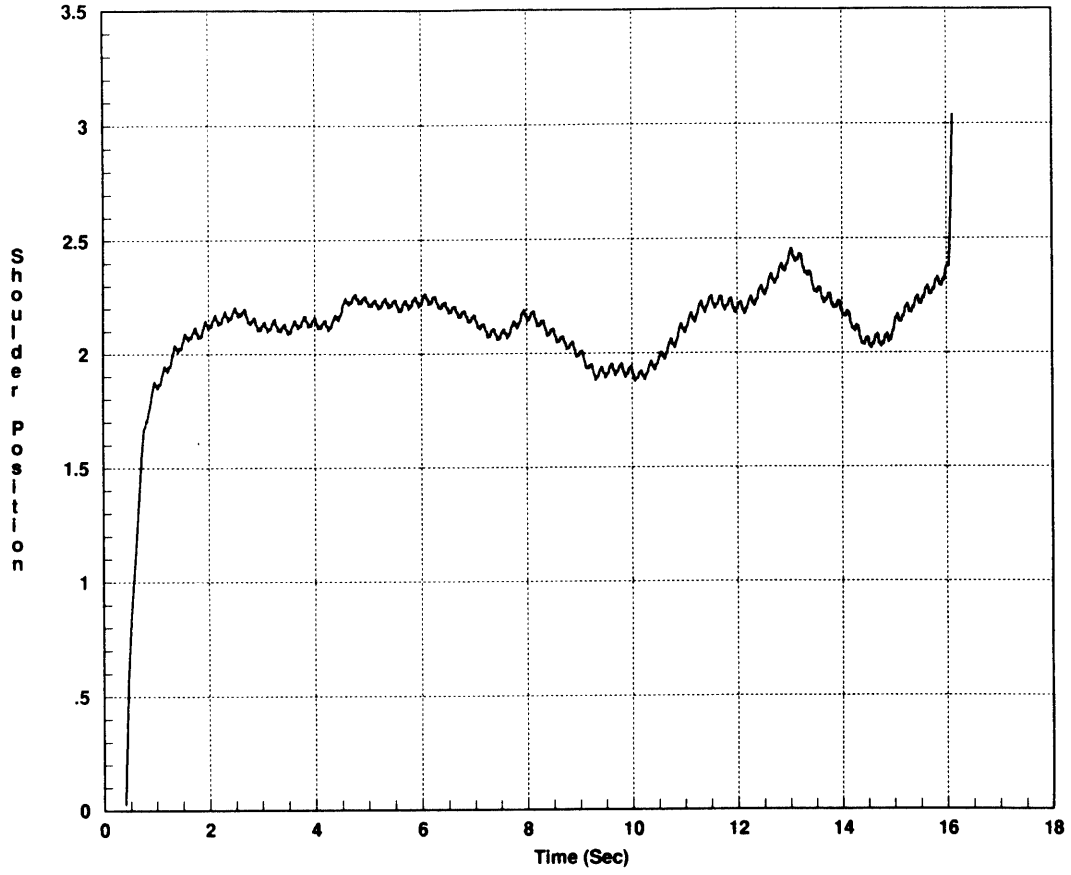

Figure 4.16 Modified Data for a Low Speed Move

Chapter 5: Conclusions

Two main areas of research have been addressed, the modeling of complex systems to produce accurate simulations, and the design and construction of a robot for the testing of torque control and Harmonic Drive performance. The main conclusions of this research are outlined in the following chapter.

In trying to build a good simulation model there are several items which must be carefully considered. The most important issue is what the model will be used for. The main goal of our model of the RRC arm was to provide simulation data which could accurately predict robot motions while running in a position control mode. We found that a simple linear model was inadequate for this system, since it predicted that some of the joints would be unstable. A more detailed non-linear model, which included Coulomb friction in the motor and joints and a non-linear model of the Harmonic Drive spring rate, provided better results.

An experimental test plan was designed and the results compared favorably to the simulation predictions. Parameter studies suggested possible areas where our model could be improved. One interesting result of these studies was that although it was important to include the non-linear friction effects to get a stable simulation, the values used for the Coulomb friction did not affect the results significantly, even when changed by up to an order of magnitude. Finally, the feasibility of using our position control model for force control was examined and it was found that the model's ability to predict such quantities as joint torque and motor current was inadequate. Some improvements had to be made in the model to in order to predict these quantities. The most important of these was adding the effects of current and voltage limits in the motor amplifier.

The next part of the research was to design and build a planar, three degree of freedom robot, the PHD, which could be used to study two areas. The primary goal was to be able to evaluate different torque control schemes. Additionally, we wanted to use the robot to determine a suitable dynamic model of the Harmonic Drive gear reducer. The robot was designed with both of these goals in mind. It consists of three planar rotary joints, shoulder, elbow and wrist. The shoulder is mounted to the base and drives the first link, which connects to the elbow. The elbow drives the second link which connects to the wrist, which has a continuously rotating output that serves as the mounting point for any end effector.

The drivetrain for each joint of the robot consists of a D.C. servo motor driving a Harmonic Drive gear reducer. There is also a torque sensor mounted in each joint to allow measurement of the torque across the joint. Position feedback is available on all three joints and velocity information is available on the shoulder and elbow. Additionally, there is an encoder mounted on the output of the shoulder to allow direct measurement of the shoulder position. This allows us to look at both the input and output positions of the Harmonic Drive, as well as the torque transmitted through it (using the torque sensor). All of this information allows us to examine the Harmonic Drive more closely to determine its important dynamic characteristics.

Experiments were then conducted to verify the robot's capabilities. The limiting factor in terms of the PHD's performance was found to be the amplifiers which drive the motors, and more powerful amplifiers would allow improved robot performance. The next experiments concentrated on determining the static properties of the Harmonic Drive, specifically the spring rate, quoted to be piece-wise linear in the product literature. We indeed found that the drive stiffened as the load was increased although we found our stiffnesses to be slightly lower. We also found that the measured stiffness was slightly different when measured from the input and the output. Although this was not an expected result, it is not surprising since the input and output mechanisms of the drive are significantly different.

Next, we moved to test how well a simple linear model of the drive would predict actual performance. To test this, the elbow and wrist joints were removed from the robot and a load inertia was added at the end of the first link. Using the linear spring model, the

predicted natural frequency of this system was estimated to be 61 Hertz. Our tests showed the actual resonance was closer to 50 Hertz. The discrepancy was attributed to the fact that the model took into account only the flexibility in the Harmonic Drive. It is apparent that there are other elements contributing flexibility to the system, such as bending in the link.

In conclusion, it was shown that the linear spring provided a fairly good model of the Harmonic Drive and could be used as a good first cut model for the drive's flexibility. The data also shows that there are other noticeable effects present in the drive whose prediction would require a more detailed model of the drive. Fortunately, these effects are small when compared to the overall joint motion. At this point we have only begun to explore the possible uses of this robot.

The PHD does possess the ability for testing and development of torque control strategies. These strategies may provide an area for the advancement of the abilities of force control, by allowing torque control to be implemented on a one, two or three degree of freedom arm. The modularity and capabilities of the PHD's design will hopefully provide a valuable tool for further research in this area. Using all three joints, the PHD can accomplish simple tasks such as planar peg in hole. Additionally, future work with the PHD can allow development of a more detailed model of the Harmonic Drive which would predict the higher order effects present in the drive.

References

[1] **Asada, H. and Lim, S-K.,**
"Design of Joint Torque Sensors and Torque Feedback Control for Direct Drive Arms", In Donath, M. and Leu, M. (editors), *Robotics and Manufacturing Automation*, ASME Winter Annual Meeting, November, 1985, Vol. PED-15, pp. 277-284.

[2] **Blevins, R.D.,**
Formulas for Natural Frequency and Mode Shape, Van Nostrand Rienhold Company, Appendix A, 1979.

[3] **Christian, A.C.,**
"Design and Implementation of a Flexible Robot", *MIT Artificial Intelligence Laboratory Technical Report AI-TR 1153*, August, 1989.

[4] **Eppinger, S.D. and Seering, W.P.,**
"Modelling Robot Dynamic Performance for Endpoint Force Control", *MIT Artificial Intelligence Laboratory Technical Report AI-TR 1072*, August, 1989.

[5] **Eppinger, S.D. and Seering, W.P.,**
"On Dynamic Models of Robot Force Control", *MIT Artificial Intelligence Laboratory Memo AIM 910*, July, 1986.

[6] **Good, M.C., Sweet, L.M. and Strobel, K.L.,**
"Dynamic Models for Control System Design of Integrated Robot and Drive Systems", *ASME Journal of Dynamic Systems, Measurement and Control*, March, 1985, Vol. 107, pp. 53-59.

[7] **Hashimoto, M.,**
"Motion Control Based on Joint Torque Sensing", *Proceedings of the IEEE Conference on Robotics and Automation*, May, 1989, Vol. 1, pp. 256-261.

[8] **Kondo, K. and Takada, J.,**
"Study on Tooth Profiles of the Harmonic Drive", *ASME Journal of Mechanical Design*, March, 1990, Vol. 112, pp. 131-137.

[9] **Luh, J.Y.S., Fisher, W.D. and Paul, R.P.C.,**
"Joint Torque Control by a Direct Feedback for Industrial Robots", *IEEE Transactions on Automatic Control*, February, 1983, Vol, AC-28, No, 2, pp. 153-161.

[10] **Maples, J.A. and Becker, J.J.,**
"Experiments in Force Control of Robotic Manipulators", *Proceedings of the IEEE Conference on Robotics and Automation*, April, 1985, Vol. 2, pp. 695-702.

[11] **Narasimhan, S., Siegel, D.M. and Hollerbach, J.M.,**
"A Standard Architecture for Controlling Robots", *MIT Artificial Intelligence Laboratory Memo AIM 977*, July, 1988.

[12] **Narasimhan, S., Siegel, D.M. and Hollerbach, J.M.,**
"Condor: A revised Architecture for Controlling the Utah-MIT Hand", *IEEE International Conference on Robotics and Automation*, April, 1988.

[13] **Narasimhan, S. and Siegel, D.M.,**
"The Condor Programmers Manual — Version II", *MIT Artificial Intelligence Laboratory Memo AIM 297*, July, 1987.

[14] **Pasch, K.A. and Seering, W.P.,**
"On the Drive Systems for High Performance Machines", *ASME Journal of Mechanisms, Transmissions, and Automation in Design*, September, 1983.

[15] **Paul, R.P.,**
"Problems and Research Issues Associated With the Hybrid Control of Force and Displacement", *Proceedings of the Workshop on Space Telerobotics*, January, 1987, Vol. 3, pp. 255-260.

[16] **Pfeffer, L., Khatib, O. and Hake, J.,**
"Joint Torque Sensory Feedback in the Control of a PUMA Manipulator", *Proceedings of the Automatic Control Conference*, June, 1988, pp. 818-824.

[17] **Sundaram, K.J.,**
"The Use of Joint Torque Feedback for Force Control", *MIT Artificial Intelligence Laboratory Memo AI-TR 1248*, July, 1990.

[18] **Tilley, S.W., Francis, C.M., Emerick, K.S. and Hollars, M.G.,**
"Preliminary Results on Noncolocated Torque Control of Space Robot Actuators", *Proceedings of NASA Conference on Space Telerobotics*, January, 1989.

[19] **Tilley, S.W., Hollars, M.G. and Emerick, K.S.,**
"Experimental Control Results in a Compact Space Robot Actuator", In Joshi, S.M., Silverberg, L. and Alberts, T.E. (editors), *Dynamics and Control of Multibody/Robotic Systems with Space Applications*, ASME Winter Annual Meeting, December, 1989, Vol. DSC-15, pp. 53-57.

[20] **Whitney, D.E.,**
"Historical Perspective and State of the Art in Robot Force Control", *Proceedings of the IEEE Conference on Robotics and Automation*, April, 1985, Vol. 1, pp. 262-268.

Appendix A: Torque Sensor Specifications

This appendix contains detailed information on the torque sensors we designed and built for the PHD. This includes: engineering drawings, a table of pertinent specifications and calibration curves for each sensor.

A.1 Shoulder

The shoulder torque sensor is a relatively simple design consisting of a cylinder which is bolted between the bottom of the Harmonic Drive flexspline and the base plate for the joint. As the torque through the joint is increased, the sensor strains, causing the strain gages on its surface to produce a voltage change proportional to the torque. The measured conversion from counts to inch-pounds for this sensor is given in Table A.1. This was measured while the A/D gain was set for a ±2.5 V range.

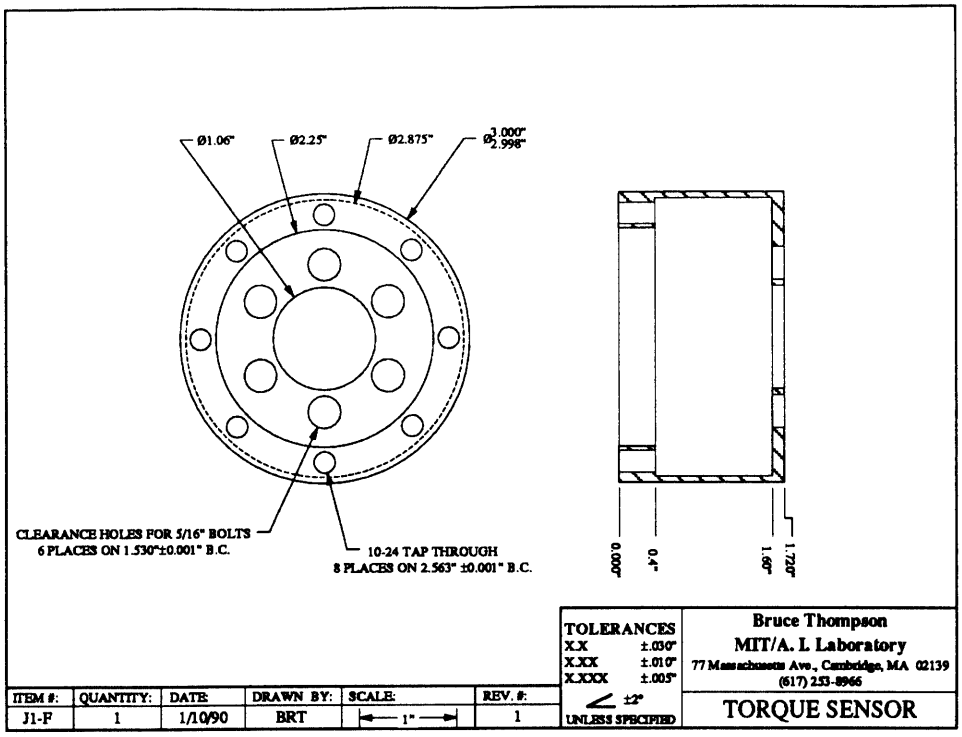

Figure A.1 Shoulder Torque Sensor Engineering Drawing

Stiffness (Theoretical):	3.88×10^6 in lb/rad
Torque to A/D Count Conversion*:	0.441 in lb/count
Number of Gages:	4
Type of Gage:	Micro Measurements CEA-13-187UV-350
Gage Factor, γ:	2
Max. Torque (limited by motor):	2600 in lb
Max. Output Voltage (before amplification):	4.41 mV
Max. Strain:	2.41×10^{-4} in/in
Max. Stress:	1807 psi

Table A.1 Specifications for Shoulder Torque Sensor

*This is with the A/D set at ±2.5 Volts

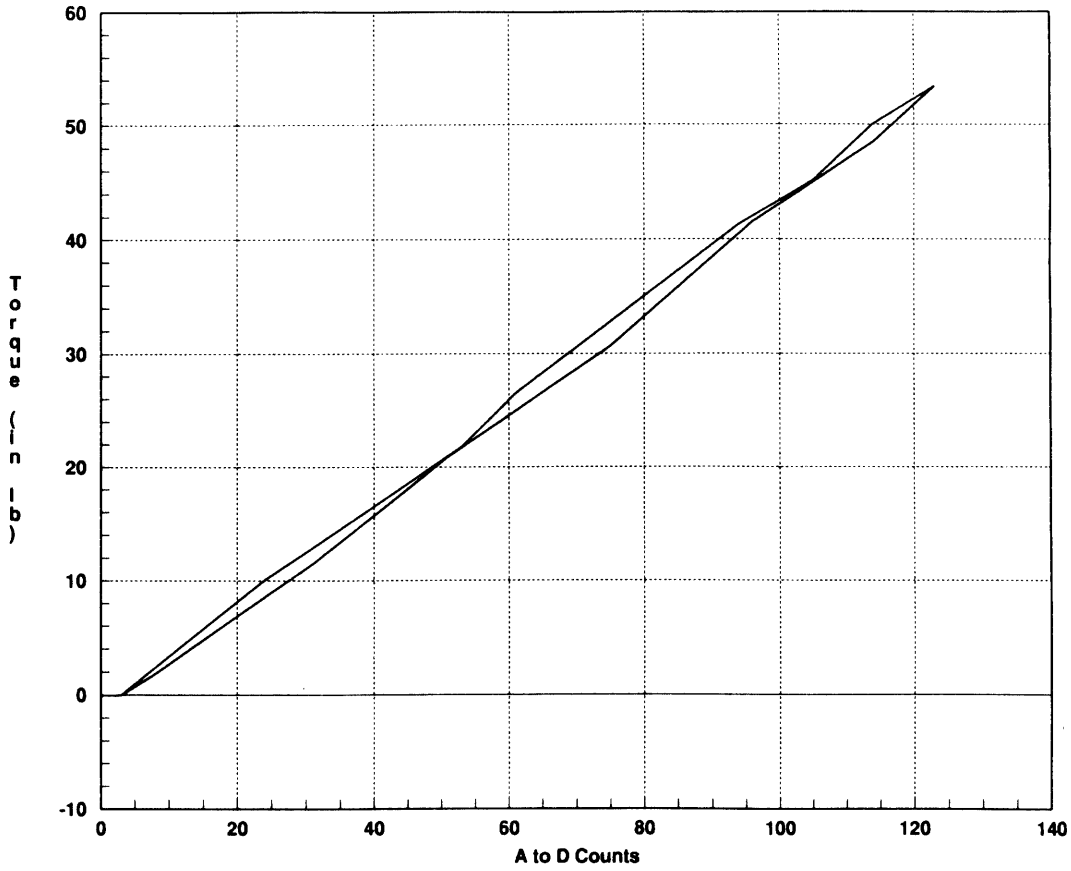

Figure A.2 Calibration Curve for Shoulder Torque Sensor

A.2 Elbow

The elbow torque sensor is nearly the same as the shoulder except it is slightly smaller. The measured conversion from counts to inch-pounds is given in Table A.2. This was measured while the A/D gain was set for a ±2.5 V range.

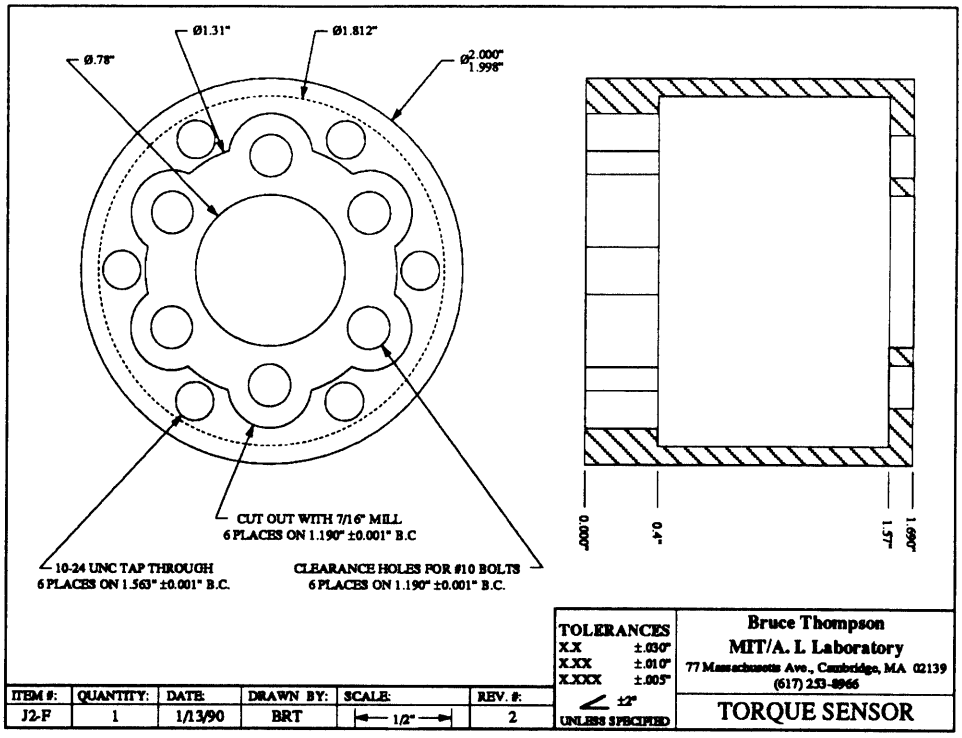

Figure A.3 Elbow Torque Sensor Engineering Drawing

Stiffness (Theoretical):	1.63×10^6 in lb/rad
Torque to A/D Count Conversion*:	0.246 in lb/count
Number of Gages:	4
Type of Gage:	Micro Measurements CEA-13-187UV-350
Gage Factor, γ:	2
Max. Torque (limited by motor):	1300 in lb
Max. Output Voltage (before amplification):	4.16 mV
Max. Strain:	2.08×10^{-4} in/in
Max. Stress:	1564 psi

Table A.2 Specifications for Elbow Torque Sensor

*This is with the A/D set at ±2.5 Volts

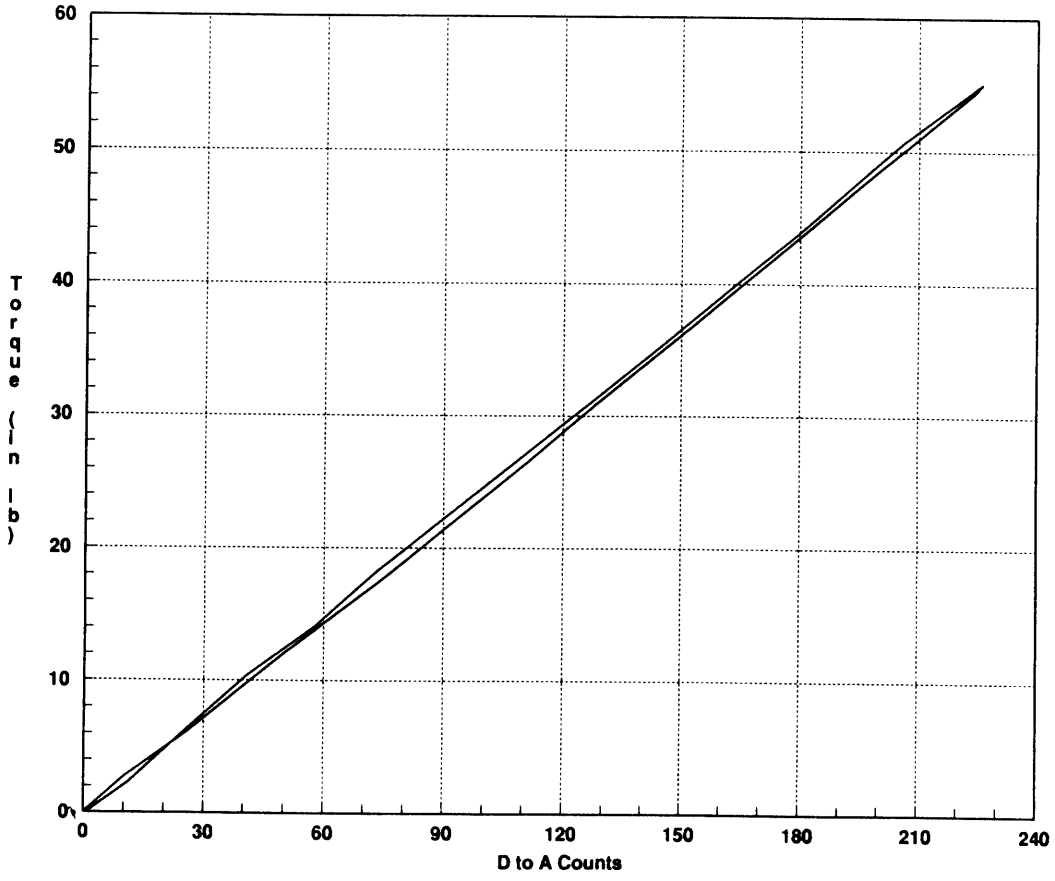

Figure A.4 Calibration Curve for Elbow Torque Sensor

A.3 Wrist

The wrist torque sensor is very different from the other two. This is because to obtain enough strain with a cylindrical design the walls would have had to be very thin (or the sensor's diameter would have had to be very large). To alleviate this problem we chose to totally remove the wall in 6 places leaving 6 equally spaced posts which would carry the torque. The four gages mounted on this sensor are not at 90° increments along the surface but on four of the six posts. The measured conversion from counts to inch-pounds is given in Table A.3. This was measured while the A/D gain was set for a ±2.5 V range. The reason for the jumps in the calibration curve is that we did not load the sensor very much, so that we were working down near the resolution of the D/A, and electrical noise caused jumps in the data.

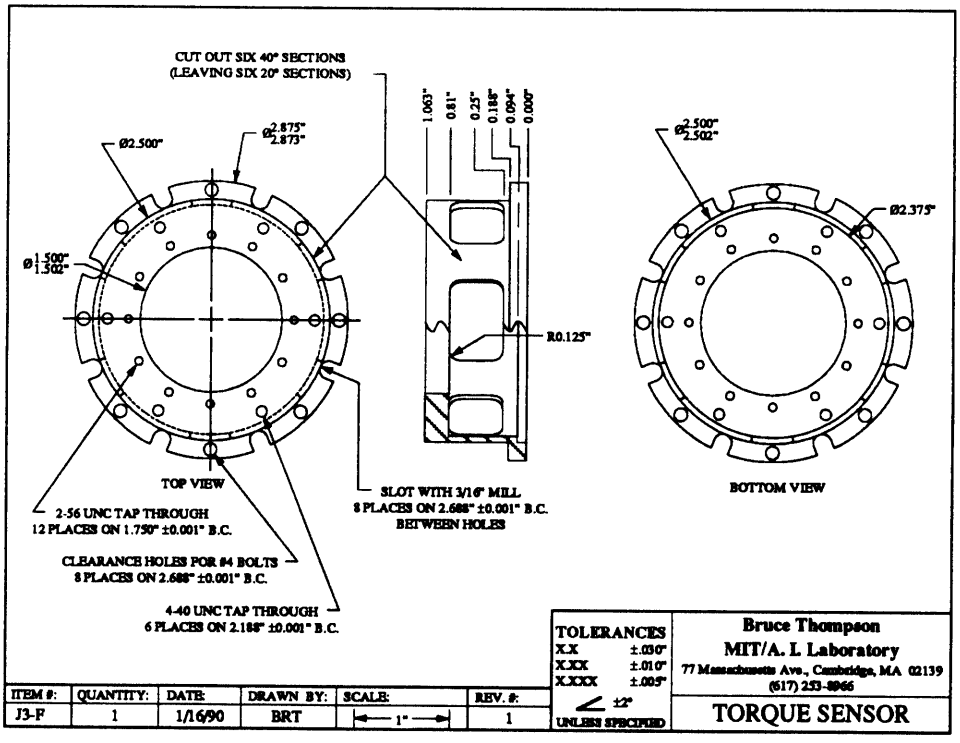

Figure A.5 Wrist Torque Sensor Engineering Drawing

Stiffness (Theoretical):	3.70×10^5 in lb /rad
Torque to A/D Count Conversion*:	0.185 in lb/count
Number of Gages:	4
Type of Gage:	Micro Measurements CEA-13-187UV-350
Gage Factor, γ:	2
Max. Torque (limited by motor):	125 in lb
Max. Output Voltage (before amplification):	6.76 mV
Max. Strain:	3.38×10^{-4} in/in
Max. Stress:	642 psi

Table A.3 Specifications for Wrist Torque Sensor
*This is with the A/D set at ±2.5 Volts

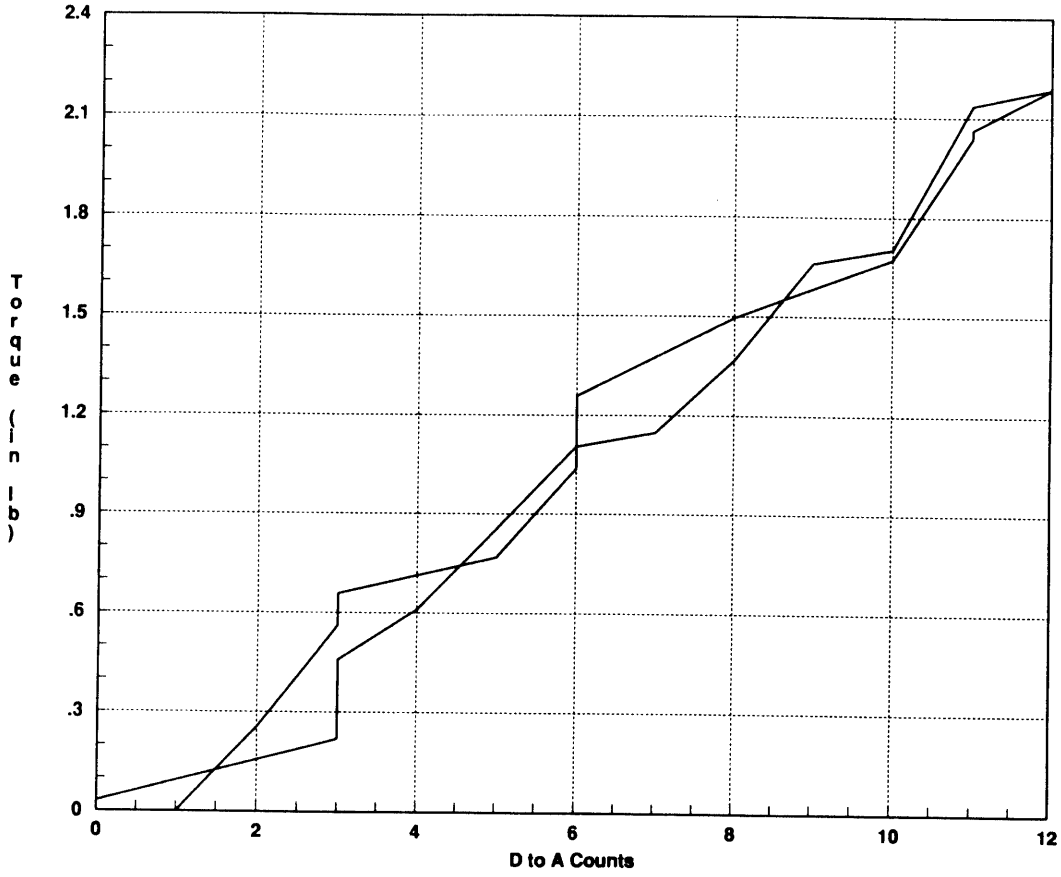

Figure A.6 Calibration Curve for Wrist Torque Sensor

Appendix B: Hardware Specifications

This appendix is broken into three sections. The first gives maintenance and safety information for the robot. The second gives pointers on the assembly of the robot and its joints. Finally, the third contains a list of all of the hardware used in the PHD robot.

B.1 Maintenance/Safety

This section outlines some important points that must be remembered when operating the PHD in order to prevent wear and accidents:

- Always keep the emergency stop switch within reach when the robot is running.
- Always make sure the work envelope is clear of obstacles before enabling the amplifiers.
- Always make sure all the limit switches are in place and operating properly.
- Be careful when working in the electronics box, the strain gage power is always on, even when power to the amplifier rack is turned off.
- Before running make sure all cables are firmly attached, especially motor cables.
- All joints should be checked periodically for loose bolts.
- Re-grease the Harmonic Drive gear teeth whenever the joints are disassembled.
- Periodically check all cables for wear, especially bending fatigue.

B.2 Assembly

This section gives instructions for the assembly of each of the joints as well as the overall robot. I assume that anyone can get the robot apart, so this section details how to get it back together. It begins with assembly of the shoulder and elbow, followed by the wrist. Finally, the assembly of the three joints to the links, along with cable routing is discussed.

B.2.1 Shoulder and Elbow Assembly

Since the shoulder and elbow joints are basically the same, the same assembly procedure applies to both. The joint is assembled in two parts, the joint housing and the drivetrain, which are then bolted together to produce the assembled joint.

First, the joint housing must be assembled. This is begun by putting the bearings into the outer tube separated by the bearing spacer ring. It may be necessary to heat the outer tube to get the bearings in. They are angular contact bearings, so you must be careful to install them correctly (back to back). Next, the base plate should be bolted to the inner tube and this assembly should be slid into the outer tube. (On the shoulder, the large gear and gear cover should be mounted before putting this base plate on.) Then the inner tube top plate should be mounted. IMPORTANT: Do not tighten the inner tube top plate down all the way or it will overload the bearings. It must just be tightened until snug (all bearing play is removed). Ideally, a shim of the proper thickness should be placed under the top plate to guarantee it is squarely mounted. If it is tightened unevenly, the bearings will exhibit varying friction as they spin. Next, the outer tube top plate should be bolted on. This completes the assembly of the joint housing.

Now the drivetrain must be assembled. First, check that there is still grease on the Harmonic Drive teeth. If most of it is gone, re-apply some more grease (H.D. calls for a NGLI #2 grease). Mount the motor adapter plate to the motor. Then the H.D. wave generator must be mounted on the motor shaft using the TranTorque coupling. It is important to mount the wave generator as far out on the shaft as possible, especially on the shoulder, as mounting it too close to the motor will not provide proper tooth preloading in the Harmonic Drive, resulting in a small amount of backlash in the output. Next, take the torque

sensor and bolt it to the H.D. flexspline. The concentricity of these two pieces must be checked. Since there is no locating mechanism, it must be adjusted by hand (by feeling or looking at the center holes to see how well they match up). If they are off, loosen and re-align them. Next, slide the flexspline onto the wave generator. Then, slide the circular spline on over the torque sensor and flexspline. To check that the H.D. has been assembled properly the motor can be turned by hand. This can be done by pulling off the encoder cover and carefully turning the motor shaft, as the circular spline is held to the motor adapter plate by hand. If assembled properly the flexspline should deflect twice per motor revolution. If it is only deflecting once, you have assembled the H.D. dedoidally and must remove the circular spline and try again.

Now the drive train can be slid into the joint housing. Be careful not to mangle the torque sensor wires. The torque sensor cable connector must slide through the hole in the base plate, and it is important to verify that the wires from the gages go through the slot on the bottom of the sensor before bolting the drivetrain on. This can be done by rotating the whole drivetrain until the slot (and hopefully wires) are seen through one of the bolt holes in the base plate. After this the torque sensor can be bolted down, be sure to tighten the bolts a bit at a time, not all at once as the sensor could then get misaligned in the joint housing. Finally, the motor plate and circular spline must be bolted to the top of the joint housing. At this point it is worth taking off the encoder cover and rotating the motor by hand to verify everything is together properly and the joint turns.

B.2.2 Wrist Assembly

Assembly of the joint housing is identical to the other two joints above except that only eight of the holes on the outer tube top plate are used to hold it down, the other eight are to hold the torque sensor. The drivetrain assembly is as follows. First bolt the motor adapter plate to the motor. Then the H.D. wave generator is affixed to the motor shaft using Loctite. Again, it is important to make sure the wave generator is far enough out on the motor shaft. Next, bolt the H.D./Output Adapter to the H.D. flexspline and slide the flexspline over the wave generator. Now the circular spline must be bolted to the torque sensor on the inside. You will notice that this only uses six of twelve holes on the bolt circle. Next, slide the torque sensor and circular spline over the flexspline and bolt them together using the other six holes. At this point you must again check to see that the Harmonic Drive has not been

assembled dedoidally. If so remove the circular spline and try again. Now slide the drivetrain into the joint housing and bolt the output plate to the bottom of the H.D./Output Adapter. Then, the torque sensor can be bolted down using the other eight holes on the top of the outer tube. Before doing this it is important to make sure the cables are properly oriented, so that the encoder and torque sensor cables will be pointing in the right direction when the joint is fully assembled. Finally, the torque sensor cover can be placed over the sensor and bolted down. Be careful not to damage the torque sensor wires.

B.2.3 Joint/Link Assembly and Wiring

The first step in this process is to take the assembled shoulder joint and mount it to the table. This is done using the "special" Allen wrench, an Allen wrench that has been shortened to fit under the gear. (This is the major flaw in the design which I would change if I had another chance by making the base 8" in diameter.) After that the extra encoder must be mounted. (This process is the other flaw in my design.) You must use either another "special" Allen wrench or a pair of needle nose pliers to tighten the two bolts holding the encoder mounting plate on. Make sure that the anti-backlash gear is preloaded before meshing the two gears. The rest of the assembly is straight forward (no more "special" tools). First, stuff the elbow and wrist torque sensor cables and elbow tach/limit switch cable through the first link (the shorter one). Make sure the right ends are through and bolt the first link onto the shoulder output. (Important note: there is a drop of epoxy on this link on the edge of one of the ends. This drop must be on the top of the elbow side of the link. It is what triggers the limit switch on the elbow.) Now bolt the elbow to the link, the elbow attaches on the *lower* mounting spot (on the inner tube so that the second link is above the first). Now run the wrist torque sensor cable through the second link and bolt it to the elbow (it doesn't matter which way) and bolt the wrist to its end. That completes the mechanical assembly.

Now the rest of the cabling must be finished. The torque sensor and tach/limit switch cables should be attached first. Then the encoder and motor cables which are routed down the outside of the links. Make sure you leave enough slack in the cables at the elbow to allow them to wrap all the way around. If you use wire ties creatively you can get this slack to stay up off the table when the joint is straightened. This completes the robot assembly, although

it is probably a good idea to check the cables are wired properly one more time before firing the robot up.

B.3 Hardware Parts List

This section gives a list of each piece of hardware purchased and the manufacturer.

B.3.1 Shoulder

Motor:	Aerotech 1035DC-01 Servo Motor
Harmonic Drive:	Harmonic Drive HDC-1M-160-2-K1
Bearings:	Kaydon KA040ARO (angular contact)
Motor Encoder:	HEDS-6000 Option B08 (1000 lines/rev)
Strain Gages:	Micro Measurements CEA-13-187UV-350
Strain Gage Signal Conditioner:	Analog Devices Model 1B31-AN
Output Encoder:	Vernitech VOEL-23-2500-AQ1-PU5-1L1 (2500 counts/rev)

B.3.2 Elbow

Motor:	Aerotech 1017DC-01 Servo Motor
Harmonic Drive:	Harmonic Drive HDC-5C-160-2-K1
Bearings:	Kaydon KA030ARO (angular contact)
Encoder:	HEDS-6000 Option B08 (1000 lines/rev)
Strain Gages:	Micro Measurements CEA-13-187UV-350
Strain Gage Signal Conditioner:	Analog Devices Model 1B31-AN

B.3.3 Wrist

Motor:	Stray Clifton from A.I. Lab Supply (similar to Clifton SmCo AS-780D Series)
Harmonic Drive:	Harmonic Drive HDC-1C-80-2-K1
Bearings:	Kaydon KA020ARO (angular contact)
Encoder:	HEDS-5000 Option A06 (500 lines/rev)
Strain Gages:	Micro Measurements CEA-13-187UV-350
Strain Gage Signal Conditioner:	Analog Devices Model 1B31-AN

Appendix C: Wiring Details

This appendix details the wiring of the PHD. It is broken down into two sections: the pinouts for all of the cables and the wiring for the two junction boxes. There are 22 cables, 5 from the computer rack to the junction boxes, 4 from the amplifier rack to the boxes, 1 from the computer rack to the robot, 1 between the two junction boxes and 11 from the junction boxes to the robot.

C.1 Cables

This section gives the pinouts at either end of each of the cables on the PHD. The number after the cable name tells how many of these cables there are. One note, on any cable where we weren't sure whether we needed the shield we connected a small black wire to it which runs out the back of the connector housing. This can then be hooked up if noise becomes a problem.

Encoder Cables (3)

Purpose: Take encoder and tachometer signals from Junction Box to Computer, one for each joint

Wire used: Low impedance cable with 6 twisted, shielded pairs

Notes: Shield wires ground to connector housing on computer end

Pinouts:

Computer End: Male DB-15

Pin #	Function
1	A/D Low
2	A/D Ground
3	N.C
4	N.C
5	Encoder +5V
6	Encoder Index
7	Encoder B
8	Encoder A
9	A/D High
10	Digital I/O Ground
11	N.C.
12	Encoder Ground
13	Not Used
14	Not Used
15	Not Used

Box End: Female DB-15

Pin #	Function
1	A/D Low
2	A/D Ground
3	N.C
4	N.C
5	Encoder +5V
6	Encoder Index
7	Encoder B
8	Encoder A
9	A/D High
10	Digital I/O Ground
11	N.C.
12	Encoder Ground
13	Not Used
14	Not Used
15	Not Used

A/D Cables (2)

Purpose: Take torque sensor signals from Junction Box to Computer, one (1) for shoulder and elbow and one (2) for wrist (with extra A/D not used)

Wire used: Two cables, each with one twisted, shielded pair

Notes: Shield wires stick out back of connector housing on computer end

Pinouts:

Computer End: Male DB-15

Pin #	Function
1	N.C.
2	N.C.
3	N.C
4	N.C
5	N.C.
6	A/D Ground
7	1st Channel High
8	2nd Channel High
9	N.C.
10	N.C.
11	N.C.
12	N.C.
13	N.C.
14	1st Channel Low
15	2nd Channel Low

Box End: Female DB-9

Pin #	Function
1	1st Channel High
2	2nd Channel High
3	N.C
4	N.C
5	N.C
6	1st Channel Low
7	2nd Channel Low
8	N.C
9	N.C

Motor Power Cables (3)

Purpose: Take motor power and limit switch signals from Motor Box to Amplifier Rack, one for each joint

Wire used: Two cables, one large gage for motor (white) and one small gage for limit switches (grey) both are twisted, shielded pairs

Notes: Shield wires on limit switch cables are floating

Pinouts:

Amp Rack End: Male DB-25

Pin #	Function
1	Motor Cable Shield
2	Motor Power
3	Motor Power
4	Motor Power
5	Motor Power
6	Motor Power
7	Motor Power
8	Limit Switch
9-13	N.C.
14	Motor Ground
15	Motor Ground
16	Motor Ground
17	Motor Ground
18	Motor Ground
19	Motor Ground
20	Limit Switch
21-25	N.C.

Motor Box End: Female DB-15

Pin #	Function
1	Motor Power
2	Motor Power
3	Motor Power
4	Motor Power
5	Motor Power
6	Motor Power
7	Motor Power
8	Limit Switch
9	Motor Ground
10	Motor Ground
11	Motor Ground
12	Motor Ground
13	Motor Ground
14	Motor Ground
15	Limit Switch

Strain Gage Power Cable (1)

Purpose: Supply power to strain gage chips from supply located in amplifier rack

Wire used: Low impedance cable with three twisted shielded pairs

Pinouts:

Amp Rack End: Male 5 Pin

Pin #	Function
A	+15V
B	Ground
D	-15V
E	Shield
H	Unused

Box End: Female 5 Pin

Pin #	Function
A	+15V
B	Ground
D	-15V
E	Shield
H	Unused

Limit Switch Jumper Cable (1)

Purpose: Take limit switch signals from junction box to motor power box

Wire used: Low impedance cable with three twisted shielded pairs

Pinouts:

Box End: Female 7 Pin

Pin #	Function
A	Shoulder Limit Switch
B	Shoulder Limit Switch
C	Elbow Limit Switch
D	Elbow Limit Switch
E	Wrist Limit Switch
F	Wrist Limit Switch
H	Shield

Motor Box End: Male 7 Pin

Pin #	Function
A	Shoulder Limit Switch
B	Shoulder Limit Switch
C	Elbow Limit Switch
D	Elbow Limit Switch
E	Wrist Limit Switch
F	Wrist Limit Switch
H	Shield

Robot Encoder Cables (3)

Purpose: Take encoder signals from motor to Junction Box, one for each joint

Wire used: Shielded ribbon cable

Notes: Shield of cable sticks out of jacket on junction box end, it is not connected to anything right now

Pinouts:

Box End: Male DB-9

Pin #	Function
1	Encoder Index
2	Encoder B
3	Encoder Ground
4	Encoder Ground
5	Encoder A
6	Encoder +5V
7	Encoder +5V
8	N.C.
	Encoder +5V

Robot End: Male 10 Pin

Pin #	Function
1	Encoder A
2	Encoder +5V
3	Encoder Ground
4	N.C.
5	N.C.
6	Encoder Ground
7	Encoder +5V
8	Encoder B
9	Encoder +5V
10	Encoder Index

Robot Motor Power Cables (3)

Purpose: Take motor power from Motor Box to motors, one for each joint

Wire used: Shielded 3 conductor 14 gage cable

Pinouts:

Color	Function
Red	+ Motor Power
Blue	Motor Ground
Yellow	Shield (only on box end)

Robot Tach/Limit Switch Cables (2)

Purpose: Take tach and limit switch signals from joint to Junction Box, one for shoulder, one for elbow

Wire used: Two, two conductor cables, each with one twisted shielded pair

Notes: There in no cable running to the wrist since there is no tach or limit switches (limit switches could be added). Instead, the connection at the box end is where the limit switches on the table are connected. Shield of cable sticks out of jacket on junction box end, it is not connected to anything right now

Pinouts:

Box End: Female 4 Pin

Pin #	Function
A	Tachometer
B	Tachometer
C	Limit Switch
D	Limit Switch

Robot End: Male 4 Pin

Pin #	Function
A	Tachometer
B	Tachometer
C	Limit Switch
D	Limit Switch

Robot Torque Sensor Cables (3)

Purpose: Take power and signal between torque sensors and Junction Box, one for each joint

Wire used: Two, two conductor cables, each with one twisted shielded pair

Notes: Shield of cable sticks out of jacket on junction box end, it is not connected to anything right now

Pinouts:

Box End: Male 4 Pin

Pin #	Function
A	Sensor Signal
B	Sensor Signal
C	+10V Power
D	Ground

Robot End: Female 4 Pin

Pin #	Function
A	Sensor Signal
B	Sensor Signal
C	+10V Power
D	Ground

Shoulder Joint Position Encoder Cable (1)

Purpose: Take signal from extra encoder on shoulder to computer

Wire used: Low impedance cable with three twisted shielded pairs

Notes: Shield wires ground to connector housing on computer end

Pinouts:

Computer End: Male DB-15

Pin #	Function
1	A/D Low
2	A/D Ground
3	N.C
4	N.C
5	Encoder +5V
6	Encoder Index
7	Encoder B
8	Encoder A
9	A/D High
10	Digital I/O Ground
11	N.C.
12	Encoder Ground
13	Not Used
14	Not Used
15	Not Used

Robot End: Female DB-9

Pin #	Function	Encoder Wire Color
1	Encoder Index	Orange
2	Encoder B	White
3	Encoder Ground	Black
4	N.C	N.A.
5	Encoder A	Blue
6	Encoder +5V	Red
7	N.C	N.A.
8	N.C	N.A.
9	N.C	N.A.

C.2 Junction Boxes

There are two junction boxes mounted on the side of the robot base: the electronics box and the motor box. They serve to re-route signals from the racks into those for the robot. The motor box handles motor power and the limit switches and the electronics box handles all other signals (except the extra shoulder encoder, which goes directly from the computer rack to the robot). The electronics box also houses three small wire wrapped boards which are used to amplify and filter the strain gage signals from the torque sensor. Figure C.1 shows a layout of the amplifier box.

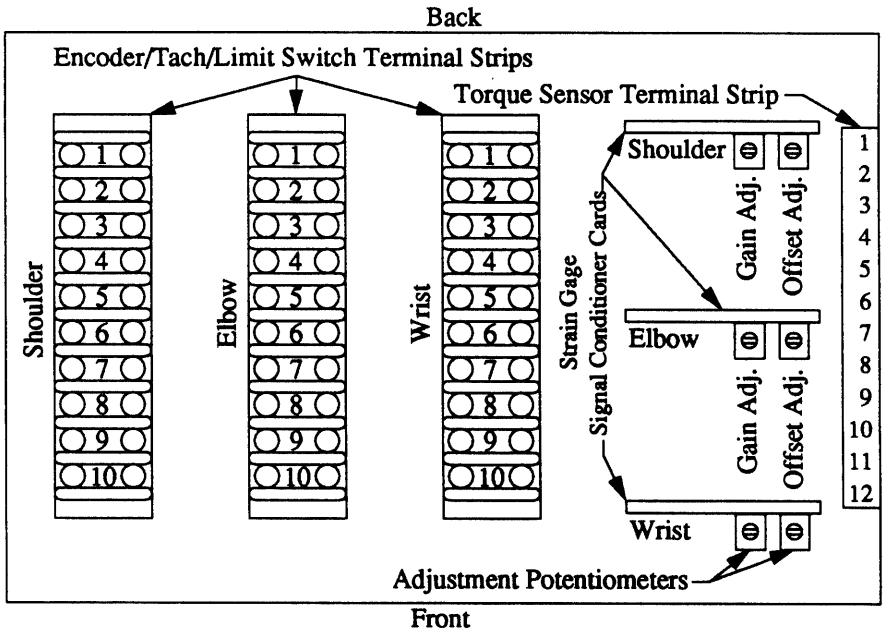

Figure C.1 Layout of the Electronics Box

Figure C.2 and C.3 show the layout of the front and back of the box where the cables plug in. Those coming from the racks plug into the front (the left side when it is mounted) and those going to the robot plug into the back (the right side when it is mounted).

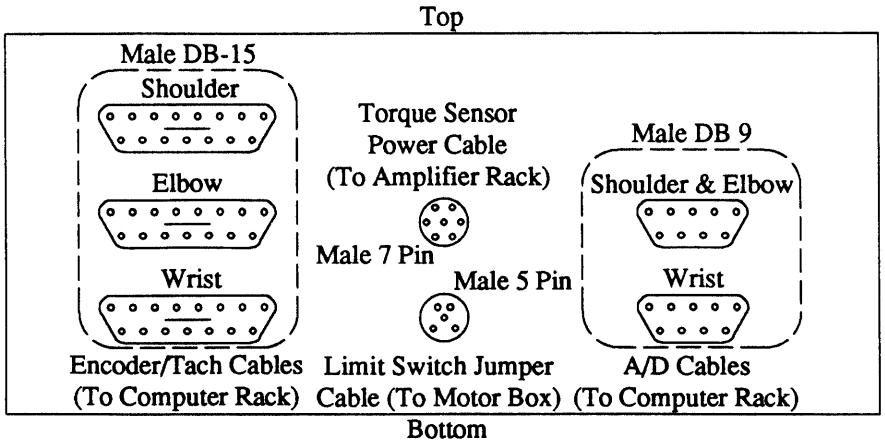

Figure C.2 Front of the Electronics Box

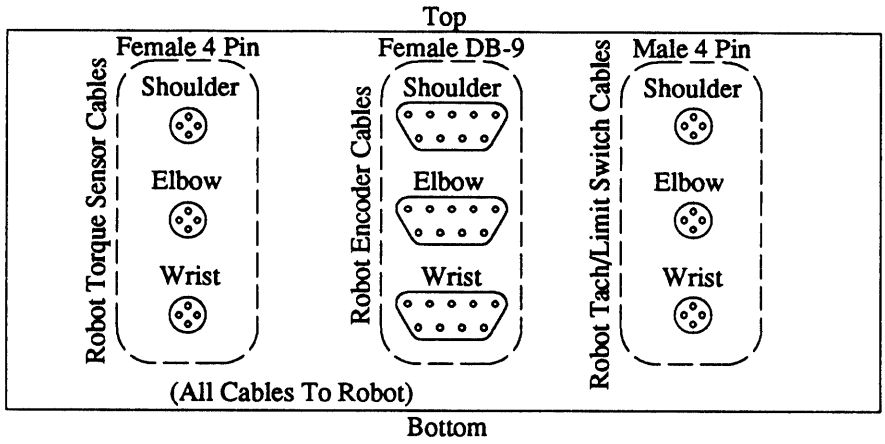

Figure C.3 Back of the Electronics Box

There are three terminal strips on the bottom of the box, one for each joint, which have the limit switch, encoder and tachometer signals running through them. Then there is one terminal strip mounted on the side of the box which routes the signals from the torque sensor signal conditioning cards. Figure C.4 and C.5 detail what each screw on the terminal strips is for.

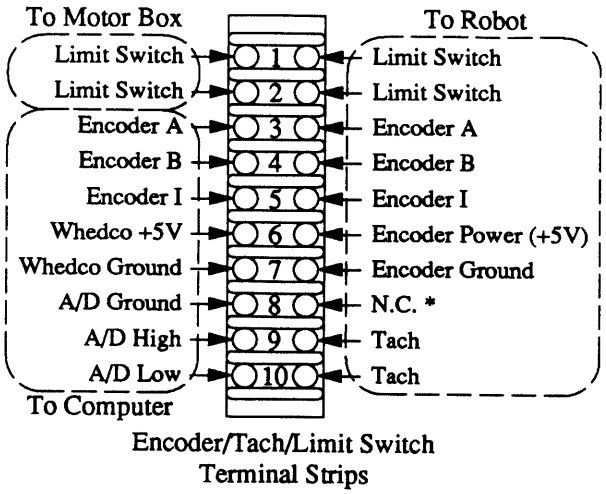

Figure C.4 Wiring for Encoder, Tachometer and Limit Switch Terminal Strips

[Note: There are few additions to this terminal strip. "Pull-up" resistors (2200Ω) are located between encoder A, B, I and +5V to allow the encoder signal to travel back to the Whedco Boards. Also, there is a voltage divider on the tach signal to keep it in the ±2.5V range which the D/A is set on. This circuit consists of a 75kΩ resistor between the tach signal and the A/D high and then a 20kΩ resistor between the A/D high and A/D low. Finally, there is a 20kΩ resistor connecting A/D low to A/D ground to keep the low close to zero volts.]

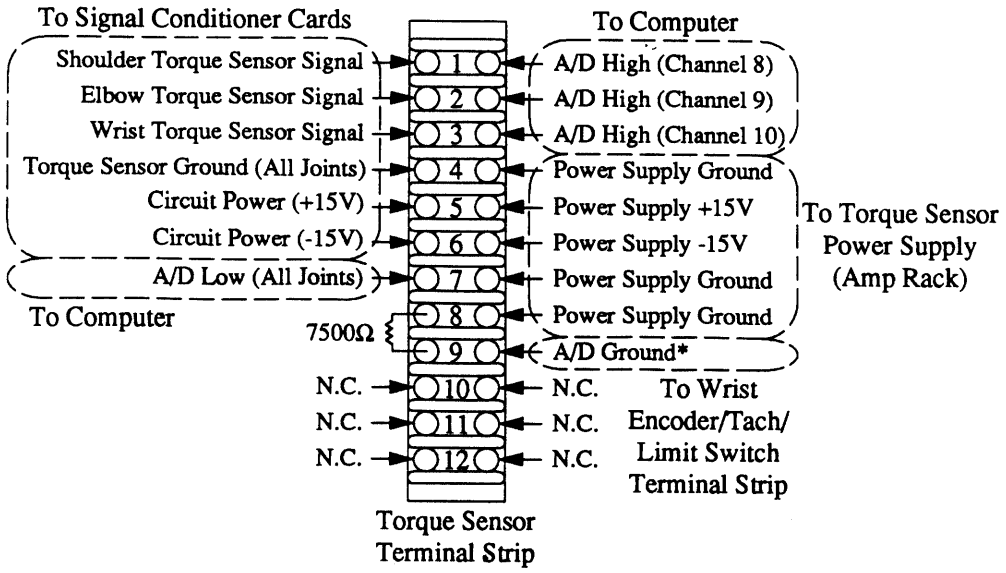

Figure C.5 Wiring for Torque Sensor Terminal Strip

[*Note: The A/D ground is connected to the A/D ground on the wrist encoder/tach/limit switch terminal strip since the A/D cables did not carry the A/D ground signals from the computer.]

Figure C.6 details the wiring of the torque sensor signal conditioning boards. There are two potentiometers in this circuit, one (blue 100Ω) allows adjustment of the gain according to formula C.1 and the other (yellow 50kΩ) allows adjustment of the output offset so the sensor can be zeroed out at no torque. [IMPORTANT: Changing the gain on the board will require re-calibration of the torque sensors.] Also, there are two capacitors (located behind the power conditioning capacitors, right next to the chip) which set the filter cut-off frequency. It is nominally at 1kHz, but we have set it to 100Hz. Formulae C.2 and C.3 give the capacitor values for a given bandwidth.

$$G = 2 + \frac{80k\Omega}{R} \qquad (C.1)$$

In this formula G is the gain and R is the total resistance between pins 3 and 4. (Note: the 16Ω resistor in series with the potentiometer must be added to the potentiometer resistance to use this formula.)

$$C_{sel}1 = 0.015\mu F\left(\frac{1kHz}{f_c} - 1\right) \quad (C.2)$$

$$C_{sel}2 = 0.0022\mu F\left(\frac{1kHz}{f_c} - 1\right) \quad (C.3)$$

In these formulae f_c is the desired cut-off frequency (in kHz).

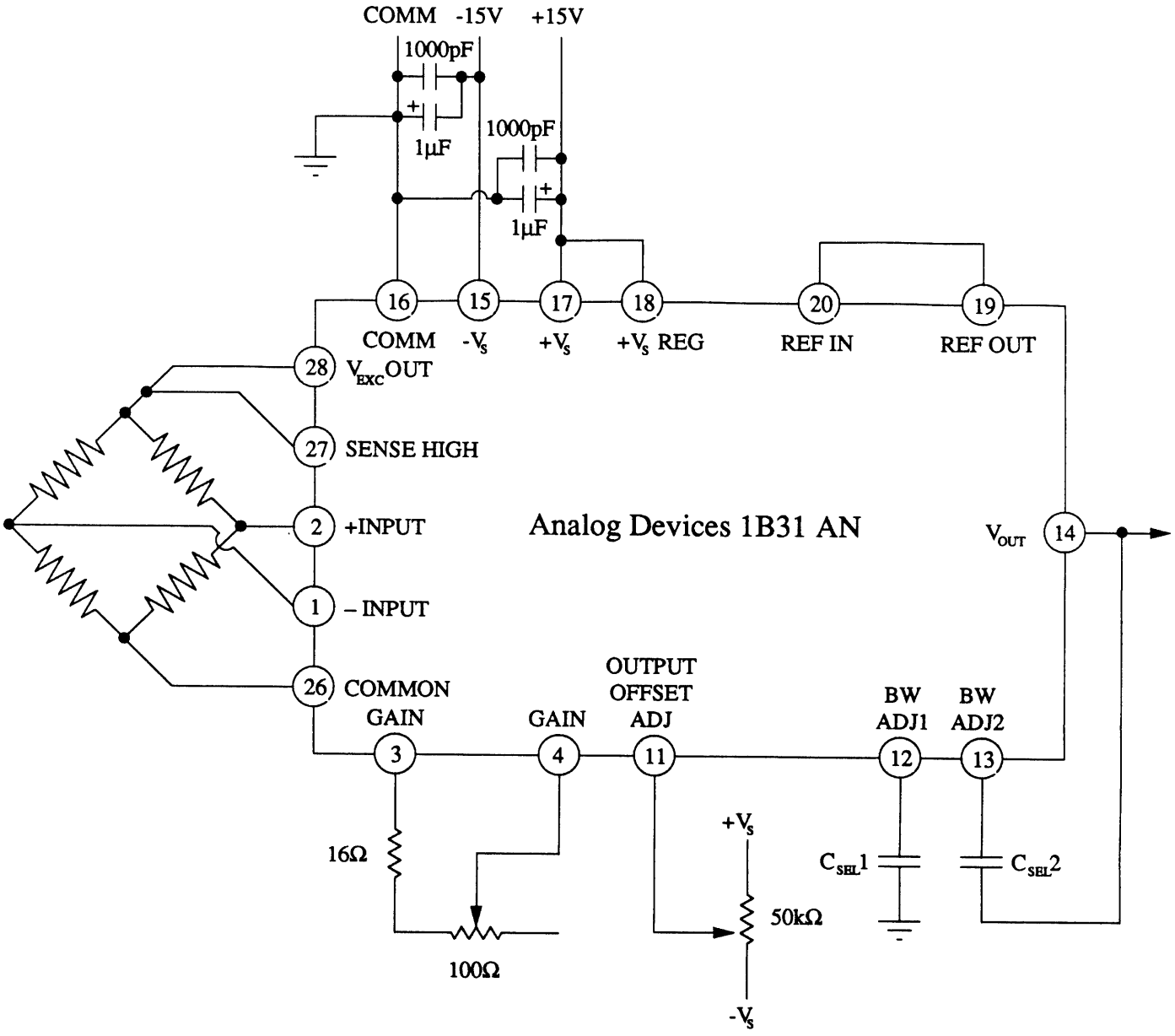

Figure C.6 Wiring for Torque Sensor Signal Conditioning Board

The motor box is pretty much self-explanatory. The motor power and limit switch come in from the amplifier rack, and the limit switch signals are routed out the front to the electronics box. The motor power and shield run out the back of the box through the white cables to the motors.

Appendix D: Motor/Drive Spread Sheet

This appendix contains a copy of the spreadsheet used to select the motor and Harmonic Drive for each joint. As you can see several motors were selected for each joint and then their combination with different Harmonic Drives was evaluated. To do this, first all the important motor data was entered (torque and speed data). The first set of motors are selections for the wrist, the second set for the elbow and the third for the shoulder. Then, the Harmonic drive data was entered (columns 9 & 11, 24 & 26) for two different drive selections. Finally, two different sets of link lengths were entered for each drive.

Next, the formulas for the various other quantities were entered. The Max. Speed and Max. Torque columns are how fast the output turns with that row's motor and that column's Harmonic Drive. The columns with TqJ1, TqJ2 and TqJ3 represent the torque that the other joints would need to produce if the robot were driving its tip into a rigid obstacle, based on the link length at the top of that column. Finally, there are two columns which determine the endpoint force and speed that could be developed (with the other joints locked).

This format allowed us to try several different drives and link length combinations to determine which ones would fit well with a particular set of motors. This was a convenient method because we could just change the drive reduction or link length and then evaluate its effect on the system. The goal was to get a set of motors, drives and link lengths that would be comparable, so no joint was significantly stronger or weaker than the others. The final motor selections we made are indicated by an asterisk (*), the Harmonic Drives we selected are in columns 24 & 26, and the link lengths were 12", 12" and 4".

	1	2	3	4	5	6	7	8
1	Motors							
2		Stall Torque	No Load Spd		Weight			
3	Who's	(oz-in)	(RPM)	PM/RE	lb.	Etc.	Price	Deliv. (wks.)
4	CAS-662-021*	50.0	8000	RE	0.42	2 shaft	$0.00	
5	Inl. QT-0805	24.0	6275	RE	0.46	2 shaft	$1,280.00	8
6	Inl. T-1262	40.0	2500	PM	1.38	2 shaft	$355.00	6-8
7					1C-.3lb			
8								
9	AST DM-326	45.0	5600	PM		Tach.	$89.00	
10	AST DM-481	50.0	5500	PM		Tach.	$42.50	
11	Inl. NT-2173	54.0	1400	PM	2.81	2 shaft	$915.00	6
12	Inl. T-1258	50.0	1700	PM	1.88	2 shaft	$385.00	6
13	Aero 1017DC-01*	80.0	6500	PM	1.70	2 shaft	$275.00	6
14					5C-1.2lb	8-9 wks.		
15								
16	AST DM-395	120.0	2800	PM		2 shaft	$49.50	
17	AST DM-486	100.0	3500	PM		Tach.	$75.50	
18	Inl. QT-1209	100.0	3500	RE	1.88	2 shaft	$1,180.00	6
19	Inl. T-1266	100.0	1350	PM	3.00	2 shaft	$645.00	6
20	Inl. T-1816	100.0	1250	PM	3.75	2 shaft	$915.00	8
21	Inl. T-1856	110.0	1550	PM	3.75	2 shaft	$915.00	8
22	Aero 1035DC-01*	150.0	4500	PM	2.50	2 shaft	$293.00	8
23					1M-2.6lb	8-9 wks.		

	9	10	11	12	13	14	15	16	17	18
1	Max. Speed		Max. Torque	Link 1	Link 2	End				Link 1
2	Model 1C	Slew Rate	(in-lb)	10	10	2	End F	End Spd		12
3	80	deg/sec	140	Tq J1	Tq J2	Tq J3	(lb)	in/s		Tq J1
4	100.00	600.00	250.00	2750.00	1500.00	250.00	125.00	20.94		1750.00
5	78.44	470.63	120.00	1320.00	720.00	120.00	60.00	16.43		840.00
6	31.25	187.50	200.00	2200.00	1200.00	200.00	100.00	6.54		1400.00
7	Model 3C		(in-lb)							
8	120		990							
9	46.67	280.00	337.50	618.75	337.50	56.25	28.13	58.64		590.63
10	45.83	275.00	375.00	687.50	375.00	62.50	31.25	57.60		656.25
11	11.67	70.00	405.00	742.50	405.00	67.50	33.75	14.66		708.75
12	14.17	85.00	375.00	687.50	375.00	62.50	31.25	17.80		656.25
13	54.17	325.00	600.00	1100.00	600.00	100.00	50.00	68.07		1050.00
14	Model 5C		(in-lb)							
15	200		2470							
16	14.00	84.00	1500.00	1500.00	818.18	136.36	68.18	32.25		1500.00
17	17.50	105.00	1250.00	1250.00	681.82	113.64	56.82	40.32		1250.00
18	17.50	105.00	1250.00	1250.00	681.82	113.64	56.82	40.32		1250.00
19	6.75	40.50	1250.00	1250.00	681.82	113.64	56.82	15.55		1250.00
20	6.25	37.50	1250.00	1250.00	681.82	113.64	56.82	14.40		1250.00
21	7.75	46.50	1375.00	1375.00	750.00	125.00	62.50	17.85		1375.00
22	22.50	135.00	1875.00	1875.00	1022.73	170.45	85.23	51.84		1875.00
23										

	19	20	21	22	23	24	25	26	27	28
1	Link 2	End				Max. Speed		Max. Torque	Link 1	Link 2
2	12	4	End F	End Spd		Model 1C/.3	Slew Rate	(in-lb)	12	12
3	Tq J2	Tq J3	(lb)	in/s		80	deg/sec	140	Tq J1	Tq J2
4	1000.00	250.00	62.50	41.89		100.00	600.00	250.00	1750.00	1000.00
5	480.00	120.00	30.00	32.86		78.44	470.63	120.00	840.00	480.00
6	800.00	200.00	50.00	13.09		31.25	187.50	200.00	1400.00	800.00
7						Model 5C/1.2		(in-lb)		
8						160		1240		
9	337.50	84.38	21.09	78.19		35.00	210.00	450.00	787.50	450.00
10	375.00	93.75	23.44	76.79		34.38	206.25	500.00	875.00	500.00
11	405.00	101.25	25.31	19.55		8.75	52.50	540.00	945.00	540.00
12	375.00	93.75	23.44	23.74		10.63	63.75	500.00	875.00	500.00
13	600.00	150.00	37.50	90.76		40.63	243.75	800.00	1400.00	800.00
14						Model 1M/2.6		(in-lb)		
15						160		2470		
16	857.14	214.29	53.57	41.05		17.50	105.00	1200.00	1200.00	685.71
17	714.29	178.57	44.64	51.31		21.88	131.25	1000.00	1000.00	571.43
18	714.29	178.57	44.64	51.31		21.88	131.25	1000.00	1000.00	571.43
19	714.29	178.57	44.64	19.79		8.44	50.63	1000.00	1000.00	571.43
20	714.29	178.57	44.64	18.33		7.81	46.88	1000.00	1000.00	571.43
21	785.71	196.43	49.11	22.72		9.69	58.13	1100.00	1100.00	628.57
22	1071.43	267.86	66.96	65.97		28.13	168.75	1500.00	1500.00	857.14
23										